UNIVERSITEIT VAN STELLENBOSCH
UNIVERSITY OF STELLENBOSCH

TRANSIENT MODELLING OF A LOOP THERMOSYPHON

TRANSIENT EFFECTS IN SINGLE AND TWO PHASE NATURAL CIRCULATION THERMOSYPHON LOOPS SUITABLE FOR THE REACTOR CAVITY COOLING OF A PEBBLE BED MODULAR REACTOR

Johannes Coenraad Ruppersberg

Departement Meganiese Ingenieurswese | Department of Mechanical Engineering

Privaatsak X1 | Tel: +27 (0) 21 808 4376 | Private Bax X1
7602 MATIELAND | Faks/Fax: +27 (0) 21 808 4958 | 7602 MATIELAND
Suid-Afrika | E-pos/E-mail: meganies@ing.sun.ac.za | South Africa

TRANSIENT MODELLING OF A LOOP THERMOSYPHON

TRANSIENT EFFECTS IN SINGLE AND TWO PHASE NATURAL CIRCULATION THERMOSYPHON LOOPS SUITABLE FOR THE REACTOR CAVITY COOLING OF A PEBBLE BED MODULAR REACTOR

Johannes Coenraad Ruppersberg

Thesis presented in partial fulfilment of the requirements for the degree
Master of Science in Engineering at the University of Stellenbosch

Thesis Supervisor: RT Dobson

March 2008

Department of Mechanical and Mechatronic Engineering
University of Stellenbosch

DECLERATION

I, Johannes Coenraad Ruppersberg, the undersigned, hereby declare that the work contained in this thesis is my own original work and has not previously, in its entirety or in part, been submitted at any university for a degree.

…….

Signature of candidate

…..… day of ……... 2008

SUMMARY

The focus of this project was the application of a passive device in the form of a loop thermosyphon as a reactor cavity cooling system (RCCS) for a Pebble Bed Modular Reactor. An extensive literature review showed that loop thermosyphons have been widely researched, both theoretically and experimentally. In the review attention has specifically been given to matters such as safety, instability, control and mathematical modelling.

One of the objectives of the project was to build one of the axially symmetric sections of Dobson's (2006) proposed full scale RCCS using a scaled down version consisting of a single loop heated by a section of the reactor pressure vessel and cooled by a tank of water. The second objective was to derive a theoretical model that could be used in a computer code to simulate the experiment. The theory and experiment would then be compared in order to verify the code.

The mathematical model created used the following three major assumptions: quasi-static flow, incompressible liquid and vapour and one dimensionality. The conservation equations in the form of a set of difference equations with the appropriate closure equations were then solved explicitly. It was found that the theoretical results were heavily influenced by the surface optical properties as well as the heat transfer coefficients. The emissivity influenced the transition point from single to two-phase flow as well as the condenser outlet temperature. The single phase heat transfer coefficients influenced the condenser outlet temperature significantly while it was found that for two phase flow the combination of the available boiling and condensation heat transfer coefficients had only minor effects on the end results.

A stainless steel and aluminium thermosyphon loop was built using water as the working fluid. A stainless steel heater plate provided the heat input while a 200 L water tank was the heat sink. Temperature and flow rate measurements were recorded as a function of time with various heating/cooling transients from start-up to steady state for three operating modes. The three operating modes were single phase, two-phase and heat pipe mode.

It was found that the theoretical temperatures correspond reasonably well with the experimental temperatures. The time predicted by the theoretical model to reach the operating temperature was however somewhat longer than for the experimental. This is to be expected when considering that there is some uncertainty pertaining to the heat transfer coefficients as well as surface emissive properties. The correspondence of the theoretical and experimental fin temperatures was poor due to significant thermal stratification of the air separating the heater plate and fins. Several shortcomings in the theoretical model as well as the experimental setup were identified and discussed.

The conclusion was reached that this exploratory study showed that the loop thermosyphon is a viable option for the RCCS and that the mathematical model is a viable theoretical simulation tool. Several recommendations were made for further study to address and overcome the shortcomings identified in the theoretical and experimental models in order to prove this conclusion. Amongst these is the determination of better material surface properties and heat transfer coefficients and improved mass flow rate measurement. Investigating scaling issues, natural convection outside the loop and updating of the computer program is also recommended.

OPSOMMING

Die fokus van hierdie projek was die toepassing van passiewe apparatuur, in die vorm van ‘n geslote lus termoheuwel, as ‘n reaktor kamer verkoellings stelsel vir die korrel bed modulêre reaktor. Die literatuur studie wys dat hierdie tegnologie reeds breedvoerig ondersoek is teoreties sowel as eksperimenteel. In die literatuur oorsig word aandag spesifiek gegee aan veiligheid, onstabiliteit, beheer en modelleering.

Een van die doelwitte van die projek was om ‘n klein skaalse model te bou van een van die aksiaal simmetriese seksies van Dobson (2006) se voorgestelde volskaalse reaktor kamer verkoellings stelsel. Die model bestaan uit n enkele lus verhit deur ‘n seksie van die reaktor drukvat en verkoel deur ‘n tenk vol water. Die tweede doelwit was die afleiding van ‘n teoretiese model wat in ‘n rekenaar program gebruik kan word om die eksperiment te simuleer. Die teoretiese en eksperimentele data kan dan vergelyk word om die geldigheid van die program te toets.

Die volgende aanames is gemaak tydens die afleiding van die wiskundige model: kwasi-statiese vloei, onsamedrukbare vloeistof en gas en een dimensionalitiet. Die behouds wette is in die vorm van ‘n stel differensie vergelykings met die toepasbare sluitings vergelykings eksplisiet opgelos. Dit is bevind dat die teoretiese resultate swaar beinvloed is deur die materiaal oppervlak eienskappe sowel as die warmteoordrag koëffisiënte. Die emisiviteit beinvloed die oorgangs punt van enkel na twee fase vloei sowel as die kondenser uitlaat temperatuur. Die enkel fase warmteoordrag koëffisiënt het n beduidende invloed op die kondenser uitlaat temperatuur terwyl dit voorkom asof die spesifieke kombinasie van die koking en kondensasie warmteoordrag koëffisiënte minimale invloed op die resultate het in die twee fase gebied.

Vlekvrye staal en aluminium is gebruik om die lus te bou met water as die verkoelings middel. Warmte is toegevoeg tot die stelsel deur ’n vlekvrye staal verhittings plaat terwyl ‘n 200 L water tenk die warmte onttrek het. Temperatuur en massa vloei tempo is aangeteken as ‘n funksie van tyd vir verskeie verhitting/verkoellings oorgangs gedragte vanaf begin tot bestendige toestand vir drie bedryfs modusse. Die drie bedryfs modusse was enkel fase, twee fase en hitte pyp modus.

Dit is bevind dat die teoretiese temperature redelik goed ooreengekom het met die eksperimentele waardes. Die tyd wat dit neem om by die bedryfs temperatuur te kom soos voorspel deur die teorie is egter langer as wat in die eksperiment gevind is. Dit is te verstane wanneer die onsekerheid in die warmteoordrag koëffisiënte en materiaal oppervlak eienskappe in ag geneem word. Die fin temperature het ‘n swakker ooreenkoms getoon as gevolg van beduidende termiese stratifikasie van die lug tussen die fin en verhittings plaat. Verskeie tekortkominge in die teoretiese model en eksperimentele opstelling is geïdentifiseer en bespreek.

Die gevolgtrekking is gemaak dat die ondersoek bewys dat geslote lus termoheuwels ‘n lewensvatbare opsie is vir ‘n reaktor kamer verkoellings stelsel en dat die wiskundige model lewensvatbaar is vir teoretiese simulasie. Verskeie aanbevelings word egter gemaak om die tekortkominge in die teoretiese en eksperimentele modelle aan te spreek om so doende die gevolgtrekking te staaf. Dit word aanbeveel dat beter waardes vir die materiaal oppervlak eienskappe en warmteoordrag koëffisiënte gevind word en verbeterde massa vloei meetings gedoen word. Dit word verder aanbeveel om skaleering asook natuurlike konveksie buite die lus te ondersoek en om die rekenaar program by te werk.

ACKNOWLEDGEMENTS

The following people are thanked for their contributions toward this project, without which the completion of this project would not have been possible:

Robert Dobson – Supervisor
Thank you for your guidance and especially your patience with me, your enthusiasm for the project was truly infectious.

Cobus Zietsman – Laboratory technician
Thank you for your many helpful suggestions and assistance with the experimental set-up.

Andre du Toit – Firga manager
Thank you for your help and understanding without which my simulations would never have gotten finished in time.

To my family for all the love and support
you have given me throughout my life

CONTENTS

LIST OF FIGURES

LIST OF TABLES

NOMENCLATURE

A	area, m^2
A_x	cross sectional area, m^2
A_z	surface area, m^2
a	acceleration, m^2/s
C_f	Fanning friction factor
c	specific heat, J/kg.K
D	diameter, m
E	energy, J
$\dot{E}$	energy transfer rate, W
e	energy per unit mass, J/kg
F	force, N
F	view factor
Fr	Froude number
f	Darcy friction factor
G	mass flux, $kg/m^2.s$
Gr	Grashof number
g	gravitational acceleration, m^2/s
h	specific enthalpy, J/kg
h	heat transfer coefficient, $W/m^2.K$
K	minor loss coefficient
k	thermal conductivity, W/m.K
L	length, m
m	mass, kg
$\dot{m}$	mass flow rate, kg/s
Nu	Nusselt number
P	pressure, Pa
Pr	Prandtl number
P_r	reduced pressure, $P/P_{critical}$
Q	heat, J
$\dot{Q}$	heat transfer rate, W
R	thermal resistance, K/W

Ra	Rayleigh number
Re	Reynolds number
S	suppression factor
S	slip factor
$\dot{S}$	heat transfer rate, W
T	temperature, K
t	time, s
U	Total internal energy, J
u	specific internal energy, J/kg
u	velocity, m/s
V	volume, m^3
v	velocity, m/s
W	work, J
We	Weber number
X	Martinelli parameter
x	thermodynamic quality, mass fraction
z	distance, m

Greek letters

α	void fraction
β	thermal expansion coefficient, K^{-1}
ε	emissivity
θ	angle, °
λ	thermal conductivity, W/m.K
μ	dynamic viscosity, $N.s/m^2$
ν	kinematic viscosity, m^2/s
ρ	density, kg/m^3
σ	surface tension, N/m
σ	Stefan-Boltzmann constant, $W/m^2.K^4$
τ	shear stress, N/m^2
ϕ^2	two phase multiplier

Superscript

t	time step

Subscript

a	air
c	core
c,af	convection, air to fin
c,fba	convection, fin to air at back of fin
c,ra	convection, rpv to air
cv	control volume
D	diameter
FC	forced convection
f	fin, saturated fluid
g	generated, gas
in	in
k	control volume number
l	liquid
lo	liquid only
m	minor
NB	nucleate boiling
out	out
pool	pool boiling
r	reactor pressure vessel (rpv)
r,rf	radiation, rpv to fin
st	stored
sys	system
t	tank
tp	two phase
tt	turbulent-turbulent
w	water, wall

1 INTRODUCTION

1.1 Why Is Energy Important

Why is energy important? This question can easily be answered by considering the power shortages of the past two years in South Africa. Due to these shortages business and industry incurred massive financial losses, according to an estimate of the Cape Town Chamber of Commerce and Industry the cost to the economy is in the order of R9 billion (Kemp, 2007). The effects cannot only be felt on an economic level but also on a personal level, for a society dependant on electrically driven technology, such shortages affect our everyday quality of life (Mangxamba et. al., 2007). For these reasons such shortages are unacceptable and in order for these shortages not to occur more power stations will have to be built. In South Africa this will in all likelihood mean the commissioning of more fossil fuel power stations, which will invariably have a serious impact on the environment due to the emissions of harmful gasses such as CO_2, SO_2 and NO_x.

Environmental damage and the current climate change phenomenon are providing the driving force for research into renewable energy systems. These systems are however not capable of providing base load capacity as yet. This begs the question: Where does one find a viable energy source for the very near future? Without debating the merits of the various energy generation methods suffice it to say that some believe the answer to lie in harnessing the energy provided by nuclear reactions. In South Africa this has led to the establishment of a company that aims to produce modular high temperature gas reactors for domestic and international use called PBMR (Pty) Ltd.

1.2 History of PBMR

The history of PBMR has its origins in Eskom's vision of adding nuclear power plants to its power generation grid as part of its integrated electricity plan (www.eskom.co.za). During the 1990's Eskom investigated the possibilities and implications of nuclear

energy addition to its arsenal and eventually acquired the necessary licenses to develop the high temperature gas reactor technology. In 2000 the PBMR company was formed in partnership with Eskom, the Industrial Development Corporation of South Africa (IDC), British Nuclear Fuels and Exelon, a US utility which later withdrew.

The design, and related processes, has continued ever since with the aim of building a demonstration plant at Koeberg. Since 2004 government has shown its support through funding and intention-of-purchasing negotiations. Then during 2005 a Chinese pebble bed developer indicated its willingness to cooperate on mutual projects. March of 2006 saw some restructuring of BNF which allowed Westinghouse, a leading nuclear power company to acquire a 15 % share in PBMR (www.pbmr.com, a). As of this date construction of the demonstration plant is set to start in 2009 with the completion date in 2013 while commercial units are expected to be in production three years later (www.pbmr.com, b).

1.3 Design Requirements

In order to facilitate future development PBMR has launched several research programs in partnership with South African universities. One of these programs entails the investigation of a suitable passive reactor cavity cooling system (RCCS). The term passive refers to a system that will accomplish the task by purely reacting in accordance with the laws of nature without the aid or incentive of manmade machines and controls. The requirements of such a RCCS are given by Matzner (2004) as follows. It must …

- Prevent thermal radiation from impinging directly onto the concrete walls of the reactor cavity.
- Remove all heat from the reactor cavity during normal operation, thereby maintaining the concrete surfaces below the design temperature, the limit being 65 °C, under normal operating condition.
- Remove all decay and residual heat generated in the reactor cavity during a pressurized and depressurized loss of forced core cooling event.

1.4 Existing RCCS concepts and designs

Several systems capable of meeting these requirements have been proposed and investigated. For the General Atomics' GT-MHR reactor, an air duct system was proposed (see figure 1) as described by Thielman et al. (2005). Air is drawn in through four separate inlets into the downcomer that completely cover the concrete wall. The air stream is then split and flows into the various risers were it is heated by radiation from the pressure vessel. Natural convection induces the air to flow up the risers to the hot plenum and eventually to the four outlets. This is a relatively simple system with no moving parts and it does not require human intervention to work. However, a limitation is placed on the reactor power in order for the heat levels not to exceed the heat removal capability of the system under accident conditions.

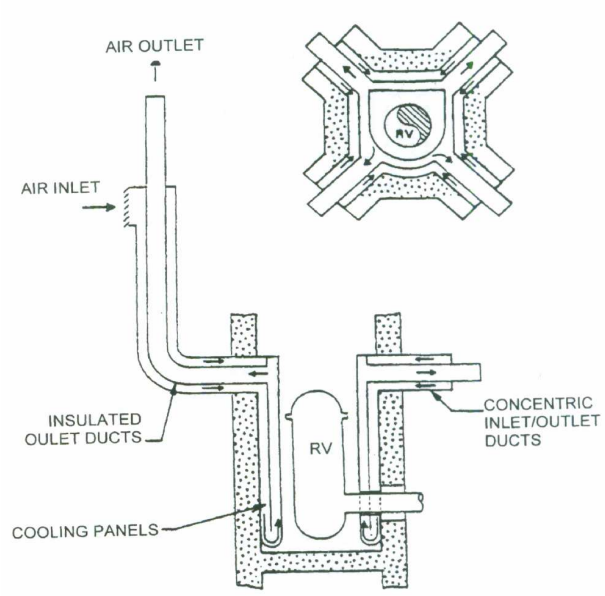

Figure 1: Schematic of GT-MHR RCCS, (Thielman et al., 2005)

Ohashi et al. (1998) conducted a preliminary study on the use of heat pipe technology as part of a passive decay heat removal system for a modular high temperature reactor (see figure 2). The evaporator is situated between the reactor pressure vessel and the containment wall shielding it from radiation. During operation the working fluid boils off and the vapour travels to the condenser section situated outside the containment building. Here the heat is transferred to the atmosphere through natural convection, enhanced by the stack. Further improvements in operation can be made by using what is termed a Variable Conductance Heat Pipe (VCHP). This calls for the addition of a

nominal amount of non-condensable gas at the outset in order to control the eventual system working temperature. There are no active components thereby giving a fully passive system.

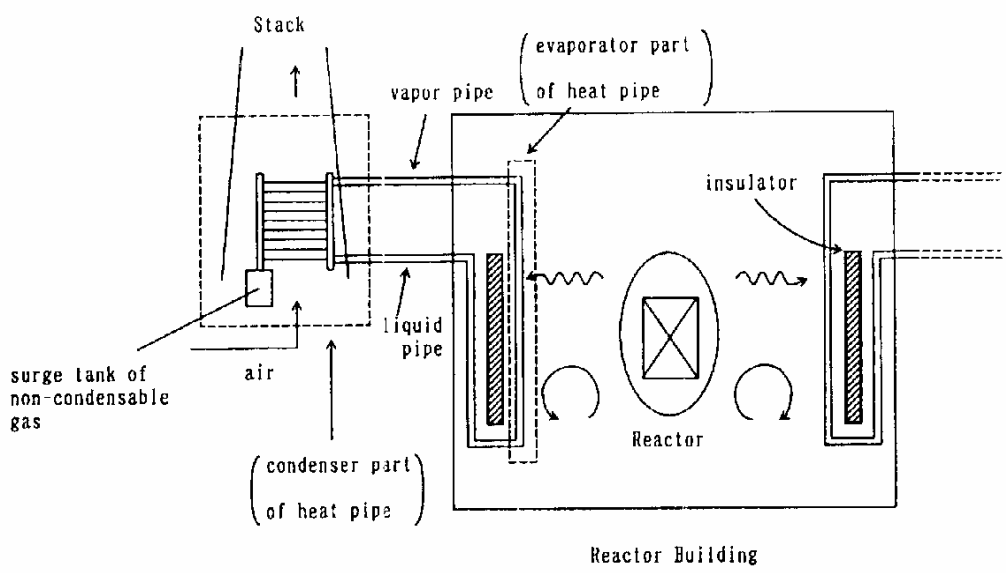

Figure 2: Schematic of VCHP decay heat removal system, (Ohashi et al., 1998)

Byun et al. (2000) (see figure 3) analysed a conceptual design for a containment cooling system for large concrete structures. This system comprises of an evaporator section, situated inside the containment structure, connected through piping and valves to a water pool at a higher elevation outside the containment structure. During operation the vapour is vented to the atmosphere while the tank level is controlled by the water supply system. The tank size is chosen to allow the containment cooling system to work for 8 hours continuously allowing the RCS to cool down to the shutdown cooling entry condition. Although gravity and buoyancy is responsible for the flow in the system the addition of DC control valves and a level control system for the tanks makes this system only semi-passive and thus vulnerable to electro-mechanical failure.

Takada (2004) (see figure 4) analysed an active system that employs a forced water-cooling panel system for modular high-temperature gas-cooled reactors (MHTGR's). This system forces cooling water through pipes surrounding the reactor pressure vessel in a reactor cavity filled with air. A similar analysis is performed by Van Staden (2004) on a forced flow RCCS for the PBMR and it is shown to be effective in maintaining the temperatures in the reactor cavity.

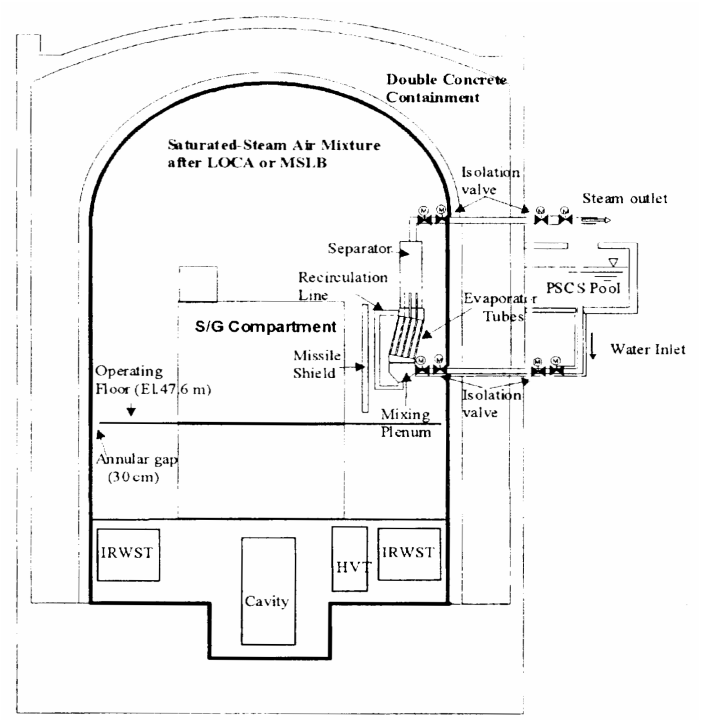

Figure 3: Schematic of containment cooling system, (Byun et al., 2000)

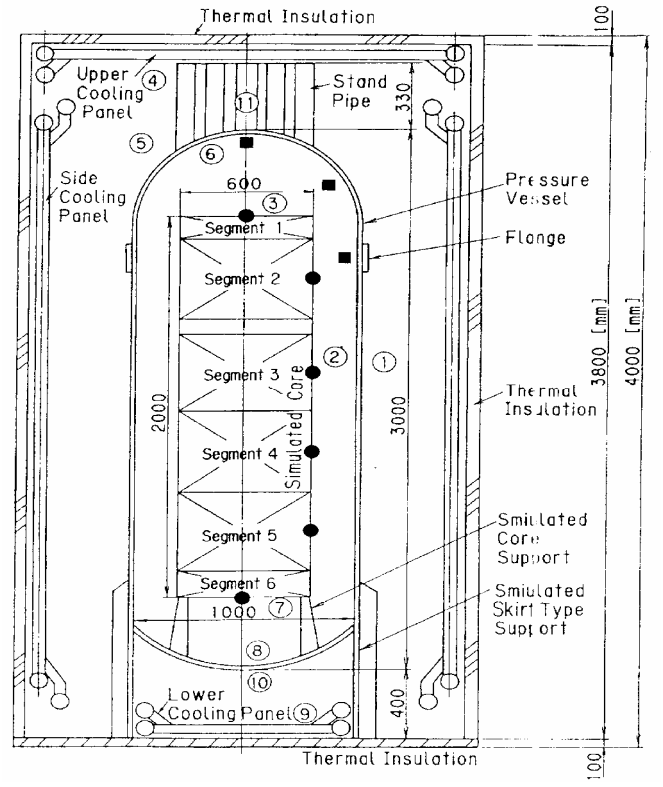

Figure 4: Schematic of MHTGR RCCS, (Takada et al., 2004)

These four methods show that the natural circulation heat pipe concept can be a very promising fully passive cooling system. It was therefore decided to further investigate the use of such a system for the use as a RCCS in a PBMR.

1.5 Objectives

The following objectives were identified at the outset of this project:

1) Do a literature review.

2) Design and build a loop thermosyphon on a small scale no larger than 2 m x 2 m. Make use of aluminium and stainless steel for the loop material rather than PVC or glass to ensure the same heat transfer characteristics present in the eventual full scale model.

3) Take experimental measurements whilst operating thermosyphon in single phase, two phase and heat pipe mode. Allow for the heat input to the system to simulate normal operating conditions as well as loss of coolant accident conditions in a PBMR.

4) Write a computer program in a commercial language that will simulate the working of the loop thermosyphon as well as the heat source and heat sink.

5) Compare the experimental and numerical data. Do a critical evaluation of the data and draw conclusions on its validity based on the physics involved as well as data obtained from published sources.

6) Attempt to predict the operation of a prototype model of this reactor cavity cooling system.

2 LITERATURE STUDY

A short history of nuclear power shows the route followed to reach the point where generation IV reactors are a viable long term option. An abbreviated description of the operation of one type of generation IV reactor, in the form of the PBMR, then show how the PBMR project originated. The focus then shifts to thermosyphons in general and thereafter onto specific areas other researchers have identified as problematic such as safety, control, instability and mathematical modelling. This gives a broad overview of the problem as well as a reference point from which to commence theoretical modelling and experimental evaluation.

2.1 Nuclear Power

The Second World War saw the first steps in nuclear research being taken by a number of countries. This was also a particularly dark time in history wherein the devastating power of nuclear weapons was demonstrated. After the war ended research focused on the use of nuclear power for electricity generation. In 1954 the fist nuclear power plant to deliver power to a national grid came on line at Obninsk in the USSR, it had a capacity of 5 MW. Two years later in 1956 the world's first commercial nuclear power station, Calder Hall in Sellafield, England was opened. It started with a 50 MW capacity that was later increased to 200 MW. In 1957 an international regulating body, the International Atomic Energy Agency (IAEA), was launched (www.iaea.org).

The early years of nuclear power saw a rapid rise in installed capacity peaking at 300 GW in the 1980's. However from the 1980's to only a few years ago anti-nuclear sentiment has dominated. The Three Mile Island accident in 1979 and the Chernobyl accident of 1986 caused a great deal of fear of possible nuclear accident and radiation. The production, transport and storage of nuclear waste are also a contentious issue. Added to this was the rising costs compared to fossil fuels. The result – orders for new nuclear power stations dried up. In 2005 the total capacity was only 366 GW, with the rise mainly attributed to the economic growth and energy requirements of China, (en.wikipedia.org).

To put this number in perspective, a report by the International Energy Agency (IEA, 2006), based on world energy data of 2004, shows nuclear power plants with a total capacity of 357 GW contribute approximately 16 % of the world's electricity.

Not only in China but the world over energy requirements increase with each passing year. In conjunction with this rising need is the need to limit pollution of which fossil fuel power plants are a large contributor. In 2002 the Generation IV International Forum (GIF) nations proposed long term research and design goals for generation IV reactors to make nuclear power safer and more viable for long term use. Combining all these factors has once again swung the favour in the direction of *nuclear* power generation.

2.2 PBMR

In South Africa this direction takes the form of the Pebble Bed Modular Reactor (PBMR) which is a helium cooled graphite moderated high temperature reactor. An appreciation for the scale of the structures involved can be given by the dimensions of the reactor pressure vessel (RPV) which is 27 m high with an internal diameter of 6.2 m. Contained in the RPV is an annular fuel core that is located between the central and outer graphite reflectors. The graphite is used as the moderator, responsible for slowing down the neutrons to the speed required for nuclear fission. The fuel elements take the form of uranium dioxide kernels coated in silicone carbide and pyrolytic carbon encased in a 60 mm diameter spherical graphite shell, termed a fuel pebble. Each pebble travelling through the reactor several times in its lifetime until the fuel is optimally spent.

The heat of fission is transferred to the helium coolant that enters the reactor at 500 °C and leaves at 900 °C to drive the turbo-machinery in a direct Brayton cycle. The turbine in turn drives the generator through a speed-reduction gearbox to produce 165 MWe. The power level is dependant on the helium mass flow rate which in turn is dependant on the system pressure. Therefore the power will be controlled by varying the system pressure. A typical thermal efficiency (electrical power output/ thermal heat input) for a light water reactor is approximately 33 %, it is however estimated that the

PBMR will have a thermal efficiency of approximately 41 % due to the high temperature and pressures involved (www.pbmr.com, c).

These high temperatures however necessitate the use of a reactor cavity cooling system that satisfies the design requirements given in section 1 to ensure that the structural integrity of the concrete containment is maintained.

2.3 Safety Issues

In the nuclear industry safety is of great importance. Great emphasis has been placed on creating an inherently safe design for the PBMR. This was achieved mainly through the reactor design and the choice of materials and fuel elements. In order to extend this safety-conscience design to the containment building and in particular the reactor cavity a reliable RCCS is required. Two options are open to the designers, design an active system with the required built-in redundancy to ensure reliability or design a passive system with no moving parts or electro-mechanical control devices that operates according to the laws of nature with a higher associated reliability.

Burgazzi (2004) however points out that there always exists the non-zero likelihood of the occurrence of failure once operation starts. The objective of Burgazzi's paper is to identify and evaluate the uncertainties identified by the failure modes of a passive cooling system. To illustrate this procedure a decay heat removal system relying on natural circulation is evaluated using two different methods namely the Failure Mode and Effect Analysis (FMEA) and hazard and operability study (HAZOP). The study shows that a great deal of uncertainty exists relating to passive system performance. The task of doing a meaningful reliability study is made difficult due to the lack of operational and experimental data. Burgazzi (2004) goes on to point out that the majority of the uncertainties identified is related to the current state of knowledge about the physical phenomena present and can thus be reduced through additional study. While this paper does not have a direct influence on the present work it is important to keep nuclear related issues such as this under consideration as it will most certainly become an issue for the designers of the reactor cavity cooling system.

2.4 Thermosyphon Loops

2.4.1 General

Looking at the varying existing concepts in the previous chapter, the heat pipe option made a great deal of sense due to its high heat transfer rate capability. It is intended in this project to investigate the use of a particular type of heat pipe called a loop thermosyphon. In the literature the two most common configurations are the toroidal and rectangular loops. This project investigated the operation of a rectangular loop since it was the more practical shape for the problem.

A loop thermosyphon is a thermodynamic device that employs temperature induced density gradients to create a natural circulation of the working fluid in the system. The operation of a thermosyphon can best be described by imagining a parcel of fluid of constant volume flowing around the loop. The parcel enters the evaporator section; heat is added to the parcel which causes the density to decrease. The parcel gets lighter and rises, moving toward the condenser section. When it passes through the condenser heat is removed and the parcel's density increase. Gravity assists and the parcel again moves toward the evaporator section.

These devices use no mechanical pumps which make it less likely to fail and are relatively noiseless and less costly to install, maintain and retire. Natural circulation loops find widespread use: in the chemical process industry in the form of thermosyphon reboilers (Arneth, 2001; Chexal, 1986); as solar water heaters and for waste heat recovery (Cheng, 1982; Chen, 1991 and Yilmaz, 1991), in the electronics industry (Khodabandeh, 2002) but particularly in the nuclear industry as passive heat removal systems under accident conditions as well as for removal of parasitic heat loss during normal operation (Hsu, 1998; IAEA, 2000; Jiang, 1995; Ohashi, 1998 and Sha, 2004).

2.4.2 Theory

Due to the widespread use of natural circulation systems it has understandably been the subject of numerous research papers. One of the pioneers of the field was Welander (1966) who considered the fluid to be driven by the pressure difference and a buoyancy force, and is retarded by a frictional force. The assumptions made included the Boussinesq approximation, the tangential friction force on the fluid is proportional to the *instantaneous* flow rate, the temperature of the fluid is uniform over each cross-sectional area, and the heat transfer rate between the pipe and the fluid is proportional to the difference between a prescribed wall temperature and the fluid. Applying these assumptions, the essentially *one-dimensional* equations of change are obtained for a single phase fluid. Using analytical as well as numerical integration a stability map was constructed on which stable and unstable operating conditions were plotted and the occurrence of transient and non-linear effects could be established. The reason why this article has been singled out is that it is one of the earliest publications giving the assumptions on which most of the theoretical work to date has been based.

Grief (1988) gives a descriptive review of a number of single phase and two-phase thermosyphon loops while Knaani and Zvirin (1990, 1993) show how the single phase loop theory may be extended for the case of a two-phase loop by specifying suitable equations for the friction factor, the two-phase frictional multiplier, the single and two-phase heat transfer coefficients and a suitable relationship for the void fraction and the mass fraction. The differential equations were solved using a relatively involved combination of analytical and numerical stages.

Dobson (1993), although only for a single phase laminar fluid, shows how a simple explicit finite difference discretization formulation scheme is able to capture transients and the highly non-linear behaviour of the loop. Vincent and Kok (1992) using ten differential equations were able to capture the transient performance of a two-phase closed loop thermosyphon. Emphasis was placed on the value of the control volume approach as a powerful tool to describe the overall performance of the thermosyphon with a limited number of variables.

Lee and Kim (1999) investigated the role of an expansion tank fitted to a two-phase natural circulation loop. It was concluded that the length and cross-sectional area of the expansion line as well as the system pressure has a significant effect on the magnitude of the pressure drop fluctuations in the two-phase system.

2.4.3 Two-phase flow

It was envisioned that the loop thermosyphon would operate not only in single phase but also in two-phase mode. The reason for this being that boiling and condensation is characterized by enhanced heat transfer coefficients that allows for rapid heat dissipation with low temperature differences which is a very attractive quality for an RCCS.

As an introduction to the current project, visualization experiments were performed on a glass loop thermosyphon that was designed and built by Le Grange (1996). This thermosyphon allows the user to visually experience the different flow patterns found in gas liquid flows with heat transfer.

The characteristics of these flow patterns are determined by surface tension, the surface wetting characteristics and gravity. Consulting different textbooks produces various names for the different flow patterns depending on the flow direction. For instance in the case of vertical flow it depends on whether the flow is co-current or counter current, up flow or down flow. Then there is also horizontal flow that has the added complication of gravity working in a different plane than that of the flow. The most common flow patterns for adiabatic co-current up flow in vertical circular tubes and horizontal circular tubes are given by Whalley (1987).

Adding heat to the boiler tube causes changes in the flow patterns. Initially the tube and fluid may be at temperatures below the saturation point. Adding heat to the tube raises the tube and fluid temperatures, at this time heat transfer to the fluid is accomplished through convection. Once the tube wall reaches a temperature slightly above the saturation temperature of the fluid, nucleation sites are activated and boiling can commence. It is found that boiling already occurs before thermodynamic quality

reaches zero, this is called sub-cooled nucleate boiling. The vapour bubbles condense shortly after formation, releasing latent heat that raises the bulk fluid temperature. Once the fluid reaches the saturation temperature the thermodynamic quality value exceeds zero and sub-cooled nucleate boiling transitions to saturated nucleate boiling. It is interesting to note that even though saturated nucleate boiling has been initiated there can still exist a sub-cooled liquid core due to the radial temperature profile.

Each of the flow regimes can be identified with one or more types of boiling. Bubbly flow is associated with both sub-cooled and saturated nucleate boiling. Plug flow falls completely within the saturated nucleate boiling region. As churn and annular flow regimes take over with a corresponding liquid film, nucleation is suppressed and vapour generation is due to evaporation from the liquid vapour interface. In other words heat is transferred by convection through the liquid film. With continued addition of heat the liquid film will eventually disappear due to entrainment and vaporisation leaving a vapour flow with entrained droplets, this is aptly called the “drop flow” regime.

The phenomenon of dry-out can have a serious effect on the integrity of the loop material. This is due to the fact that once dry-out occurs the heat transfer rate is reduced and the tube wall temperature increases markedly. Koizumi and Ueda (1994) studied dry-out using an experimental setup with R113 as the working fluid. It was found that under natural circulation dry-out is primarily a function of the flow rate and only weakly influenced by the surface texture of the loop. It was also found that for high vapour generation situations local dry-out patches occur in the thin liquid film associated with the annular flow regime.

2.4.4 Instabilities

During the literature review process it has become clear that under certain initial and boundary conditions a number of undesirable flow characteristics are exhibited. Flow oscillations can cause mechanical vibration that can potentially damage the system, as well as affect the heat transfer characteristics, possibly causing the critical heat flux to be induced prematurely.

In general two-phase flow instabilities can be divided into two categories namely static and dynamic instability. A flow exhibits static instability when during steady state operation the flow is subjected to a disturbance and instead of returning to the previous undisturbed state the system shifts to a different steady state operating point or exhibits periodic oscillating flow behaviour. Dynamic instability is caused by thermal and hydrodynamic inertia in the system leading to flow oscillation.

Bouré et al. (1973) gives a detailed description of experimentally observed flow instabilities. The instabilities of interest are:

Static instabilities

Ledinegg instability

This type of instability occurs when the following criterion is met: $\left(\frac{\delta \Delta P}{\delta G}\right)_{\text{int}} < \left(\frac{\delta \Delta P}{\delta G}\right)_{ext}$. This criterion can be met in two-phase flow when the sum of the friction, momentum and gravity terms of the pressure drop decreases with increased mass flow rate.

Relaxation instability

Instability is experienced as periodic transition between flow regimes, normally between bubbly flow and annular flow. The oscillations is characterised by alternative accelerating and deceleration behaviour.

Bumping, geysering, chugging

Bumping occurs at irregular intervals for low heat fluxes. The instability occurs when the wall temperature shifts back and forth between the values required for nucleate boiling and natural convection. Geysering occurs when a sufficient amount of superheat is introduced to the base of a non-boiling system, this allows for increased vapour generation that leads to the forcible expulsion of the vapour. As sub-cooled liquid returns the non-boiling conditions is restored. Chugging is the cyclic expulsion of coolant from a flow channel which can range from a slight variation of flow rate to a violent outburst. The cycle takes much the same form as geysering.

Dynamic instabilities

Acoustic (or pressure wave) instability

Acoustic waves propagate at a frequency of 10-100 hz through a system that is experiencing sub-cooled nucleate boiling, saturated nucleate boiling or film boiling. The wave period is in the same order as that of a pressure wave travelling through the system at the speed of sound. In general acoustic waves have little influence on the flow, it has however been observed that acoustic pressure fluctuations can be large compared to steady state values.

Density wave instability

Density wave oscillation is the most common type of dynamic instability and has been extensively studied. Density wave oscillation is a low frequency oscillation with a period approximately that of a particle travelling through the system. In a boiling system these oscillations result from multiple regenerative feedbacks between the flow rate, vapour generation rate and pressure drop.

Fukuda and Kobori (1979) observe two types of density wave instability during experimentation. Type I instability occur in the low power region with nearly zero steam quality while type II instability occur in the high power region with high steam quality. Through dynamic analysis, transfer functions are derived that show the dominant pressure drop term associated with each type of instability. It was found that the dominant term for type I instability is the gravitational pressure drop while for type II instability it is the two-phase frictional pressure drop.

Two-phase flow instability is a major concern during the start-up phase of a natural circulation nuclear system. Jiang et al. (1995) investigated the thermo-hydraulic behaviour of a natural circulation system using a test loop with a riser of 3 m to simulate the geometry and system design of the primary loop of a 5 MW nuclear reactor. Three types of instability, namely geysering, flashing and low steam quality density wave oscillations were identified for attention during the start-up process from atmospheric to operating conditions. A method was devised to reach operating conditions whilst bypassing all instability. This method required control of the system pressure, through the use of a non-condensable gas, and the heat flux.

Various factors have an influence on the stable behaviour of natural circulation systems. Wu et al. (1996) studied chaotic oscillations in a low temperature two-phase natural circulation loop and found that power input and inlet sub-cooling has a large effect on the oscillating behaviour of the loop. Wang and Pan (1998) using Taguchi methods share Wu's conclusions, but add that, flow restrictions and compressible volumes in the system are also factors influencing stability.

2.4.5 Control

Control of the loop is a central issue due to the need to avoid potential unstable situations, especially during start-up. One of the objectives of a passive design is for the loop thermosyphon to be self-controlling i.e. there should be no electronics involved. In order to do this it has been proposed to add minor quantities of non-condensable gasses to the loop. These gasses, for instance nitrogen or air, have a noticeable influence on the condensation heat transfer present. This type of phenomenon has been investigated by Anderson et al. (1997) who choose to use a heat/mass transfer analogy to successfully model the heat transfer. Liu et al. (2000) investigated the condensation characteristics of steam when air or air/helium mixture was added. The lack of an appropriate correlation prompted the creation of an empirical heat transfer coefficient correlation using experimental data.

Ohashi et al. (1998) undertook a preliminary study of the use of a two-phase natural circulation loop concept to remove decay heat from a high temperature reactor (HTR). The loop was evacuated and charged with water as working fluid, temperatures at different levels in the condenser could be measured (the loop dimensions were not given). The loop was heated using an electrical heating element wrapped round the outside of the evaporator and the condenser portion of the loop was cooled with water using a forced-flow tube-in-tube heat exchanger. It was shown that the temperature of the working fluid increased in step with the increase in heat input. For a given input it was found that the temperature along the length of the tube varies very little, approximately 2-3 °C. Introducing nitrogen gas into the system however gives a large variation of approximately 60 °C. Ohashi et al. (1998) call this a variable conductance

heat pipe. Through the proper selection of non-condensable gas initial amount and pressure it is possible to have passive temperature control.

2.5 Mathematical Modelling

2.5.1 General

The prediction of fluid flow and heat transfer in the two-phase loop thermosyphon is a complicated matter due to the imperfect knowledge of the processes involved. It is known that certain factors for example heat flux, pressure, void fraction, mass flow rate, fluid properties, etc have a marked influence on these processes.

This dependence can be illustrated by considering boiling. The heat transfer coefficient in flow boiling is dependant on the interaction between the nucleate and convective boiling which is in turn dependant on the vapour fraction. For heat fluxes below that necessary to achieve nucleate boiling only convective boiling is present and the heat transfer coefficient is independent of the heat flux over a wide range of mass velocities and vapour fractions. With increased heat flux the nucleate heat transfer coefficient is increased, which in turn increases nucleation. In the fully developed nucleate boiling region the boiling coefficient is independent of the velocity and vapour fraction. The convective heat transfer coefficient increases with increased mass flow rate; which corresponds to lower wall temperatures and reduced nucleation and thus reduced nucleate boiling.

In an attempt to create a numerical model of loop thermosyphons Lee and Rhi (2000) describes two different simulation methods, namely lumped and sectorial, that can be used in computer simulations. The lumped method considers the two phase region as a single entity allowing for the use of a single correlation to describe the forced convective boiling taking place. The sectorial method on the other hand divides the two-phase region into smaller regions characterized by definite flow patterns. This requires more than one correlation related to each flow pattern. An added complication is introduced in the form of the transition regions between the flow patterns.

Comparing the two methods it is found that the lumped method is by far the easier to program but it cannot possibly analyze the flow in as much detail as the sectorial method.

Lee and Rhi (2000) then compare the numerical results with data for experimental loops of various sizes to gauge the efficacy of their numerical model. This comparison shows that possibly the biggest influence on the eventual solution lies in the choice of boiling and condensing correlations used. Each different combination gives a different answer and none of these solutions compare well to the experimental results obtained. Lee and Rhi (2000) proceed to find the best suited combination of correlations to each situation and apply a modification to these correlations. The end result compares very well to the experimental data. An important conclusion is reached: Computer simulation without experimental validation cannot deliver meaningful quantitative results!

2.5.2 Heat transfer correlations

Chen was the first to formulate a popular flow boiling method. Chen's correlation uses a simple additive method with a nucleate suppression factor to describe the interaction of nucleate and convective boiling. Kutateladze improved upon this thought by proposing a power addition equation. This had the effect that the boiling heat transfer coefficient approached the larger of the two boiling terms.

A different approach to the above mentioned methods was proposed by Shah. This method uses a boiling number to describe the nucleate heat transfer and a convection number to describe the convective heat transfer. This method had its draw backs in terms of range and accuracy.

Other more involved correlations have been created that are variants of the above methods. These are the methods of Kandlikar, Liu and Winterton (1991) and Klimenko (1988, 1990) to name but a few. Steiner and Taborek (1992) followed a somewhat different path from these researchers and developed an asymptotic model using 13 000 database points collected from various research works for vertical flow of water in tubes.

2.5.3 Hydrodynamic considerations

In order to do a meaningful numeric study not only heat transfer correlations are required but also hydrodynamic correlations. Vijayan et al. (2000) did an extensive review of published pressure drop and void fraction correlations. These correlations were then compared to the in-house data bank of experimental data and found the method of Chexal et al. (1996) to give the best void fraction comparison. This correlation is then used to calculate a void fraction that is used in the pressure drop correlations. It was found that the Lockhart-Martinelli pressure drop correlation (as can be found in the textbook of Carey, 1992) performed the best.

A generalized frictional pressure loss coefficient correlation based on non-dimensional numbers as proposed by Vijayan et al. (1991) was formulated in the attempt to compare the friction and heat transfer coefficients of natural and forced flow closed loops. It was found that the pressure loss coefficient in natural flows exceed that of forced flow due to buoyancy induced secondary flow. It would therefore be unwise to resort to the use of forced-flow correlations.

3 MATHEMATICAL MODELLING

3.1 Simplifying Assumptions

The three most important assumptions made to produce the computational code are that the flow is quasi-static, incompressible for both the liquid and vapour phase, and one-dimensional.

The quasi-static assumption for the solution of the momentum equation is reasonable due to the fact that the average velocity of the working fluid in the loop is two to three orders of magnitude less than the speed of sound in the fluid. This means that the rate at which pressure waves are propagated through the working fluid are much faster than the rate at which mass and heat moves in the loop. In other words the pressure change is assumed to occur instantaneously throughout, bringing the system to a new state at each time step. The heat and mass flow can then be determined by regarding the flow as steady for that time step. Given small enough time steps, this succession of steady flow solutions numerically approximate the transient flow being simulated.

The assumption of incompressibility of the liquid and gas phase can be made since the pressure varies little throughout the loop and stays in the vicinity of one atmosphere. This assumption does introduce some error for the vapour flow since the density does change due to the temperature rise. This inaccuracy is offset by the simplicity the assumption offers to the solution procedure. It however excludes the possibility of pressure (acoustic) waves. The boiling heat transfer coefficient depends, inter alia, on the size of the vapour bubbles. The effect of pressure on bubble size can thus not be taken into account.

The buoyancy force that *drives* the flow varies according to temperature, constant density can therefore not be applied in the buoyancy term of the momentum equation. This problem can be overcome by adopting the Boussinesq approximation whereby the density is assumed constant except in the buoyancy term and where the density is assumed to be a function of temperature only.

It was decided to create a one dimensional model of the system. The system was divided into discrete control volumes as shown by figure 5 and the conservation equations formulated for each control volume as shown in section 3.2. In figure 5 heat from the reactor pressure vessel is transferred by radiation and convection through the air gap to the fin, by conduction from the fin to the pipe. Finally the heat is transferred from the looped pipe to a large water tank.

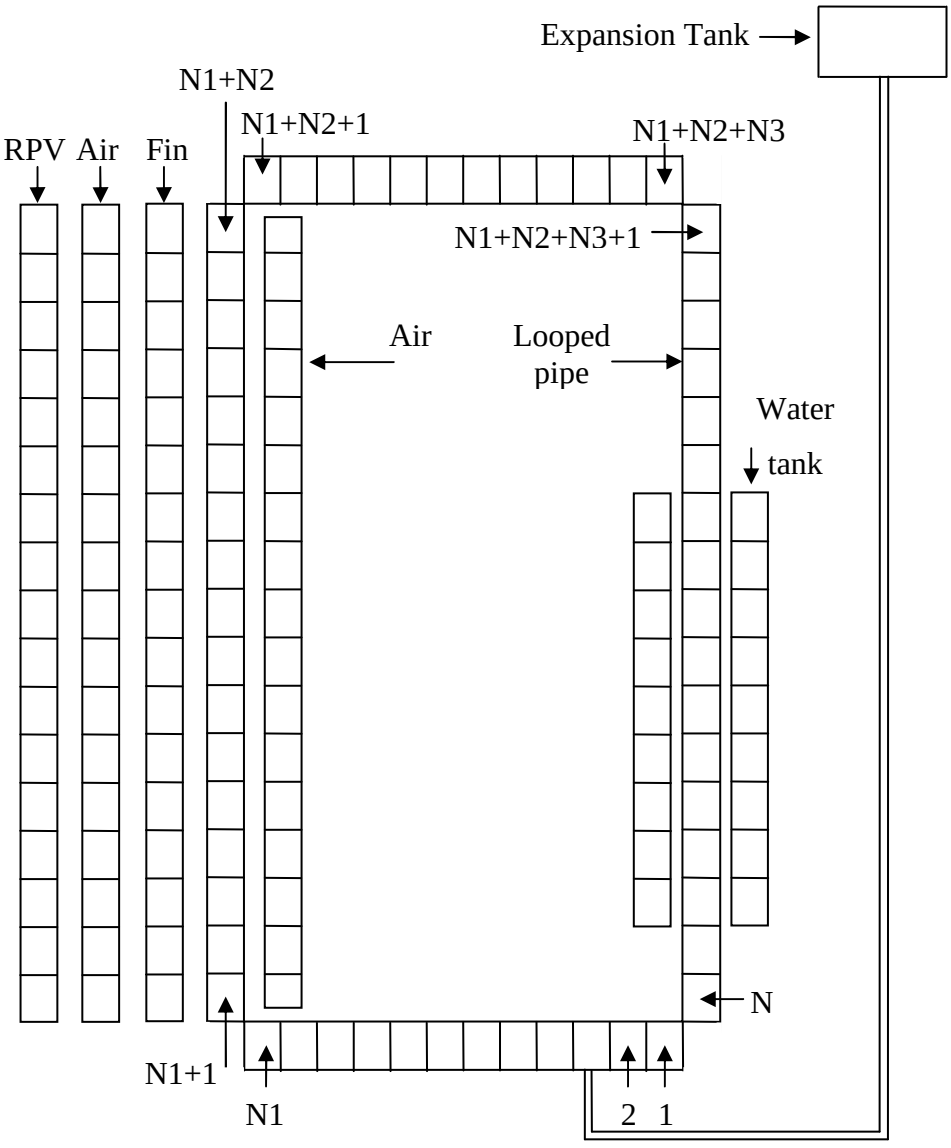

Figure 5: The discretized system

3.2 Formulation of the Differential Equations

The laws of mechanics are written for a system of arbitrary mass that experience interactions with its surroundings. These equations are:

Conservation of mass: $$\frac{dm}{dt} = 0 \qquad \textbf{(3.1)}$$

Newton's second law: $$\boldsymbol{F} = m\boldsymbol{a} = \frac{d}{dt}(m\boldsymbol{v}) \qquad \textbf{(3.2)}$$

The first law of thermodynamics: $$\frac{dQ}{dt} - \frac{dW}{dt} = \frac{dE}{dt} \qquad \textbf{(3.3)}$$

In order to proceed with a control volume based flow analysis it is necessary to reformulate these equations to apply to a specific region rather than an individual mass. This conversion is called the Reynolds transport theorem as given by White (1999). For a one-dimensional fixed control volume the general form of the Reynolds transport theorem becomes:

$$\frac{d}{dt}(B_{sys}) = \frac{d}{dt}\left(\int_{cv} \beta\rho dV\right) + (\beta\rho Av)_{out} - (\beta\rho Av)_{in} \qquad \textbf{(3.4)}$$

Where B represents mass, momentum or energy and β represent the intensive value of B i.e. $\beta = \frac{dB}{dm}$

The momentum equation follows from equations 3.2 and 3.4:

$$B = mv \quad \text{and} \quad \beta = \frac{d(m\boldsymbol{v})}{dm} = \boldsymbol{v} \quad \text{thus} \quad \beta\rho Av = \boldsymbol{v}\rho Av = \dot{m}\boldsymbol{v}$$

Through substitution equation 3.4 becomes:

$$\frac{d}{dt}(m\boldsymbol{v})_{sys} = \frac{d}{dt}\left(\int_{cv} \boldsymbol{v}\rho dV\right) + (\dot{m}\boldsymbol{v})_{out} - (\dot{m}\boldsymbol{v})_{in} \qquad \textbf{(3.5)}$$

Substituting equation 3.5 into equation 3.2 gives:

$$\sum \boldsymbol{F} = \frac{d}{dt}\left(\int_{cv} \boldsymbol{v}\rho dV\right) + (\dot{m}\boldsymbol{v})_{out} - (\dot{m}\boldsymbol{v})_{in} \qquad \textbf{(3.6)}$$

The energy equation follows from equations 3.3 and 3.4:

$$B = E \quad \text{and} \quad \beta = \frac{d(E)}{dm} = e$$

Through substitution equation 3.4 becomes:

$$\frac{dE_{sys}}{dt} = \frac{d}{dt}\left(\int_{cv} e\rho dV\right) + (e\rho Av)_{out} - (e\rho Av)_{in} \qquad \textbf{(3.7)}$$

Substituting equation 3.7 into 3.3 gives:

$$\frac{dQ}{dt} - \frac{dW}{dt} = \frac{d}{dt}\left(\int_{cv} e\rho dV\right) + (e\rho Av)_{out} - (e\rho Av)_{in} \qquad \textbf{(3.8)}$$

Where $e = u + 0.5v^2 + gz$

Sections 3.2.1 to 3.2.5 shows the differential equations applied to each of the control volumes as well as the equivalent difference equation used in the computer model expressed explicitly. See appendix B for the detailed derivation of the explicit difference equations for the various differential equations describing the flow and heat transfer in the loop.

3.2.1 Reactor pressure vessel

In the case were the core heat flux is known the reactor pressure vessel temperature can be calculated as shown below. In order for the program to simulate the experiment however the reactor pressure vessel temperature is an input value found from the log files created with each experiment.

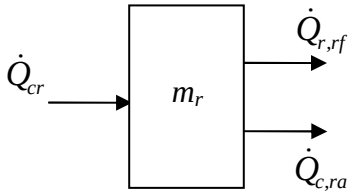

Figure 6: Reactor pressure vessel control volume

Rewriting equation 3.3 with the work term equal to zero, the heat transfer term consisting of the elements shown in figure 6 and the energy term equal to the internal energy gives the following differential and difference equations:

$$\dot{Q}_{cr} - \dot{Q}_{r,rf} - \dot{Q}_{c,ra} = \frac{dU_r}{dt} \qquad \textbf{(3.9)}$$

$$T_r^{t+\Delta t} = T_r^t + \frac{\Delta t}{m_r c_r}\left(\frac{T_c^t - T_r^t}{R_{cr}} - \frac{T_r^t - T_f^t}{R_{r,rf}} - \frac{T_r^t - T_a^t}{R_{c,ra}}\right) \qquad \textbf{(3.10)}$$

3.2.2 Air

Figure 7 represents an air element situated between the heating plate and the fin.

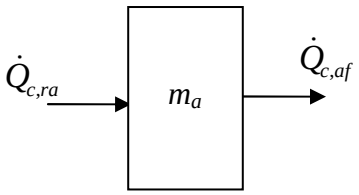

Figure 7: Air control volume

Rewriting equation 3.8, with the heat transfer term consisting of the elements shown in figure 7 the following differential and difference equations can be derived:

$$\dot{Q}_{c,ra} - \dot{Q}_{c,af} = \frac{dU_a}{dt} \qquad \textbf{(3.11)}$$

$$T_a^{t+\Delta t} = T_a^t + \frac{\Delta t}{m_a c_a}\left(\frac{T_r^t - T_a^t}{R_{c,ra}} - \frac{T_a^t - T_f^t}{R_{c,af}}\right) \qquad \textbf{(3.12)}$$

Figure 8 shows an air element situated between the fin and the back wall of the heating chamber, which is assumed to be perfectly insulated. The heat transfer rate calculated in this way gives an indication of the heat losses from the back of the fin.

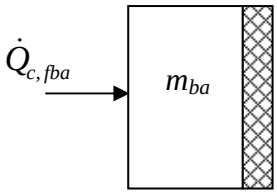

Figure 8: Air control volume at back of fin

Rewriting equation 3.8, with the heat transfer term consisting of the elements shown in figure 8 the following differential and difference equations can be derived:

$$\dot{Q}_{c,fba} = \frac{dU_{ba}}{dt} \tag{3.13}$$

$$T_{ba}^{t+\Delta t} = T_{ba}^{t} + \frac{\Delta t}{m_{ba} c_{ba}} \left(\frac{T_f^t - T_{ba}^t}{R_{c,fba}} \right) \tag{3.14}$$

3.2.3 Fins

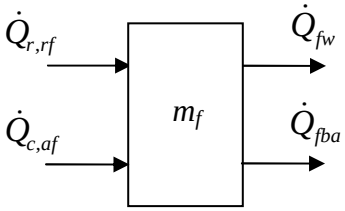

Figure 9: Fin control volume

Rewriting equation 3.3 with the work term equal to zero, the heat transfer term consisting of the elements shown in figure 9 and the energy term equal to the internal energy gives the following differential and difference equations:

$$\dot{Q}_{r,rf} + \dot{Q}_{c,af} - \dot{Q}_{fw} - \dot{Q}_{c,fba} = \frac{dU_f}{dt} \tag{3.15}$$

$$T_f^{t+\Delta t} = T_f^t + \frac{\Delta t}{m_f c_f} \left(\frac{T_r^t - T_f^t}{(R_{r,rf}^{-1} + R_{c,af}^{-1})^{-1}} - \frac{T_f^t - T_w^t}{R_{fw}} - \frac{T_f^t - T_{ba}^t}{R_{c,fba}} \right) \tag{3.16}$$

3.2.4 Working fluid

Figure 10 shows the energy flow across the boundaries of a fluid control volume in the loop and equations 3.17 and 3.18 are the corresponding differential and difference energy equations.

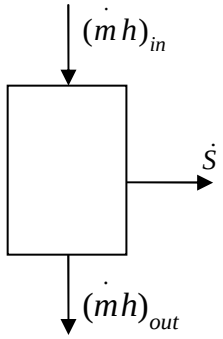

Figure 10: Loop fluid control volume

$$-\dot{S} = \frac{d}{dt}(um) + (\dot{m}h)_{out} - (\dot{m}h)_{in} \qquad \textbf{(3.17)}$$

$$u^{t+\Delta t} = \frac{U^t}{m^{t+\Delta t}} + \frac{\Delta t}{m^{t+\Delta t}}\left((\dot{m}h)_{in} - \dot{S} - (\dot{m}h)_{out}\right) \qquad \textbf{(3.18)}$$

The derivation of the differential and difference energy equations from equation 3.8 can be seen in appendix B. In reference to the differential equations note the following: The heat transfer term is represented by $\dot{S}$ which can be either heat added or removed from the system as dictated by the position of the control volume in the loop, axial conduction is however not taken into account. In the heat transfer sections of the loop not in thermal contact with the heat source or cooling water tank the $\dot{S}$ term represents the losses due to convection to the atmosphere.

The work term consist of machine work, pressure work and shear work due to viscous stresses. Since this is a passive system there is no machine work and the shear work is negligible due to the choice of the control volume boundaries. Each of the control volumes has two wall boundaries, one inlet and one outlet boundary. At the walls the velocity is zero hence shear work is zero. At the inlet and outlet boundaries the flow is

normal to the control volume cross section. The only viscous work terms come from the normal shear stress that is so small that it can safely be neglected. The pressure work term is lumped with the internal energy to form the fluid property enthalpy. The rest of the energy term is neglected since the contribution of viscous dissipation, kinetic and potential energy will be negligible compared to the internal energy term.

The knowledge of the internal energy of the control volume allows for the calculation of the control volume temperature and thermodynamic quality.

If $u^{t+1} < u_f$ then

$$T_w^{t+1} = \frac{u^{t+1}}{c} \qquad \text{and} \qquad x^{t+1} = 0 \tag{3.19}$$

If $u^{t+1} > u_f$ then

$$T_w^{t+1} = T_{sat} \qquad \text{and} \qquad x^{t+1} = \frac{u^{t+1} - u_f^{t+1}}{u_{fg}^{t+1}} \tag{3.20}$$

Using the momentum equation, equation 3.21 can be derived and used to calculate a new mass flow rate. Figure 11 shows the forces experienced by the fluid in the loop for a typical control volume.

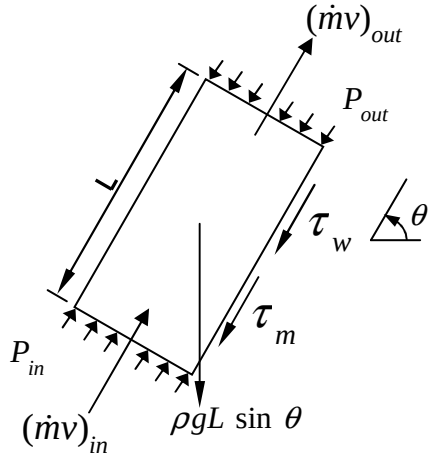

Figure 11: Conservation of momentum for a typical control volume

$$\dot{m}^{t+1} = \dot{m}^t + \Delta t \left(- \frac{\sum_{k=1}^{N} \rho_k g L_k \sin\theta_k}{\sum_{k=1}^{N} \frac{L_k}{A_{x,k}}} - \frac{\sum_{k=1}^{N} \frac{1}{2} \frac{(C_f + K)}{\rho_k} \frac{A_{z,k}}{A_{x,k}^3} (\dot{m}^t)^2}{\sum_{k=1}^{N} \frac{L_k}{A_{x,k}}} \right) \tag{3.21}$$

3.2.5 Water tank

It was deemed worthwhile to simplify the analysis of the water tank due to the complexities involved in the evaporative heat transfer that takes place from the tank surface as well as the natural convection and stratification that takes place in the water tank. Assuming a well insulated tank, the heat transfer across the tank control volume (not for the surface control volume) boundaries is shown in figure 12. Equation 3.22 and 3.23 are derived in appendix B.

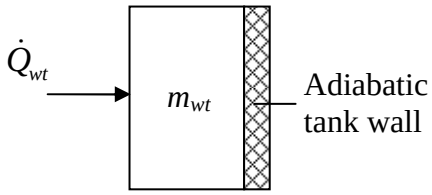

Figure 12: Water tank control volume

$$\dot{Q}_{c,wt} = \frac{d(u_{wt} m_{wt})}{dt} \qquad \textbf{(3.22)}$$

$$T_{wt}^{t+\Delta t} = T_{wt}^{t} + \frac{\Delta t}{m_{wt} c_{wt}} \left(\frac{T_{w}^{t} - T_{wt}^{t}}{R_{wt}} \right) \qquad \textbf{(3.23)}$$

Heat and mass transfer to the atmosphere can be taken into account by a surface control volume with two added heat transfer components, evaporative heat transfer and convection to the atmosphere as shown in figure 13. The complexity lies in determining the amount of evaporation taking place. The mass transfer convection coefficient, h_m, has to be determined experimentally or a heat and mass transfer analogy must be applied to determine h_m from the convection heat transfer coefficient h, which is determined in turn from empirical correlations.

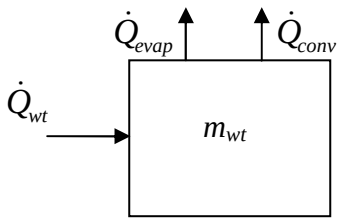

Figure 13: Water tank surface control volume

$$\dot{Q}_{c,wt} - \dot{Q}_{evap} + \dot{Q}_{conv} = \frac{d(u_{wt} m_{wt})}{dt} \quad \textbf{(3.24)}$$

$$T_{wt}^{t+\Delta t} = T_{wt}^{t} + \frac{\Delta t}{m_{wt} c_{wt}} \left(\frac{T_w^t - T_{wt}^t}{R_{c,wt}} - \dot{m}_{evap} h_{fg} + \frac{T_{wt}^t - T_{air}^t}{R_{c,wta}} \right) \quad \textbf{(3.25)}$$

Noting that $\dot{m}_{evap} = h_m A_s (\rho_{wt,s} - \rho_{wt,\infty})$ (Incropera & De Witt, 2002) where $\rho_{wt,s}$ is the vapour density at the surface of the water tank and $\rho_{wt,\infty}$ is the density of the vapour in the air so that the equation becomes:

$$T_{wt}^{t+\Delta t} = T_{wt}^{t} + \frac{\Delta t}{m_{wt} c_{wt}} \left(\frac{T_w^t - T_{wt}^t}{R_{c,wt}} - h_m A_s (\rho_{A,s} - \rho_{A,\infty}) h_{fg} + \frac{T_{wt}^t - T_{air}^t}{R_{c,wta}} \right) \quad \textbf{(3.26)}$$

3.3 Numerical Considerations

Section 3.2 shows the derivation of the conservation equations for the control volumes. In order to complete the mathematical model closure equations are required for C_f, h, α and ϕ^2. Unless otherwise stated the correlations presented are for forced flow due to the lack of availability of the relevant natural flow correlations. It is therefore assumed that some error will be introduced in the model. As shown by Vijayan et al. (1991) this can cause either the under- or over prediction of the coefficients due to the fact that the flow may not always be fully developed and the effects of secondary flows present in natural circulation are not accounted for.

3.3.1 Friction factor

Correlations for the laminar and turbulent Fanning friction factor were found in Incropera and De Witt (2002). Assuming fully developed flow an approximation for the smooth surface condition for laminar flow is given by:

$$C_f = \frac{16}{Re_D} \tag{3.27}$$

and turbulent flow by:

$$C_f = 0.079 Re_D^{-0.25} \qquad Re_D \le 2*10^4 \tag{3.28}$$

$$C_f = 0.046 Re_D^{-0.2} \qquad Re_D \ge 2*10^4 \tag{3.29}$$

The transition point between laminar and turbulent flow was taken at a Reynolds number of 1181 as suggested by Dobson (2005). This point was found by extrapolating the smooth pipe curve until it met the laminar flow curve on the Moody chart.

3.3.2 Heat transfer correlations

Several heat transfer correlations are required for the model. These heat transfer coefficient correlations are divided into single phase and two phase correlations. Unless otherwise stated the heat transfer coefficient is determined from the Nu number as follows:

$$h = \frac{Nu_D * k}{D} \tag{3.30}$$

For the single phase, laminar flow heat transfer coefficient, the correlation of Collier (1994) is:

$$Nu_D = 0.17 Re_D^{0.33} Pr^{0.43} \left(\frac{Pr}{Pr_w} \right)^{0.25} Gr^{0.1} \quad Re_D \le 2000 \tag{3.31}$$

For the single phase, turbulent flow heat transfer coefficient, the correlation of Gnielinski as given by Mills(1999) is:

$$Nu_D = \frac{(f/8)(Re_D - 1000)\,\mathrm{Pr}}{1 + 12.7(f/8)^{0.5}(\mathrm{Pr}^{2/3} - 1)} \qquad 3000 \le Re_D \le 10^6 \tag{3.32}$$

Gnielinski's correlation was developed for forced flow conditions. In order to take into account the secondary flow effects present in natural circulation a Rayleigh number correction factor as proposed by Yang et al. (2006) was introduced so that:

$$Nu_D = Nu_D Ra^{-0.011} \quad \textbf{(3.33)}$$

For convenience sake, the boiling and condensation heat transfer coefficient correlations are given in full in appendix C but only the final equations and a short description of the terms are given in the present text.

In flow boiling there are two types of boiling, nucleate boiling and convective boiling. Although these two types are usually treated separately they can coexist and as the quality increases the contribution of the nucleate boiling decreases until eventually convective boiling is the dominant form of boiling. It is therefore required to find a correlation that incorporates both. The first correlation of this kind was developed by Chen mainly for flow boiling of water. This correlation was incorporated into the model using the equations given by Whalley (1987):

$$h = h_{NB} + h_{FC} = Sh_{FZ} + Fh_l \quad \textbf{(3.34)}$$

The nucleate boiling term consist of the suppression factor *S* that decreases from 1 to 0 as the quality increases to account for the suppression of nucleate boiling as convective boiling becomes stronger. The nucleate pool boiling heat transfer coefficient is calculated from the Forster-Zuber equation (Carey, 1992), which predicts water fairly well. The forced convection term consist of a two phase heat transfer coefficient multiplier *F* that is always greater than 1 and a single phase liquid convective heat transfer coefficient based on the liquid mass flow rate.

This correlation tends to over-predict the heat transfer coefficient in the high quality region and under-predicts it in the low quality region. An improvement proposed by Kutateladze (1961) was the addition of the square of the two boiling heat transfer coefficients thus further suppressing the nucleate boiling term as convective boiling become the dominating heat transfer mechanism:

$$h^2 = (Sh_{pool})^2 + (Fh_l)^2 \quad \textbf{(3.35)}$$

Lui and Winterton (1991) used equation 3.35 as the departure point and made the assumption that S was a function of F and Re_l. Using this assumption, Kutateladze's equation with h_{pool} calculated using the Cooper pool boiling correlation, (Cooper, 1984) and experimental data, expressions for S and F were determined. Manipulating the equations as shown in appendix C gives the following equation:

$$h = Fh_l q_*^{3/2} \quad \textbf{(3.36)}$$

Where F is the two phase heat transfer coefficient multiplier, that is always greater than 1, h_l is the single phase liquid convective heat transfer coefficient based on the liquid mass flow rate and q_* is function of F, S, q, p_r and ΔT_s.

Steiner and Taborek (1992) also followed the power type addition route for the combination of the heat transfer coefficients. The reason given was that it was a simple model where the components were independent of each other with the interaction governed by equation 3.37 alone.

$$h = \left[(F_{nbf} h_{nb,o})^n + (F_{tp} h_l)^n\right]^{1/n} \quad \textbf{(3.37)}$$

In this equation F_{nbf} is a correction factor that compensates for the differences in pool and flow boiling and $h_{nb,o}$ is the nucleate pool boiling coefficient based on normalised conditions. F_{tp} is the two-phase multiplier and h_l is the liquid only heat transfer coefficient calculated from equation 3.32. The value of the exponent n determines the transition between the two types of boiling. Regression analysis of their 13 000 data points showed that the best value for n was 3.

For internal flow condensation various correlations have been developed from the assumption that the flow regime is annular. This may lead to some inaccuracy at the point where the condensation process ends, where other flow regimes take over. The correlations used were that of Soliman et al. (1968), Traviss et al. (1973), Shah (1989) and Chen et al. (1987).

Soliman et al. (1968) acknowledged the importance of the shear stresses in the heat transfer across the liquid film in annular flow, writing the correlation in the form:

$$h = 0.036 \frac{k_l \rho_l^{0.5}}{\mu_l} \mathrm{Pr}_l^{0.65} \tau_w^{0.5} \quad \textbf{(3.38)}$$

Where the τ_w term consist of the shear terms due to friction, gravity and momentum change in the fluid.

Traviss et al. (1973) proposed the following correlation:

$$Nu = \frac{0.15 Pr_l Re_l^{0.9}}{F_T} \left[\frac{1}{X_{tt}} + \frac{2.85}{X_{tt}^{0.476}} \right] \quad \textbf{(3.39)}$$

Where X_{tt} is the turbulent-turbulent Martinelli parameter and F_T is a function of Pr_l and Re_l number.

A correlation based on empirical data for convective condensation in round tubes proposed by Shah (1989) is given by:

$$\frac{h}{h_{lo}} = (1-x)^{0.8} + \frac{3.8 x^{0.76} (1-x)^{0.04}}{P_r^{0.38}} \quad \textbf{(3.40)}$$

The three correlations presented above are primarily for horizontal flow as this is most often encountered in industrial heat exchangers. Chen et al. (1987) developed a correlation for annular flow condensation in vertical tubes based on analytical and theoretical results from the literature. This correlation takes the form:

$$Nu_x = \left[\left(0.31 Re_x^{-1.32} + \frac{Re_x^{2.4} Pr_l^{3.9}}{2.37 \times 10^{14}} \right)^{1/3} + \frac{A_D Pr_l^{1.3}}{771.6} (Re_{ter} - Re_x)^{1.4} Re_x^{0.4} \right]^{1/2} \quad \textbf{(3.41)}$$

Here Nu_x is defined as: $Nu_x = \frac{hv_l^{2/3}}{k_l g^{1/3}}$ where v is the kinematic viscosity, k the thermal conductivity, g the gravitational acceleration and h the two phase heat transfer coefficient.

3.3.3 Void fraction and the two phase multiplier

Two two-phase flow models were investigated. The general separated flow model, where the liquid and vapour flows at different velocities, as well as the homogenous flow model were the phases are assumed to be well mixed and travelling at the same velocity.

The void fraction is defined as the fraction of the cross-sectional area which is occupied by the gas phase. The general equation is:

$$\alpha = \frac{1}{1+\left(\frac{u_g}{u_l}\frac{1-x}{x}\frac{\rho_g}{\rho_l}\right)} \qquad \textbf{(3.42)}$$

The ratio of the phase velocities is called the slip ratio: $S = \frac{u_g}{u_l}$. For homogeneous flow the slip ratio value is one while for the separated flow model it is greater than one so that the vapour velocity is always greater than the liquid velocity. Many of the void fraction correlations derived using experimental data are really correlations for the slip ratio. A correlation like this is the Chisholm correlation giving

$$S = \left[1 - x\left(1 - \frac{\rho_g}{\rho_l}\right)\right]^{0.5} \qquad \textbf{(3.43)}$$

and the CISE correlation which is somewhat more involved (see appendix C), both given by Whalley (1987). Butterworth (1975) showed that many correlations take the general form of equation 3.44:

$$\alpha = \frac{1}{1 + B\left(\frac{1-x}{x}\right)^{n1}\left(\frac{\rho_g}{\rho_l}\right)^{n2}\left(\frac{\mu_l}{\mu_g}\right)^{n3}} \quad \textbf{(3.44)}$$

One such is the Lockhart-Martinelli correlation were B = 0.28, n_1 = 0.64, n_2 = 0.36 and n_3 = 0.07 as given in Carey (1992). Whalley (1987) suggested that the CISE correlation may be the most accurate correlation available.

In two-phase flow the frictional pressure drop is calculated using the single phase pressure drop, which is more easily determined, and a two-phase multiplier. The two-phase, liquid only multiplier is defined as $\phi_{lo}^2 = \frac{(-dP/dz)_F}{(-dP/dz)_{lo}}$, that is to say, it is the ratio of the two phase frictional pressure drop and the single phase pressure drop due to the liquid flowing alone in the tube at the same total mass flow rate as the two-phase fluid. Similar definitions exist for liquid flow, gas flow and gas only flow.

For the homogeneous model it can be shown that the two phase multiplier is given by:

$$\phi_{lo}^2 = \frac{C_{fh}\rho_l}{C_{flo}\rho_h} \quad \textbf{(3.45)}$$

Where C_{fh} is the friction factor calculated using homogenous properties.

For the separated flow model the two-phase multiplier is correlated from experimental data. The model employed the Lockhart-Martinelli correlation as given by Carey (1992). Assuming turbulent-turbulent flow the equation is given as:

$$\phi_l^2 = \left(1 + \frac{20}{X} + \frac{1}{X^2}\right)^{1/2} \quad \textbf{(3.46)}$$

Where X is the Martinelli parameter defined as: $X = \left[\frac{(-dP/dz)_l}{(-dP/dz)_v}\right]^{1/2}$ and given by:

$$X_{tt} = \left(\frac{1-x}{x}\right)^{0.9}\left(\frac{\rho_v}{\rho_l}\right)^{0.5}\left(\frac{\mu_l}{\mu_v}\right)^{0.1} \quad \textbf{(3.47)}$$

This is a fairly simple correlation that does not take the effect of mass flux on the two-phase multiplier into account. A more involved correlation with an increased accuracy was proposed by Friedel (1979), where the two-phase multiplier is given by:

$$\phi_{lo}^2 = C_{F1} + \frac{3.24 C_{F2}}{Fr^{0.045} We^{0.035}} \qquad \textbf{(3.48)}$$

Whalley (1987) suggested that this correlation may be the most accurate correlation available.

3.3.4 Solution parameters

Section 3.2 shows the conservation equations derived in explicit form. That is to say each equation has one unknown that is a function of variables calculated at the previous time step. The explicit solution scheme requires each equation to be solved consecutively rather than simultaneously like the implicit scheme. This is therefore a very simple scheme but it does put limitations on certain parameters in order to avoid numerical instability. In order for the stability criteria to be met some restrictions are placed on the control volume length and time step size. This criterion is easiest explained by considering a particle moving through the loop. The combination of control volume length and time step must be such that the particle does not travel through more than one control volume at any given time step, preferably no further than half a control volume length at a time.

The initial conditions were set to correspond to the system in thermal equilibrium with the surroundings. Consequently all temperatures are equal to the ambient temperature and the initial mass flow rate of the working fluid is zero kilograms per second since there can be no driving force if there is no density gradient. Throughout the solution procedure a pressure boundary is applied at the liquid-air interface in the expansion tank with a value equal to the atmospheric pressure.

3.4 Solution Procedure

The solution procedure proceeds stepwise as follows, see appendix E for sample calculations:

1) Apply initial values, as defined in the user interface, to all variables.
2) Read the heating plate temperature from the text file created during the experiment. Through interpolation determine the temperature at each control volume. Using the temperature of the heating plate as the input parameter calculate the heat transfer rate and temperatures of the air and fin for the individual control volumes from equations 3.12, 3.14 and 3.16.
3) Calculate the change in internal energy of the loop control volume using equation 3.18.
4) Using the given criteria concerning the internal energy, calculate the loop temperature and quality from equations 3.19 and 3.20.
5) With the new temperatures now known calculate the new void fraction using the chosen correlation.
6) From the knowledge of the void fraction calculate the fluid density and mass.
7) Calculate the two phase multiplier using the chosen correlation.
8) The momentum equation provides the mass flow rate in the form of equation 3.21.
9) The pressure drop can now be calculated as well as the nodal pressures from the combined knowledge of pressure drop and the boundary value at the top of the expansion tank.
10) Calculate the saturation temperature from the equation by Kröger (1998), giving temperature as a function of pressure.
11) Calculate the water tank temperature using equation 3.23.
12) Calculate mass balance, determine amount of mass moving into or out of the expansion tank in the time step. Calculate energy loss to atmosphere from tank.
13) Calculate sum of heat transferred to and from thermosyphon loop.
14) Write output data to text file.
15) Repeat steps 2 to 14 until final time step is reached.

4 EXPERIMENTAL MODEL

4.1 Introduction

A concept drawing of a potential reactor cavity cooling system (RCCS) for the PBMR as proposed by Dobson (2006) is given in figure 14. In this concept the RCCS may be represented by a number of axially symmetrical elements: the reactor core, reactor pressure vessel, air in the cavity between the reactor vessel and the concrete structure, the concrete structure, a heat sink situated outside the concretes structure, and a number of closed loop thermosyphon heat pipes with the one vertical leg in the hot air cavity and the other leg in the heat sink. The heat pipe loops are spaced around the periphery of the reactor cavity at a pitch angle θ. Vertical fins are attached to each length of the heat pipe in the cavity to shield the concrete structure from radiation and convection from the reactor vessel through the gap between the pipes and to conduct the heat to the pipes.

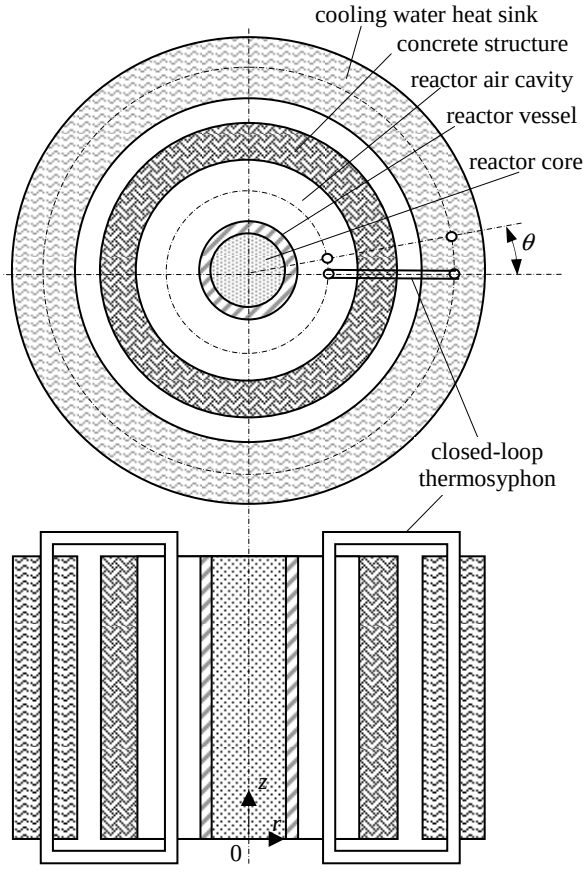

Figure 14: Schematic representation of the proposed RCCS, Dobson (2006)

Section 3 describes the one dimensional theoretical model created to simulate a single loop thermosyphon. However as shown by Lee et al. (2000) the data generated by such a theoretical model is highly suspect until proven by experimental means. It was therefore the aim of the experimental setup to simulate one of the axially symmetric sections of the proposed full scale RCCS using a scaled down version consisting of a single loop heated by a section of the reactor pressure vessel and cooled by a tank of water in order to verify the code.

Three operating modes were identified beforehand. The first is the single phase flow mode where single phase flow exists from start to finish; this does not however make for very spectacular flow. The second is the single to two-phase mode where the flow starts in single phase mode but due to the addition of heat turns into two-phase flow. The third mode is the so called heat pipe mode were the experiment starts off with a loop partially filled with liquid at saturation conditions. As heat is added the liquid starts to boil, and a characteristically oscillatory two-phase flow and heat transfer rate between the evaporator and condenser is established.

Temperature and mass flow rate measurements were made with the experimental apparatus shown in figure 15 to compare with the theoretically determined values. The following paragraphs will give details about the experimental setup and procedures followed to obtain results.

4.2 Experimental Setup

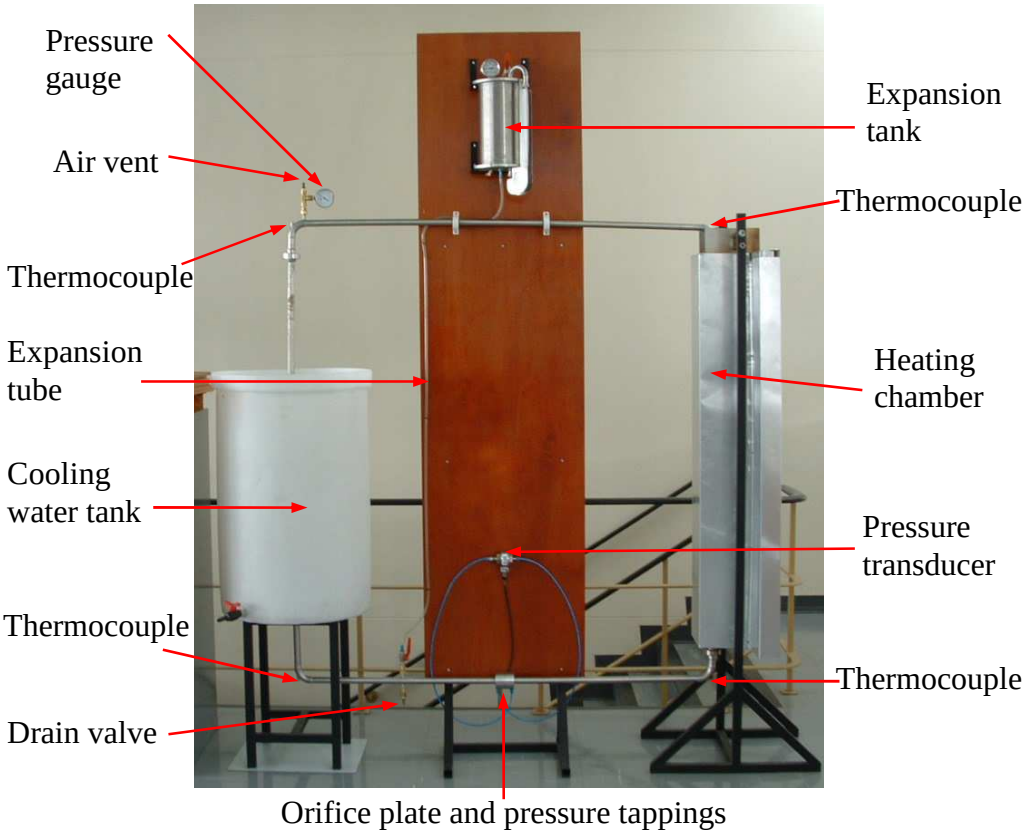

Figure 15: Experimental setup

4.2.1 Geometry and materials

Figure 16 shows a diagrammatic representation of the thermosyphon loop that was constructed from 25.4 mm aluminium and stainless steel tubes with overall dimensions of 1.6 m width and 1.8 m height. The aluminium was used for the heat transfer sections due to its low thermal resistance. Union-type couplings and flanges were used to connect the various parts of the loop.

Water was chosen as the working fluid. Factors that influenced this choice were the low cost involved, abundance and ease of use associated with water. A side effect of this choice was that the loop had to operate under sub-atmospheric conditions in order to allow boiling at temperatures below 100 °C.

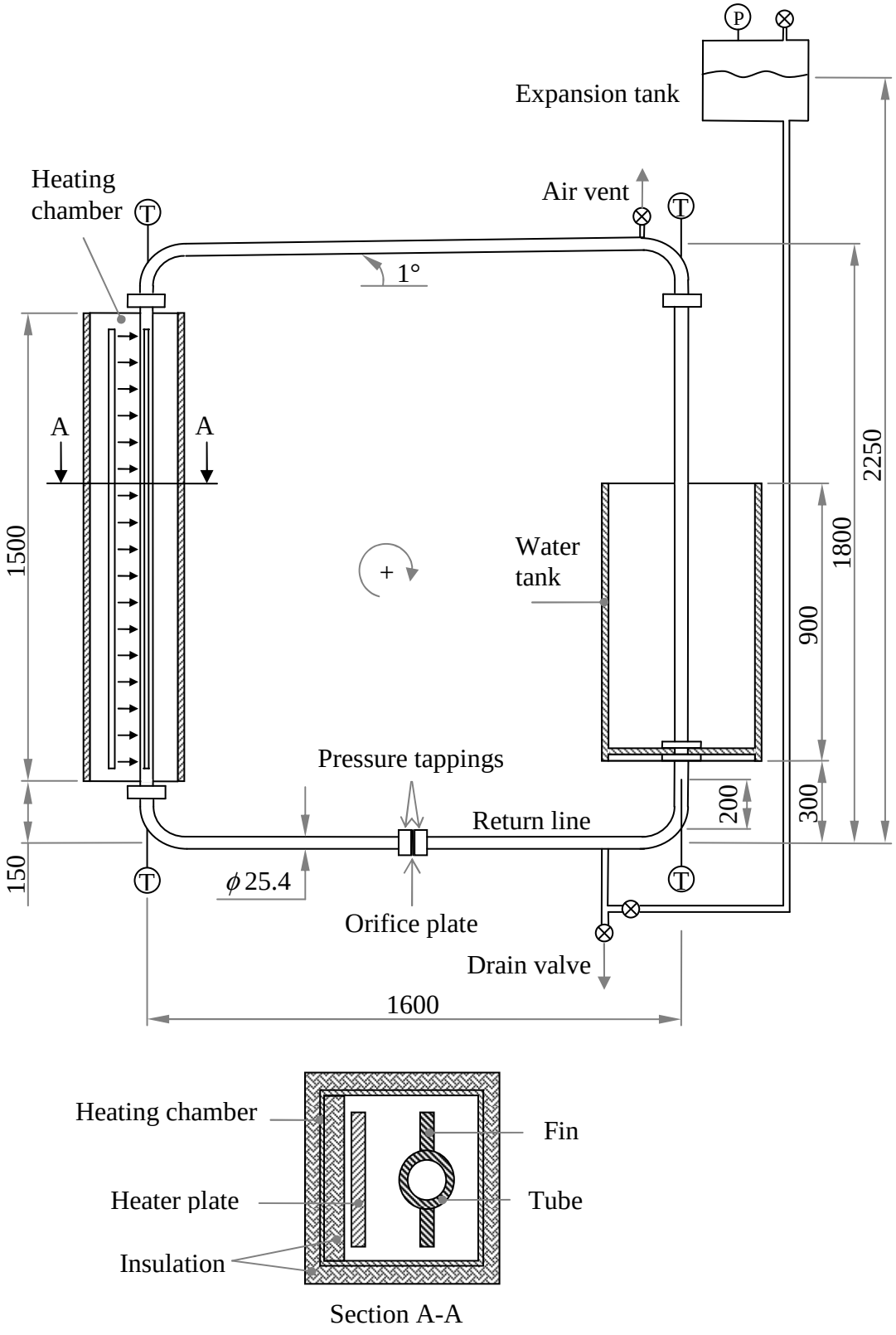

Figure 16: Thermosyphon Loop

It was expected that flow oscillations would occur during the course of experimentation. Therefore an orifice plate capable of measuring flow in both directions, which was not bevelled with an orifice to tube diameter ratio β of 0.33, was manufactured. The orifice plate with flange tappings was installed in the centre of the return line. There were straight lengths of at least 30 diameters on both sides of the orifice plate to minimize any swirl induced by the 90º elbows. British Standards (1981) recommend a minimum length of 12 diameters upstream and 5 diameters downstream of the orifice plate. The standard further states that for research at least twice the minimum value for the upstream case should be used. Two and a half times the minimum value was therefore deemed satisfactory.

The heat source was a stainless steel plate that represented a section of the hot reactor pressure vessel. Energy was imparted to the system via nine 1.3 kW spiral stove heating elements attached to the plate, giving a total heat capacity of 11.7 kW. The power to the heating elements was controlled using individual on/off timer switches. This made it possible to create a temperature profile along the plate.

Rectangular fins, 1.5 m high, 60 mm long and 3 mm thick, were welded along the length of the tube in the portion of the loop adjacent to the heating plate. The heating plate and fins were placed parallel to each other, spaced 100 mm apart and insulated as shown in section A-A, figure 16. The heating chamber was then insulated from the surroundings by a ceramic wool blanket.

The heat sink was a 200 L plastic drum filled with water at ambient temperatures. The water in the tank was not agitated during the experiment. This meant that as the experiments progressed and temperatures in the loop increased the water in the tank took on a two dimension temperature profile. The water temperature was observed to cool down in both the radial measuring from the centre outwards and longitudinal directions measuring from top to bottom.

A stainless steel expansion tank fitted with a sight glass was assembled and placed at a height of 2 m above ground level. It was attached to the loop by an expansion line via a valve attached to the loop return line.

Figure 17 shows a cutaway view of the heating chamber. The figure shows the five equally spaced K-type thermocouples on the heating plate face and the six equally spaced T-type thermocouples on the fins. Thermocouples were placed on both fins so that alternative thermocouple indicated in figure 17 is on the same fin.

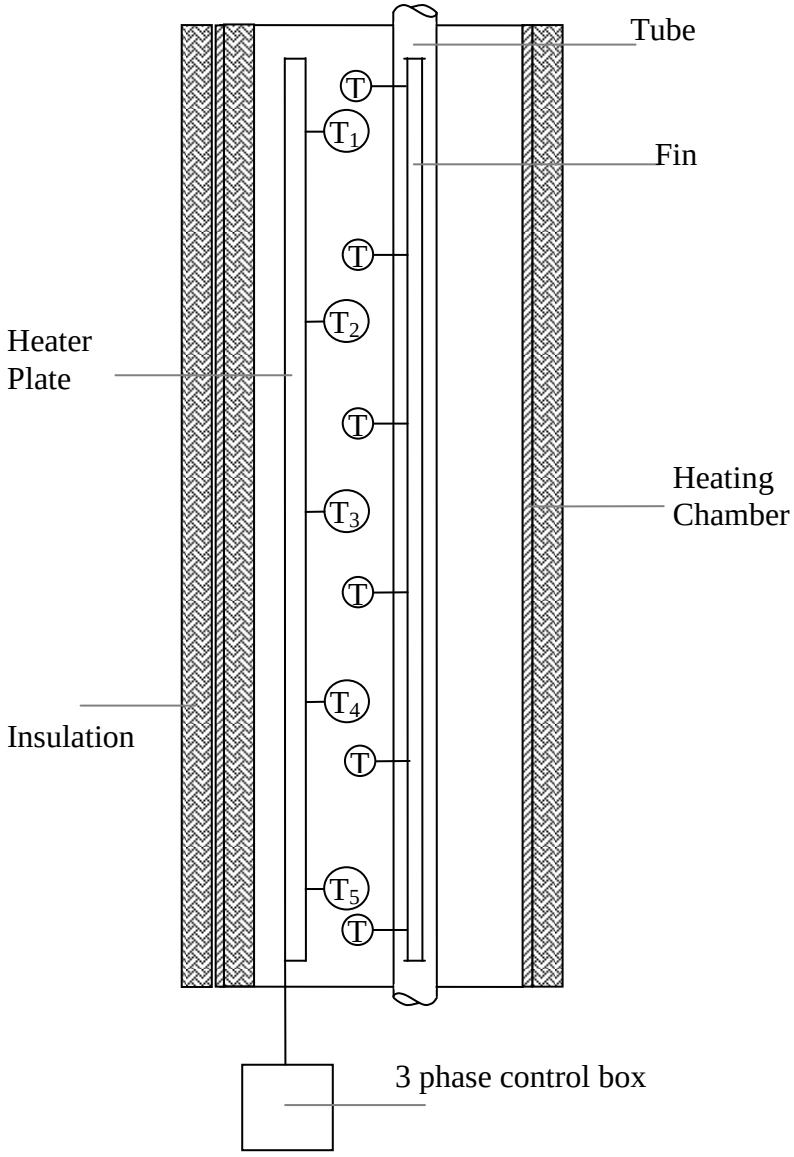

Figure 17: Evaporator assembly cross-section

4.2.2 Sensors

In addition to the thermocouples shown in figure 17, four 1.6 mm T-type thermocouple probes were used to measure the temperature of the working fluid at the inlet and outlet of both the evaporator and condenser.

In order to account for variation in the characteristics of different batches of thermocouple wire it was decided to take each set of thermocouples from the same roll. The accuracy was then verified by testing the thermocouples against a calibrated sub-standard platinum resistance thermometer manufactured by Isotech with model number 935-14-72. The tests indicated all the thermocouples measured within an acceptable accuracy range with little deviation between thermocouples of the same set, see appendix D.

The mass flow rate was measured using an orifice plate, differential pressure transducer and bridge amplifier. In order to determine the relationship between the mass flow rate and the pressure-drop across the orifice, a system calibration was performed. This is to say the orifice plate was not calibrated separately but as part of the system with the associated idiosyncrasies of the loop itself part of the calibration. Several tests showed repeatable results leading to a satisfactory calibration curve, see appendix D.

Two differential pressure transducers were used during the course of experimentation. Initially a HBM DP1-type transducer, F.Nr. 25021, with a 0.1 bar full scale reading working up to a nominal pressure of 50 bar was used. It was however found that the measured values fell in the lower portion of the transducer's range causing the accuracy to be questioned. The transducer was then replaced with a HBM DP1-type transducer, F.Nr. 2929, with a 0.01 bar full scale reading working up to a nominal pressure of 50 bar.

As for the bridge amplifier, a HBM KWS 3073 frequency amplifier was used, F.Nr. 74230, in conjunction with a HBM DA3418 display unit, F.Nr. 75792.

4.2.3 Data acquisition

The temperature and mass flow rate sensors were connected to a Schlumberger SI 35951C IMP data logger, serial number 302523. Data integration took place over a period of 20 ms and was logged every second.

4.3 Experimental Procedure

The first step was to fill the loop with the working fluid. Ordinary, untreated tap water was used. Once the loop was filled, air trapped in the water was removed. If left unchecked this air would create an insulating layer in the condenser section negatively affecting the heat transfer rate. The air was removed by boiling the water and purging the air-steam mixture from the highest point in the system. The release valve was opened and closed at regular intervals until no more air escaped. A simple test to gauge the amount of air in the system involved two temperature measurements at the top of the loop. If there were still air in the system it would accumulate in the pipe connecting the release valve to the loop and the temperature in the upper portion of the pipe would be less than the temperature of the saturated liquid.

For the single and single to two-phase operating mode experiments air removal was the only preparation that was required. The power was switched off and the loop allowed to cool down until the system was once again in thermal equilibrium with its surroundings. Before each test run a data sheet was filled in that included values for the water level in the water tank, water level in the expansion tank, ambient temperatures and pressures as well as checks to indicate that the loop was inspected for leaks, the electrical connections were checked to prevent accidents and the bridge amplifier settings was correct. Once this initial procedure was completed the tests to determine the start-up and transient behaviour of the system could begin. Heat was added to the system and the temperatures and pressure drop across the orifice logged.

For the heat pipe mode experiments however further preparation was required. Two methods of charging the system with working fluid were considered. The first method involved drawing a vacuum in the loop using a vacuum pump. While the second

method allowed hot working fluid to cool down in a constant volume container thus drawing the required vacuum.

Method one followed the air purge operation described previously. Enough water was allowed to enter the expansion tank to fill the loop later on. Once this happened a shut off valve was closed separating the loop and the expansion tank. After a sufficient cool down period the loop drain valve was opened and whatever water remained was drained out. The drain valve was closed and a vacuum pump connected to the loop and allowed to suck a vacuum. The shut of valve was opened and water from the expansion tank was drained into the loop. A simple calculation showed how much the water level in the expansion tank had to drop to attain a certain fill ratio in the loop.

The second method, which was the method eventually used, also followed the air purge operation described previously. Once the system had cooled down and was in thermal equilibrium with the surroundings the water level in the expansion tank was measured. Heat was then added to the system allowing the water to boil. A simple calculation determined how much water had to be expanded into the expansion tank in order to have the required amount of liquid left in the loop. With the required fill ratio reached the shut off valve connecting the loop and expansion tank was closed and the working fluid allowed to cool down. The vacuum was created by the constant volume cool down process so that the loop pressure corresponded to the saturation pressure at ambient temperatures.

Before each experiment a data sheet was filled in that included values for the water level in the water tank, water level in the expansion tank, ambient temperatures and pressures as well as checks to indicate that the loop was inspected for leaks, the electrical connections were checked to prevent accidents and the bridge amplifier settings was correct. Once this initial procedure was completed the tests to determine the start-up and transient behaviour of the system could begin. Again heat was added to the system and the temperatures and pressure drop across the orifice logged.

5 RESULTS

In this section the results obtained with the experimental setup, shown in section 4, are discussed at the hand of different sets of representative test data. The results generated by the mathematical model described in section 3 are then discussed with the focus on how the various parameters and correlations influence the end result. Finally a comparison is made between the theory and experiment.

5.1 Experimental Results

Figure 18 shows a typical set of experimental results for the heating plate, fin and working fluid temperatures and mass flow rate. Figure 18(a) shows the heating plate temperatures at different positions along the plate as a function of time. Figure 18(b) shows the different fin temperatures; figure 18(c) the working fluid temperatures and figure 18(d) shows the working fluid mass flow rate. [Please note all subsequent graphs have the same layout.]

Figure 18(c) shows the temperature rise of the working fluid. The evaporator top temperature $T_{e,t}$ increases steadily to a peak of 94 °C at 2 150 s, thereafter for about 150 s it decreases slightly until boiling starts to occur at 2 300 s at the top of the evaporator, where the pressure is at its lowest, and manifests itself as a periodic temperature oscillation varying between 90 and 100 °C. At 2 150 s the bulk fluid temperature peaks at 94 °C (as indicated in figure 18(c)), the fin temperature exceeds 100 °C at this point and thus the wall temperature must also exceed the saturation temperature of the bulk fluid, and hence boiling occurs at the pipe wall. The driving force as a result of the pressure difference between the heated and cooled portions increases and hence so too does the mass flow rate. As a result of the now cooler fluid flowing over the thermocouple its temperature drops. The mass flow rate slows down slowly until this sub-cooled boiling at the wall changes to bulk boiling throughout the fluid at 2 300 s.

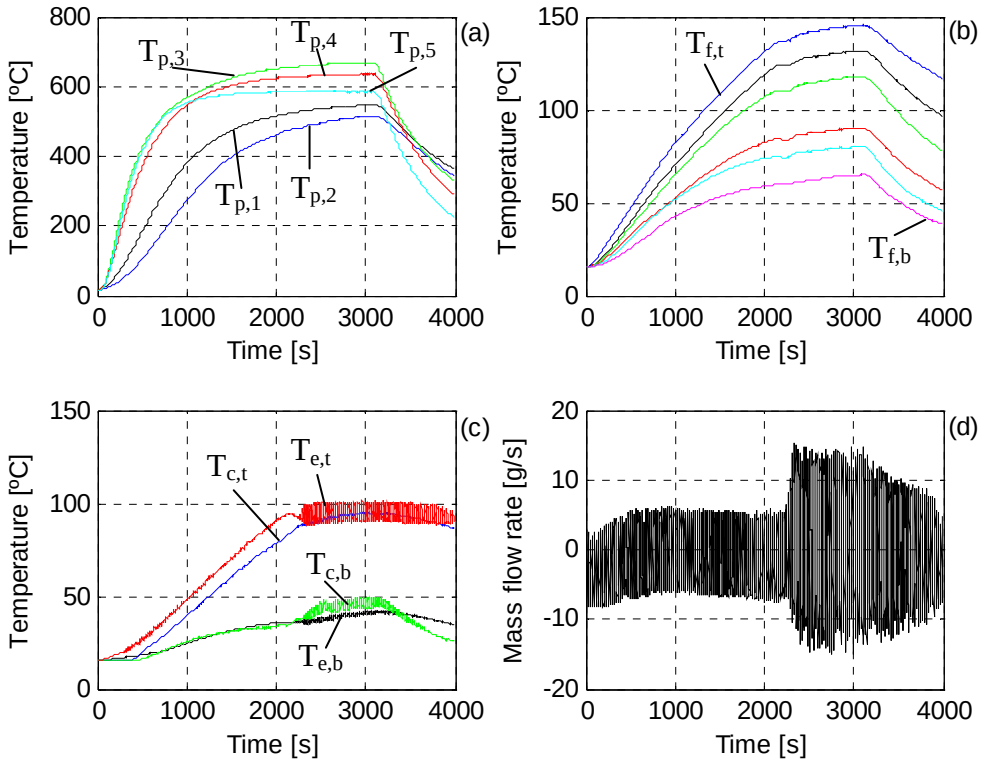

Figure 18: Single to two phase flow operating mode, type 1, plate (a), fin (b), working fluid (c) temperatures and mass flow rate (d)

The temperatures at the top of the condenser at 2 300 s starts to oscillates (it is not visible in the figure as it is shadowed by the evaporator top temperature) with an amplitude of 1 °C, at the bottom it oscillates with a larger amplitude of up to 5 °C. These oscillations are due to the mass flow rate oscillating back and forth. At the top of the condenser, warm working fluid flows over the thermocouple in the positive direction, then returns, without reaching the water tank below and is now only slightly cooler due to the relatively poor convection heat transfer to the air. At the bottom of the condenser the working fluid flows over the thermocouple and afterwards continues to be cooled by the water tank, much more than is possible by convection to the air. Thus when the mass flow reverses its direction a larger temperature oscillation at the bottom of the condenser compared to the top occurs.

In figure 18(d) it is seen that the mass flow rate increases to a peak at 650 s, thereafter decreasing slightly until boiling occurs at 2 300 s when the flow meter reads a relatively large change in the flow from the one direction to the other. After the power to the

heating elements were switched off, at 3 000 s, the amplitude of the oscillations decrease.

Experimentation stopped and was resumed again at a later date at which point the results shown in figure 19 were obtained. In contrast to the results shown in figure 18, a large increase in fin temperature is seen to occur when boiling starts. The top portion of the loop is filled with vapour as evidenced by the condenser thermocouple measuring constantly above 100 °C, after boiling starts. The smaller heat transfer rate associated with convective heat transfer to the vapour (as opposed to liquid) causes local superheating of the vapour. Figure 19(c) shows fin temperatures well above 200 °C. Since the thermocouple in the loop is surrounded by vapour only it is not unreasonable to expect the measured thermocouple temperature to be approximately the average of the wall and vapour temperatures. The wall being heated by a radiation source of above 500 °C and a fin at the top is seen to be approaching 300 °C.

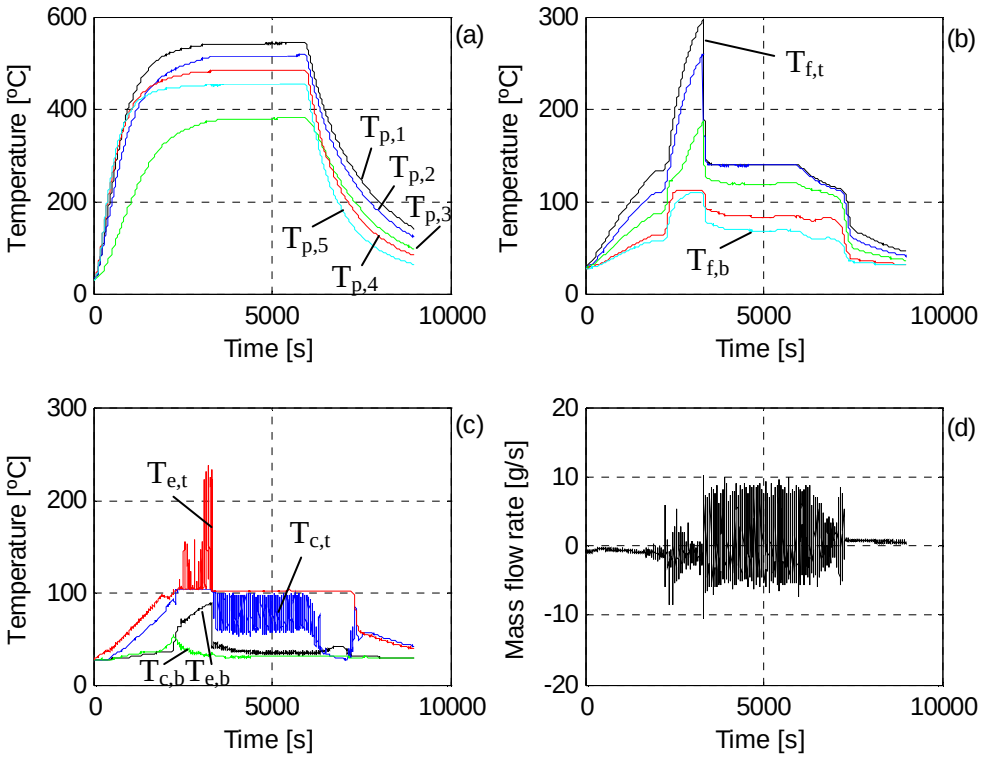

Figure 19: Single to two phase flow operating mode, type 2, plate (a), fin (b), working fluid (c) temperatures and mass flow rate (d)

In order to prevent overheating the upper portion of the condenser, i.e. not in contact with the water in the tank, was cooled by a steady stream of water. This had the effect that the evaporator top temperature stopped its oscillations, but the condenser side temperature however now starts to oscillate. This oscillation can be due to two reasons. Firstly, there is the liquid carried over by the vapour flow. Liquid and vapour of different temperatures come alternatively into contact with the thermocouple. The second possibility is the change in water level in the condenser caused by the carryover and the vapour that condenses. This could cause the thermocouple to be periodically immersed in hot water from the evaporator and then cooler water rising from the condenser section.

When the power input to the heaters is decreased the mass flow rate starts to decrease allowing a temporary increase in temperature at the bottom of the evaporator as the fluid spends a little more time in the heating section. At the same time the temperature at the top of the condenser drops sharply. The stream of cooling water flowing down the length of pipe above the cooling water level in the tank results in a large heat transfer rate, cooling this slower flow to approximately 30 °C where the mass flow rate reaches its minimum value. This however causes an increase in the density gradient again and the mass flow rate increases. As the mass flow rate starts to increase again the reverse happens to the temperatures. At one point the combination of lower heat input and increased flow rate does not allow for boiling anymore and the single phase mass flow rate can once again be identified in figure 19 at approximately 7300 s. The liquid filled loop causes the temperatures measured at the two top thermocouples to be approximately the same but with the condenser side being slightly higher. Consider the loop at the point power is switched off. The liquid in the hot leg moves to the cold leg, the new liquid coming into the hot leg at approximately the same temperature as before is heated less than before causing this difference in the two temperatures.

The difference in boiling behaviour between the two types might be attributed to the atmospheric temperatures. The experiments that correspond to that of figure 19 were conducted during the summer months where the average temperature of the surroundings was 10-15 °C higher than that experienced during the winter month tests characterized by figure 18. The smaller temperature difference between the loop and the surroundings resulted in less heat loss to the ambient. Also the temperature of the water

in the cooling water tank was higher in the summer thus changing the inlet sub-cooling experienced by the working fluid.

Before the heat pipe mode results are presented some thoughts on what is expected to happen in this operating mode. Consider a loop that is half filled with liquid as indicated by figure 20.

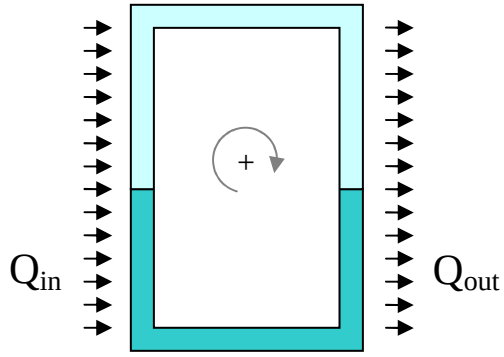

Figure 20: Heat pipe mode

Consider what happens when the heat input is approximately the same as the heat output. The heat input causes the liquid to boil while at the same time increasing the temperature of the vapour far from the interface raising the system pressure. At the same time some of the vapour is condensed at the cold leg. The difference in density causes a positive flow rate to occur sending cooler liquid to the hot leg causing boiling to cease temporarily. Over time the temperature of the liquid increase to the boiling point and the cycle continues with the temperature and pressure continually rising. At a given temperature and pressure however, that will be dependant on the cooling heat transfer rate, the rate of vapour generation and condensation will be approximately equal and the system pressure and thus saturation temperature will stabilize.

The mass flow rate will continually oscillate during the process. Given a large enough fill ratio it is likely that during the bubbly and plug flow regime liquid carryover from the evaporator to condenser will take place that will cause large amplitude oscillation. Once the evaporator liquid fill drops below a certain point liquid carryover will cease and the liquid carried upwards by the vapour drops back causing smaller amplitude oscillations.

With the expected results established the test results can now be examined. The heat pipe mode operation was investigated with fill ratios of 75, 50, 33 and 25 % where the fill ratio is given as the percentage of the evaporator volume that is filled with liquid at 20 ºC.

Figure 21 shows the results for the 75 % fill ratio experiment. Note in figure 21(b) there are only 5 lines. Experiments indicated that the thermocouple situated at the bottom of the fin measured a significantly lower temperature than the thermocouple situated closest to it. Due to the proximity of the thermocouples and the excellent heat transfer characteristics of aluminum it was deemed somewhat suspicious. Upon the completion of the set of tests the rig was disassembled and it was found that the thermocouple had in fact come loose from the fin. Upon reflection it was decided that the other five thermocouples provided enough data to determine the temperature profile over the length of the fin so that it would not be necessary to redo the experiments.

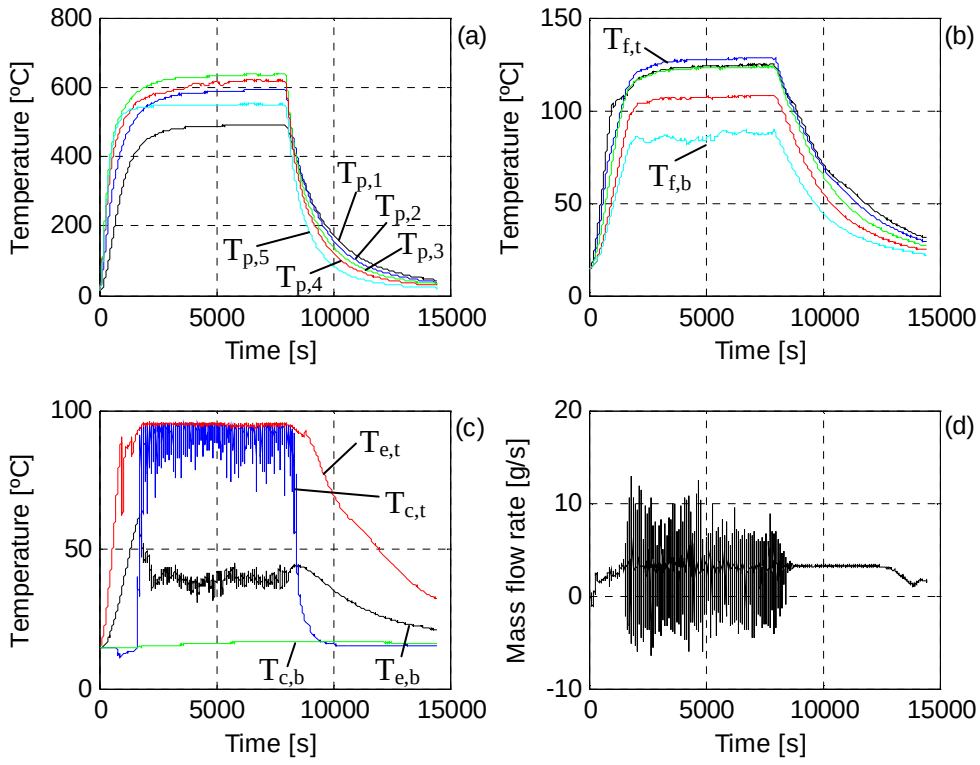

Figure 21: Heat pipe operating mode, 75 % fill ratio, plate (a), fin (b), working fluid (c) temperatures and mass flow rate (d)

Looking at figure 21(c) and (d) the flow response was as outlined in the previous paragraphs. It will be noted that the temperature at the top of the condenser, $T_{c,t}$

remains at approximately 16 ºC due to an insignificant vapour flow rate and continual cooling at the top of the condenser. Once bulk boiling is sustained the mass flow rate is appreciable and hot vapour reaches the condenser pushing $T_{c,t}$ up to the maximum of approximately 95.7 ºC. During the course of experimentation it was observed that $T_{c,t}$ is highly dependant on the condensation heat transfer rate. Increasing the condensation heat transfer rate lowers the temperature.

The increase in mass flow rate also allows the liquid a shorter residence time in the evaporator thus causing a drop in $T_{e,b}$ measured at the bottom of the evaporator. It can be seen that the temperature oscillates due to the alternative flow of hot vapour and cooler condensate past the thermocouple in quick succession. The condensate forms quickly due to the high heat transfer rate, this is also the reason $T_{c,b}$ measured at the bottom of the condenser does not rise appreciably during the test.

The results obtained for the 50 % and 33 % fill ratio experiments shows the same general trends as the 75 % experiments. In all cases when the temperature at the top of the heater plate was lowered and/or an increase in the cooling rate at the top of the condenser occurred, the maximum fin and loop temperature decreased.

The 25 % fill ratio experiments however were quite different from the 33 %, 50 % and 75 % experiments. To start off with the input plate temperature profile is different, see figure 22(a). Due to the fact that the upper portion of the loop is filled with vapour it was thought prudent to keep the temperatures at the top of the heater plate low by decreasing the electrical input. This would prevent possible damage to the system due to elevated temperatures. As can be seen in figure 22(b) even with this modification the fin temperatures still surpass 100 ºC. Figure 22(c) and (d) shows that boiling does not occur as soon as heat is added to the system. A finite time must pass while the system temperature and pressure adjust to the point where boiling starts to occur. When the working fluid boils, vapour and entrained liquid are rapidly forced upwards travelling around to the condenser raising the temperature in a short time span after which rapid condensation takes place to lower the temperature measured at the condenser inlet. This behaviour can also be observed in figure 22(d) as spikes in the mass flow rate.

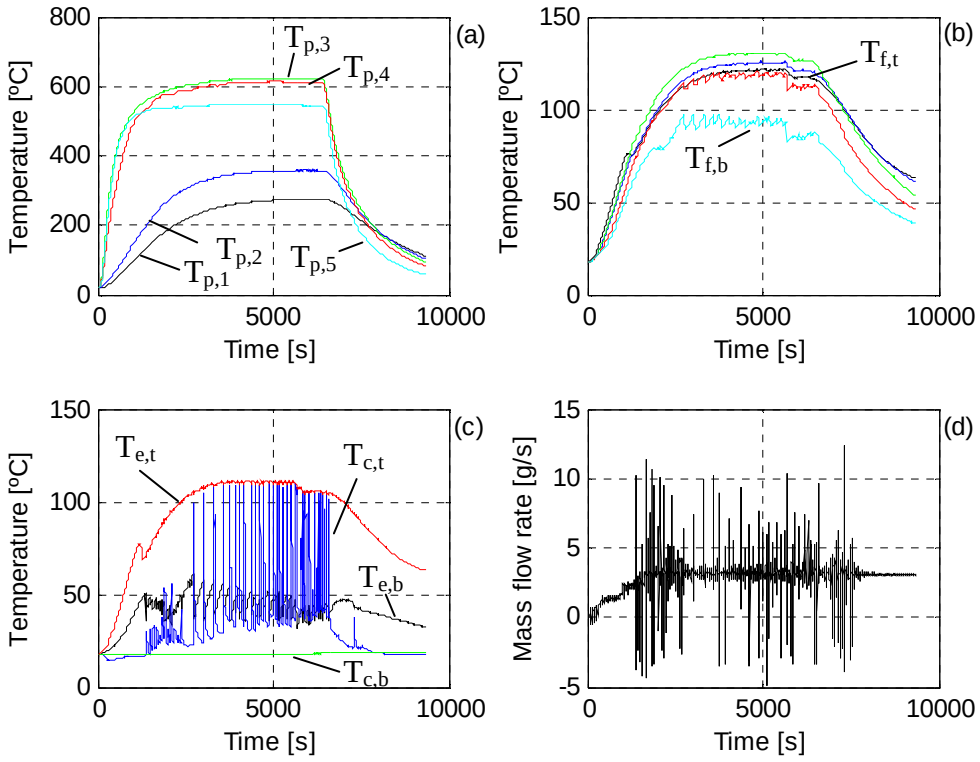

Figure 22: Heat pipe operating mode, 25 % fill ratio, plate (a), fin (b), working fluid (c) temperatures and mass flow rate (d)

Closer inspection of these mass flow rate spikes shows the process repeats itself over time giving a saw tooth response as shown by figure 23. As the temperature increases so to does the frequency of the response until a steady state is reached or the power is switched off.

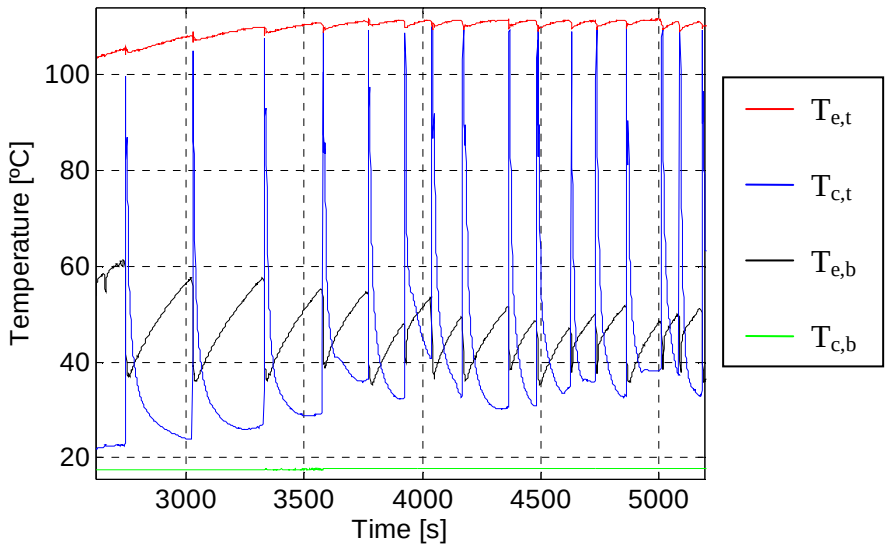

Figure 23: Heat pipe operating mode, 25 % fill ratio, working fluid temperatures

5.2 Theoretical Results

From the literature is clear that the theoretical results are dependant on the choice of correlations used. In order to gauge the effect of the correlations used in the mathematical model comparative data was generated for a heat input profile as shown in figure 24, this is the same input used in the first experiment described in section 5.1.

Table 5.1 shows the correlations used for heat transfer, void fraction and two phase multiplier for the base case to which all other combinations will be compared. The table also shows the values chosen for the material surface properties of the fin and heater plate, since it turned out to be a very influential parameter in obtaining certain results. These values were found at www.infrared-thermography.com, see appendix A.

Table 5.1: Base case parameters and correlations

ε_{fin}	0.09	
ε_{hp}	0.85	
α	Lockhart-Martinelli	Eq 3.44
ϕ^2	Lockhart-Martinelli	Eq 3.46
$h_{evap,\ single\ phase}$	Collier(laminar flow) Gnielinski(turbulent flow)	Eq 3.31 Eq 3.32
$h_{cond,\ single\ phase}$	Collier(laminar flow) Gnielinski(turbulent flow)	Eq 3.31 Eq 3.32
$h_{evap,\ two\text{-}phase}$	Chen	Eq 3.34
$h_{cond,\ two\text{-}phase}$	Traviss et al.	Eq 3.39

Figure 24 shows the results obtained for the base case. Figure 24(a) shows the heat input in the form of the heater plate temperatures; figure 24(b) the fin temperatures at positions corresponding to the positions of the thermocouples in the experiment, figure 24(c) gives the loop temperatures at the evaporator and condenser inlet and outlet and figure 24(d) the mass flow rate. [Please note all subsequent graphs have the same layout.]

From figure 24(c) it is clear that the condenser does not cool the working fluid appreciably so that the entire loop operates at a relatively high temperature. It can also be seen that boiling starts fairly late at approximately 2 650 seconds. Comparing

figures (b) and (c) it can be seen that the fin and corresponding loop evaporator temperatures are closely related throughout the simulation with a difference of approximately 20 ºC. As will be discussed later, this close relationship was not observed in the experiment. The mass flow rate shown in figure 24(d) clearly shows the transition from single to two-phase flow. The flow is characterised by a very low single phase flow rate that transitions into wildly oscillating two-phase flow.

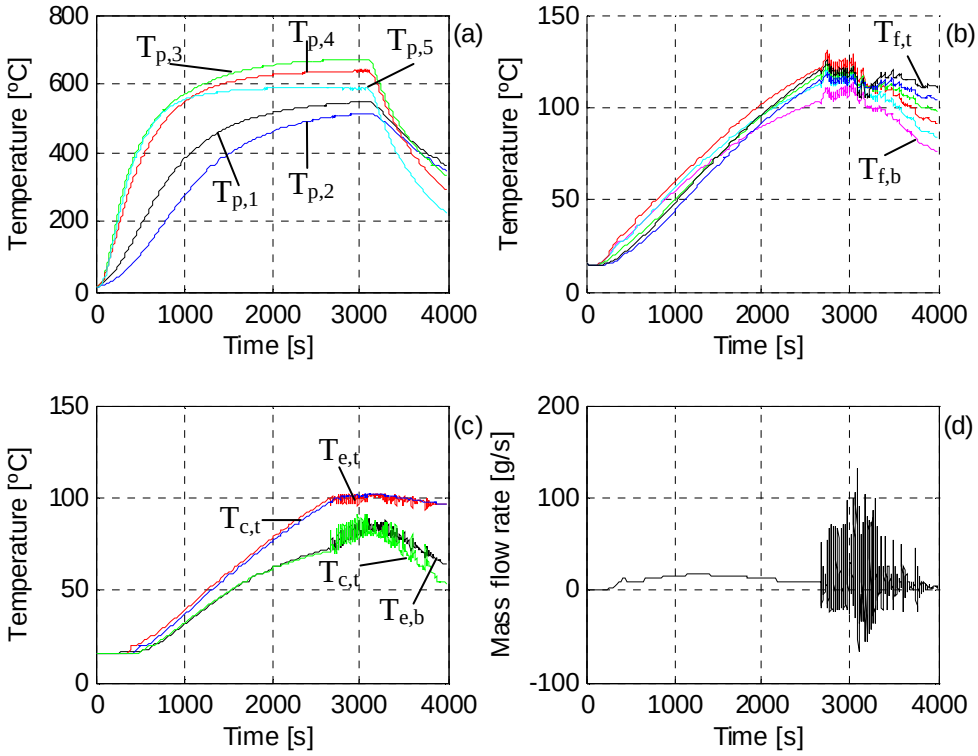

Figure 24: Base case results, plate (a), fin (b), working fluid (c) temperatures and mass flow rate (d)

In order to gauge the effect of the two phase heat transfer correlations on the results, all possible combinations of the heat transfer coefficient correlations for two-phase flow as mentioned in section 3 were used to produce results. The comparison showed that there are minor differences in the minimum and maximum values of the temperatures and mass flow rates but the trends remain the same. The conclusion is that for the two-phase condensation and boiling heat transfer coefficient correlations available to this model it makes very little difference what correlations are actually used.

Changing the void fraction and two phase multiplier correlations give results that closely match that of the base case from the onset of the experiment until the time that the power input is switched of. Hereafter smaller mass flow rate oscillations take place and temperature oscillations cease.

Since figure 24 indicates that the loop spends a large portion of the time in the single phase regime, the influence of the single phase heat transfer coefficient on the final result was investigated. One option was to use constant values for the heat transfer coefficients, this would however make it completely independent of the flow conditions, the decision was made to rather calculate a value using the correlations of Collier (laminar flow) or Gnielinski and then use a multiple of the calculated value.

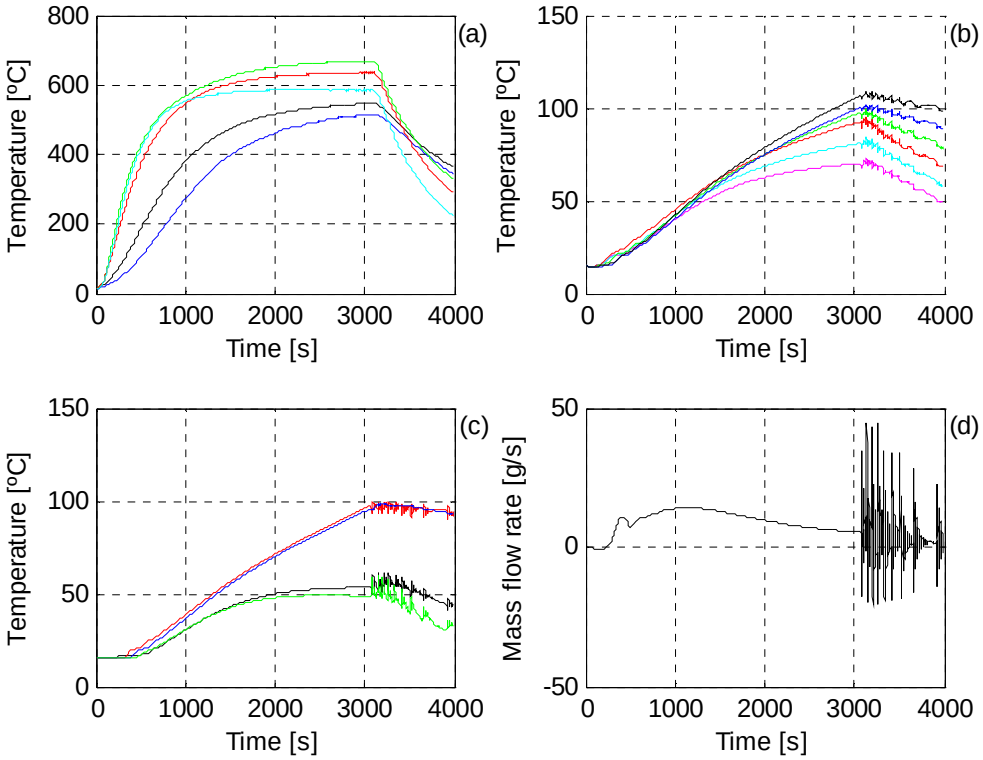

Figure 25: Different single phase heat transfer coefficient, plate (a), fin (b), working fluid (c) temperatures and mass flow rate (d)

Figure 25 show the result of using a single phase heat transfer coefficients three times larger than the correlation value. Temperatures and mass flow rate drops significantly compared to the base case. The temperature in the loop at the condenser outlet drops by approximately 30 ºC. Note also that it takes longer to reach the transition point from single to two-phase flow. In fact boiling is initiated mere seconds before the power

input is switched off and the heater plate temperature starts to decrease. In the single phase region the mass flow rate value is approximately the same as in the base case however the two-phase oscillations shows an amplitude that is smaller by approximately half. Two reasons for this exist. In the first place boiling is initiated shortly before the heat input is terminated thus decreasing the driving force and secondly due to the much larger heat transfer coefficient a much smaller mass flow rate is required to get the same heat transfer rate.

In order to shift the transition point to an earlier time an attempt was made to increase the heat transfer rate to the working fluid. This was done by increasing the emissivity of the fin, from 0.09 recommended for commercial sheets to 0.18 recommended for oxidized aluminium, thereby decreasing the resistance to heat transfer. The results are shown in figure 26.

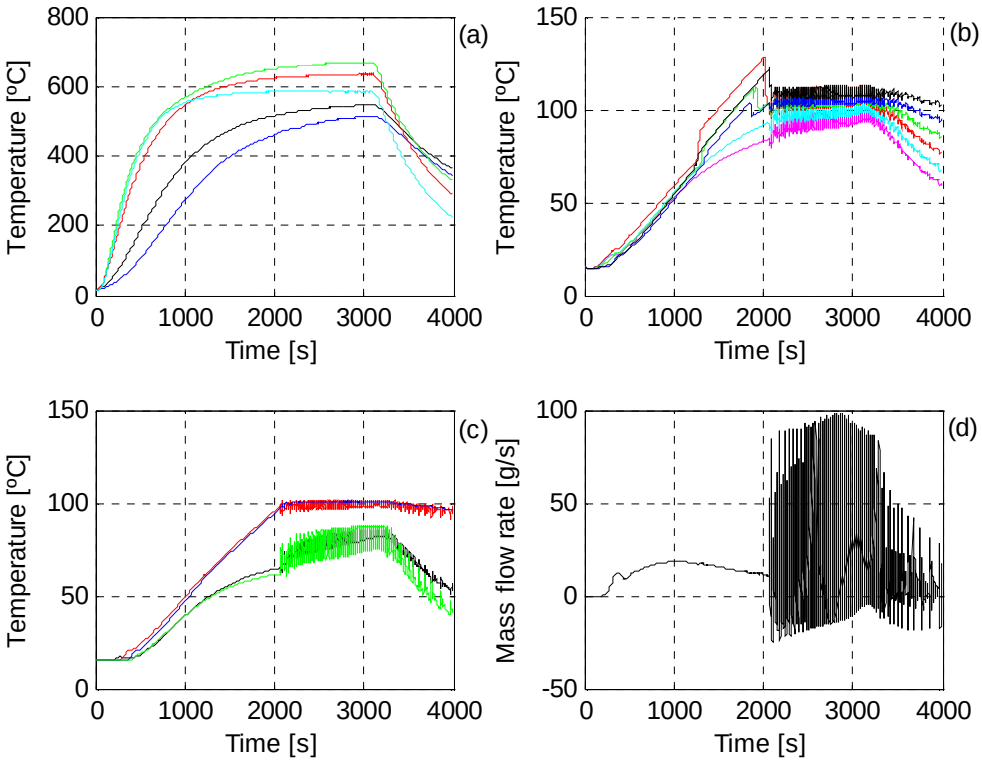

Figure 26: Influence of fin emissivity, ε = 0.18, plate (a), fin (b), working fluid (c) temperatures and mass flow rate (d)

Figure 26(c) shows that the increased heat transfer rate does indeed shift the transition point to an earlier time. Although not unexpected it is rather disappointing to see that

the condenser outlet temperature is again very high. Figure 26(b) shows the influence on the fin temperatures which is again well above 100 ºC but it also shows the influence of the increased heat transfer rate associated with two-phase flow that allows the temperatures to drop by as much as 20 ºC at the top of the fins. Figure 26(d) shows large mass flow rate oscillations during the two-phase period.

This result prompted another attempt to lower the working fluid temperature at the condenser outlet whilst maintaining as close as possible the transition point from single to two-phase flow. This was done by again doubling the heat transfer coefficient values so that it was 6 times the value calculated by the correlations. This had a small effect on the results lowering the condenser outlet temperatures by less than 10 ºC. At this point there is no reason to further increase the internal heat transfer coefficient since by now the external convection heat transfer coefficient to the water tank had become the dominant factor in the resistance to heat transfer in the condenser section. The convection heat transfer coefficient was then multiplied by 3 and the results are shown in figure 27.

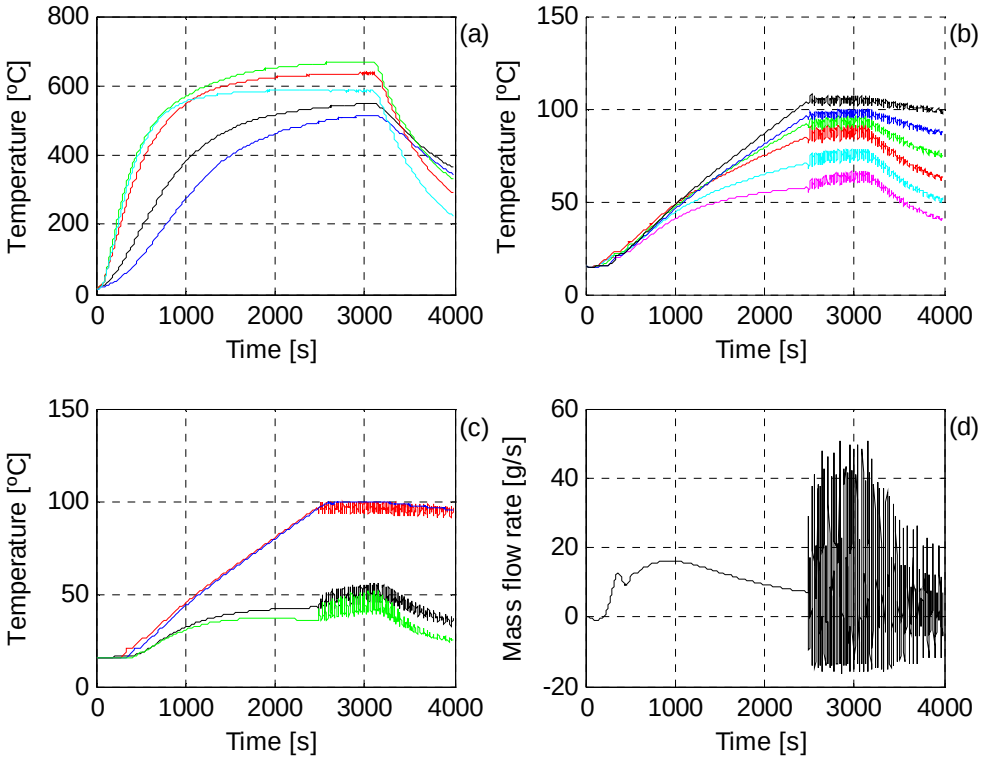

Figure 27: Theoretical results, plate (a), fin (b), working fluid (c) temperatures and mass flow rate (d)

Figure 27(c) shows a significant reduction in condenser outlet temperatures while the transition point from single to two-phase flow has unavoidably been shifted along again. The fin temperatures are seen to have a more even spread in figure 27(b). This result is a better approximation of the experimental results as will be shown in section 5.3. It was therefore decided to maintain these parameters for the simulation of other experimental test runs.

5.3 Comparison of Results

The experimental results shown in figure 18 and the theoretical results shown in figure 27 are combined and presented as figures 28 through 30 showing separately the loop temperatures, fin temperatures and mass flow rate.

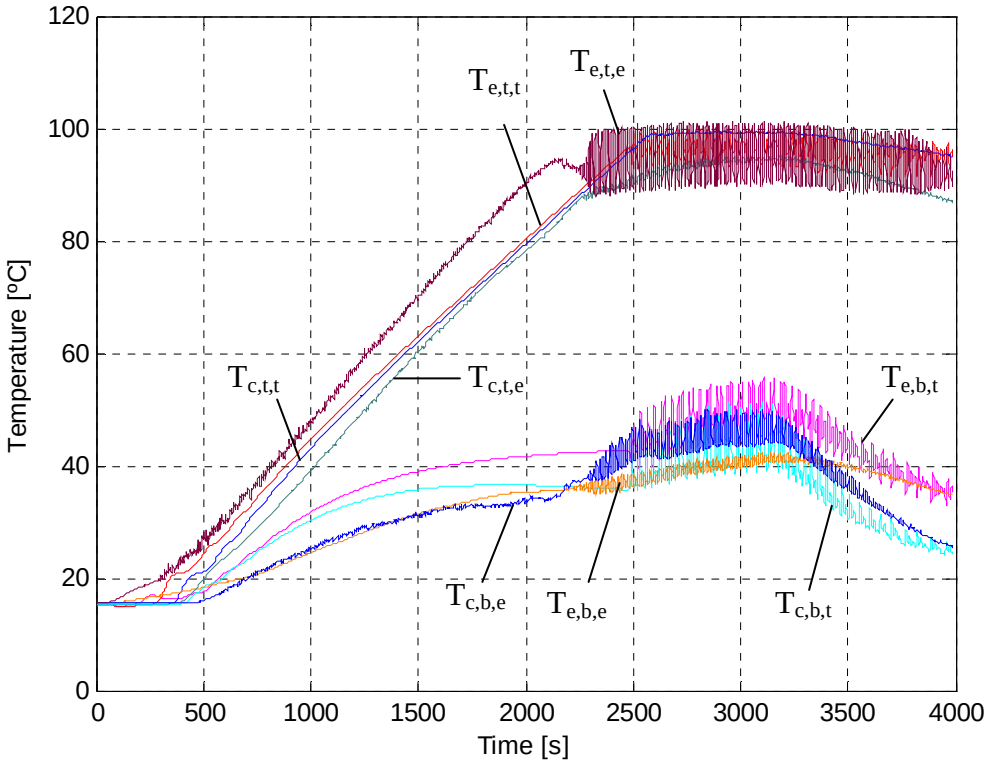

Figure 28: Loop temperature comparison

Overall it seems that the loop temperatures are well predicted by the theory. Some discrepancies do however exist. The theory does not predict the temperature peak at the top of the evaporator caused by sub-cooled boiling. This is because the theoretical model does not make provision for sub-cooled boiling only bulk boiling. It can also be

seen that a larger temperature oscillation is present at the top of the evaporator in the experiment. This may be due to the length of the thermocouple and the frequency of data measurement. When the evaporator temperatures for the top three control volumes is plotted on the same graph as that of the experiment the upper boundary of the top control volume and the lower boundary of the bottom control volumes gives approximately the same boundaries as the experiment. Furthermore the temperatures are seen to be slightly over-predicted and in comparison the transition point is somewhat delayed in the theory.

Figure 29 shows that the temperatures of the fins on the lower portion of the loop are fairly well predicted. However the upper portion is poorly predicted due to the thermal stratification of air that takes place. The model would have to calculate heat transfer in two dimensions in order to approximate the experimental temperatures better in this regard.

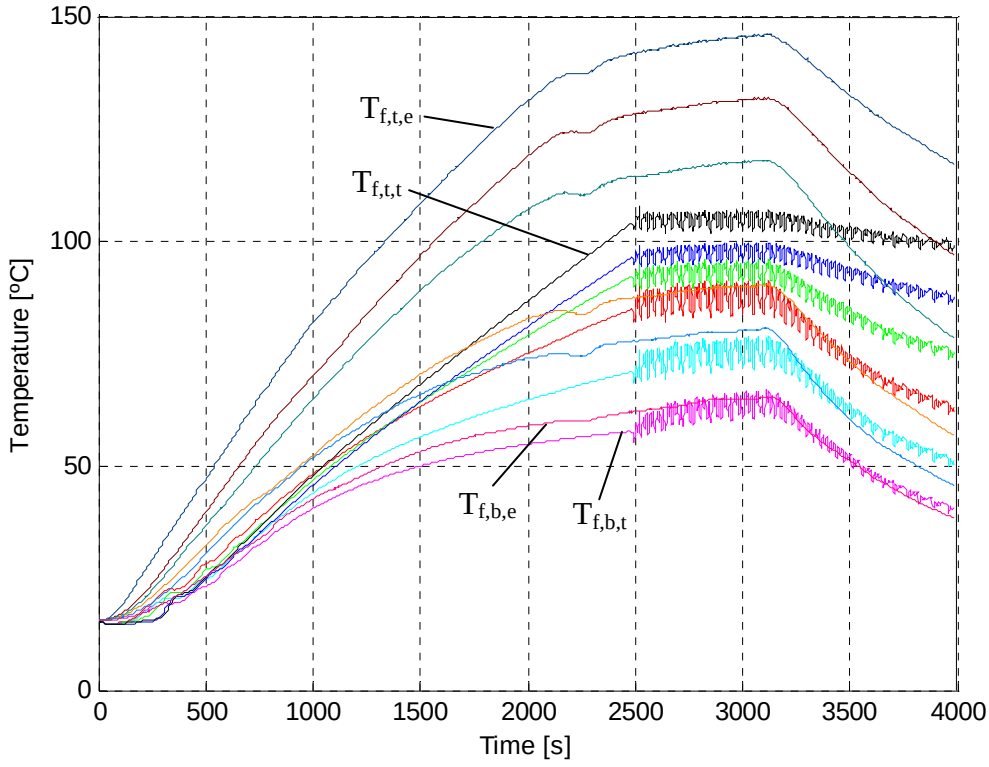

Figure 29: Fin temperature comparison

Figure 30 shows the mass flow rate graphs. The theoretical model predicts a mass flow rate more than twice that measured in the experiment. There is a large degree of uncertainty about the measured mass flow rate in the single phase region. This is mainly due to the small pressure drop across the orifice plate that caused the pressure transducer to measure in a region below which was optimal. On the theoretical side of the equation error could have been introduced due to the decision to use general frictional loss coefficient correlations rather than correlations specific to the various flow patterns that arise during the simulation (as suggested by Chisholm, 1983).

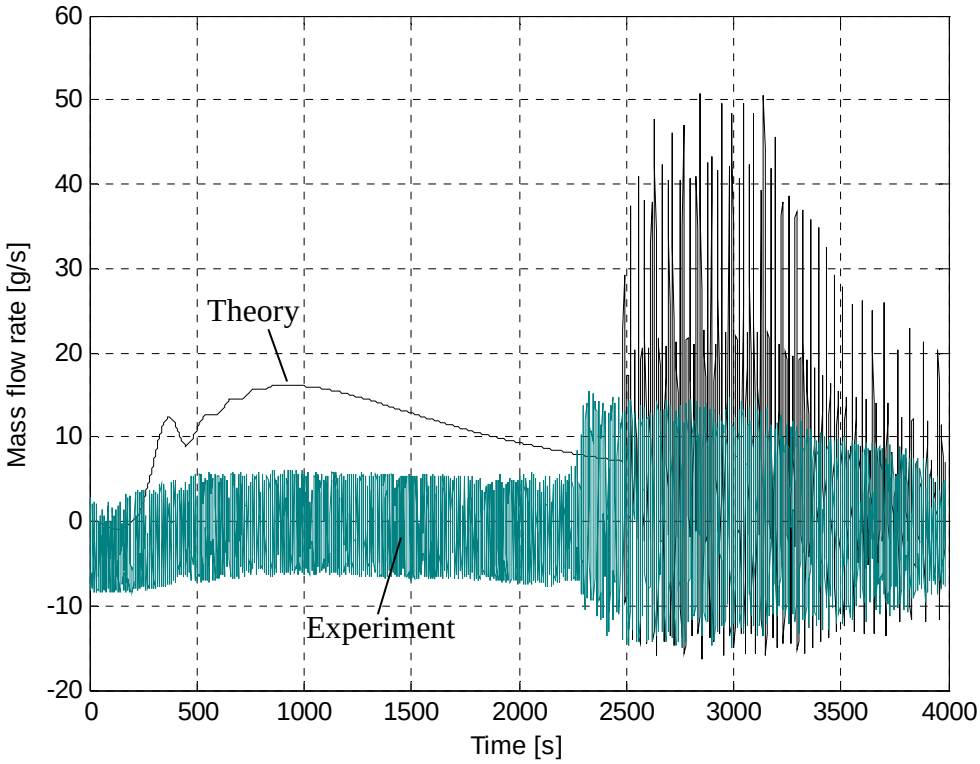

Figure 30: Mass flow rate comparison

A comparison for the second type of single to two-phase experiment shown in figure 19 will not be given since the program cannot predict the dry-out that occurs. A comparison for the heat pipe modes can also not be given due to the inability of the program to produce a stable solution. These issues will be addressed in the recommendations.

6 DISCUSSION AND CONCLUSIONS

In 2002 the Generation IV International Forum (GIF) nations proposed long term research and design goals for generation IV reactors to make nuclear power safer and more viable for long term use. One of these goals is to use passive safety features in the design. This then is the goal for the PBMR RCCS, to be totally passive while operating under normal and loss of coolant accident conditions. A literature survey showed several proposed passive solutions for reactor cavity cooling in other reactor designs. Of these solutions the heat pipe type method seems to be the most feasible.

The focus of this project then was the application of a loop themosyphon as a reactor cavity cooling system. A loop thermosyphon can be defined as a thermodynamic device that employs temperature induced density gradients to create a natural circulation of the working fluid in the system. Loop thermosyphons have been widely researched with the focus on both the theoretical and the experimental aspects. A great deal of research has been in the characterization of the stability of thermosyphons since instability can cause heat transfer excursions that may ultimately lead to system failure. Various types of instability exist with the density wave oscillation being the most common. Researchers have found that stability is mainly influenced by the following factors: power input, inlet sub-cooling, flow restrictions and compressible volumes. On the theoretical side it has been shown that computer simulation without experimental validation cannot deliver meaningful quantitative results.

One of the objectives of the project was to build one of the axially symmetric sections of Dobson's (2006) proposed full scale RCCS using a scaled down version consisting of a single loop heated by a section of the reactor pressure vessel and cooled by a tank of water. The second objective was to derive a theoretical model that could be used in a computer code to simulate the experiment. The theory and experiment would then be compared in order to verify the code.

The mathematical model created used the following three major assumptions: quasi-static flow, incompressible liquid and vapour and one dimensionality. The differential equations were formulated using the laws of mechanics and the Reynolds transport

theorem for a control volume based analysis. The equivalent difference equations were then formulated explicitly. While closure equations for the heat transfer coefficients *h*, void fraction α, the friction factor C_f and the two phase multiplier ϕ^2 were found from the literature.

It was found that the theoretical results were heavily influenced by the surface optical properties as well as the heat transfer coefficients. The emissivity influenced the transition point from single to two-phase flow as well as the condenser outlet temperature. The single phase heat transfer coefficients influenced the condenser outlet temperature significantly while it was found that for two phase flow the combination of the available boiling and condensation heat transfer coefficients had only minor effects on the end results.

A stainless steel and aluminium thermosyphon loop was built using water as the working fluid. A stainless steel heater plate provided the heat input while a 200 L water tank was the heat sink. Refrigerant 134A was also tested as a possible working fluid but it was found that the amount of wall superheat, (T_{wall}-T_{bulk}), that the apparatus could generate was insufficient to initiate boiling, thus the apparatus did not work in heat pipe mode and this course of action was abandoned. It was decided that three operating modes would be tested namely, single phase, two-phase and heat pipe mode. Temperature measurements were made with thermocouples and the mass flow rate was measured through the combination of an orifice plate, differential pressure transducer and bridge amplifier. Data was logged for comparison with the theoretical results.

A two-phase closed loop thermosyphon is a highly non-linear system were all the system parameters are interlinked so that even a relatively small changes in start-up and operating conditions can have a significant influence on the experimental results obtained as illustrated by the papers of Wu et al. (1996) and Wang and Pan (1998).

As discussed in the literature review, Wu et al. (1996) studied chaotic oscillations in a low temperature two-phase natural circulation loop and found that power input and inlet sub-cooling has a large effect on the oscillating behaviour of the loop. Wang and Pan

(1998) using Taguchi methods share Wu's conclusions, but add that, flow restrictions and compressible volumes in the system are also factors influencing stability

Operational procedures were put in place in order to provide consistency in the method of experimentation as well as ensure the safety of the equipment. This did however not lead to consistent sets of single to two-phase flow data as might be expected but rather to two distinct sets of experimental results. It has been postulate that seasonal temperature fluctuations might be the cause of this discrepancy between the two sets of data, influencing the factors mentioned by the authors above that in turn influenced the oscillating behaviour of the system.

An important objective of the experimental work was to assist in determining the accuracy of the theoretical model. Figure 28 shows the theoretical results superimposed on the experimental results. The same heating plate temperature profile was used in both instances. It can be seen that the theoretical temperatures correspond reasonably well with the experimental temperatures. The time predicted by the theoretical model to reach the operating temperature is however somewhat longer than for the experimental value of 2 000 s. This is to be expected when considering that there exists some uncertainty pertaining to the heat transfer coefficients as well as surface emissive properties. The correspondence of the theoretical and experimental fin temperatures is poor due to significant thermal stratification of the air separating the heater plate and fins.

Shortcomings identified in the theoretical model are:

- Only steady-state correlations for single and two-phase heat transfer coefficients were found in the literature; whereas in the actual experimental loop it is clear that oscillating flow occurs. In trying to simulate the experimental loop theoretically it would appear that significantly higher correlating heat transfer coefficient values, than are given by existing correlations, are needed.

- Inaccurate prediction of the heating response time. Attention must be paid to the heat transfer coefficients and surface emissive properties. The calculations of losses to the surroundings from the heating chamber and loop might have to

be revised.

- Convection in the air-space between the heating plate and the fin was not completely addressed. Significant stratification occurred resulting in a larger than expected variation in the temperature between the top and the bottom ends of the air space. This caused the relatively large temperature variation along the fin that was not theoretically predicted as shown in figure 29.

- General homogenous frictional loss coefficient correlations were used rather than correlations specific to the various flow patterns.

- Dryout is not addressed in the model and the model has difficulty with calculating heat pipe mode. Updating of theoretical model and computer program is required.

Shortcoming identified in the experimental setup:

- It was not possible to accurately verify experimentally whether the heat input balanced the heat removed by the cooling water. For instance, it is difficult to accurately measure the temperature distribution in a naturally convective stratifying tank of water; nor is it easy to accurately measure the heat transfer rate due to both radiation and convection in the space between the heating plate and the fin. It was also not possible to measure liquid carryover from the heated to the cooled legs of the loop during two-phase flow.

- The effect of thermally induced strains on the weld seams and pipe wall were not initially taken into account. It was difficult to maintain the vacuum for extended periods of time even after better seal materials were used and silicon applied liberally. It was only later that closer inspection revealed small cracks in the weld seam at the top of the evaporator were the thermocouple fitting was attached to the loop. The seals in the union type fittings also became hard and brittle as time passed causing leaks, this problem was however solved with *Viton* O-ring seals.

- In figure 18(c) it is seen that the differential pressure transducer exhibited a significantly large noise level as well as a large difference between the theoretical and experimental flow rates.

In conclusion the simple one-dimensional theoretical model can predict the internal temperatures of the thermosyphon loop fairly well, there are however areas of uncertainty that must be resolved, for instance, the determination of the fin temperatures, the heat transfer in the water tank, as well as the calculation of dryout. The theory also predicts an average heat removal rate of 2 kW for the test case shown in figure 18 during two phase flow. This is a significant value for the size of the system which makes a strong argument for the use of a loop thermosyphon as a RCCS.

7 RECOMMENDATIONS

Looking at this project in retrospect it is clear that the following areas require further research in order to come to a more meaningful conclusion on the application of this concept to the PBMR RCCS.

7.1 Material Surface Properties

In section 5.2 it was shown that the material surface properties of the fins and heater plate played a major role in determining the end result. The values used for these parameters were found from tables of average values not necessarily at the same conditions as in the experiments. These conditions would include different temperatures, levels of oxidation and the amount of fouling. In order to gain more confidence in the theoretical model a more accurate value for these properties are required. This can be done by using industry standard equipment to measure the surface properties, note though that this equipment is generally expensive.

In the event that a similar system is installed it should be remembered that the properties would most certainly change during the lifetime of the installation. It is therefore further recommended that the degradation of the surface optical properties over time should be investigated.

7.2 Heat Transfer Coefficients

The literature study as well as the theoretical results of section 5.2 clearly shows the dependence of the temperatures and mass flow rate on the heat transfer correlations used in the model. It is recommended that experiments be performed with a suitably constrained experimental setup to allow for the accurate measurement of energy entering and leaving the system so that an energy balance can be found. This data can then be used in a regression analysis to find appropriate heat transfer correlations for both single and two-phase flow.

7.3 Mass Flow Rate Measurement

Comparing the experimentally measured mass flow rate and the theoretically predicted mass flow rate a large discrepancy is evident. It is therefore recommended to investigate alternative methods of measuring the mass flow rate. These methods can include the use of more sensitive differential pressure transducers, high speed photography, hot-film anemometers or laser optical equipment.

7.4 Natural convection

There are two areas outside the thermosyphon loop where natural convection takes place that need further investigation. This can be done using a commercial computational fluid dynamics package to show the flow path of the various particles.

The first area to investigate is natural convection of the air inside the heating chamber that flows between the fin and heater plate as well as the air that flow between the back of the fin and the back of the heating chamber. The graphs of section 5.1 indicate thermal stratification that causes the fins to heat up to temperatures far above that predicted by the theory.

The second area is the natural convection in the water tank that serves as the heat sink. Tactile tests showed a definite two dimensional temperature profile. It would be most informative to see how quickly thermal stratification takes place as well as what the critical size of the water tank, height and diameter, would have to be to maintain the loop at a given temperature for a given heat input.

7.5 Scaling

Scaling is a complex issue especially when two-phase flow is present. An attempt must be made to gauge the effect of the following parameters: tube diameter, tube shape, loop height, loop width, ratio of tube length to diameter, type of working fluid, working fluid fill ratio and fin size and configuration.

7.6 Mathematical model

The mathematical model should be updated to include the two dimensional heat transfer in the heating chamber and water tank. The dry-out phenomenon should be addressed and the alterations required to generate stable heat pipe mode results should be made. Attention should also be paid to finding appropriate frictional energy loss coefficients to better approximate flow pattern dependant conditions in the thermosyphon loop.

8 REFERENCES

Anderson, M.H., Herranz, L.E. & Corradini, M.L., 1997, Evaluation of condensation modeling based on heat/mass transfer analogy, *AIChE symposium series, heat transfer-Baltimore 1997*, Vol. 93, No. 314, pp.108-113.

Arneth, S. and Stichlmair, J., 2001, Characteristics of thermosyphon reboilers, *International Journal of thermal sciences*, Vol. 40, pp. 385-391.

Bouré, J.A., Bergles, A.E., Tong, L.S., 1973, Review of two-phase flow instability, *Nuclear Engineering and Design*, Vol. 25, pp. 165-192.

British Standards, 1981, *BS 1042 section 1.1: 1981*.

Burgazzi, L., 2004, Evaluation of uncertainties related to passive systems performance, *Nuclear Engineering and Design*, Vol. 230, No. 1-3, pp. 93-106.

Byun, C.S., Jerng, D.W., Todreas, N.E. & Driscoll, M.J., 2000, Conceptual design and analysis of a semi-passive containment cooling system for a large concrete containment, *Nuclear Engineering and Design*, Vol. 199, pp. 227-242.

Carey, V.P., 1992, *Liquid-vapour phase change phenomena: An introduction to the thermodynamics of vaporization and condensation processes in heat transfer equipment*, Hemisphere publishing corporation, Washington.

Cengel, Y.A. & Boles, M.A., 2002, *Thermodynamics an engineering approach*, 4th ed., McGraw Hill, New York.

Chen K.S., Tsai, S.T., & Yu, W.T., 1991, Experimental study of the heat transfer characteristics of a two-phase double-loop thermosyphon, *Experimental Heat Transfer*, Vol. 4, pp. 171-188.

Chen, S.L., Gerner, F.M. & Tien, C.L., 1987, General film condensation correlations, *Experimental Heat Transfer*, Vol. 1, pp. 93-107.

Cheng, K.C., Morioka I., Ichimiya K., Sadler G.W., 1982, Experimental study of a two-phase thermosyphon system, *Alternative Energy Sources* (ed. Veziroğlu, T.N.), Vol. 1, Solar Collector Storage, Ann Arbor, pp. 151-170.

Chexal, V.K. and Bergles, A.E., 1986, Two-phase instabilities in a low pressure natural circulation loop, *AIChE Symposium Series*, Vol. 69, No. 131, pp. 37-45.

Chisholm, D., 1983, Two-phase flow in pipelines and heat exchangers, George Godwin, London.

Cole-Parmer Technical library, *Emissivity of specific materials*, http://www.coleparmer.com/techinfo/techinfo.asp?htmlfile=Emissivity.htm&ID=254.

Collier, J.G. & Thome, J.R., 1994, *Convective boiling and condensation*, 3rd ed., Clarendon press, Oxford.

Cooper, M.G., 1984, Saturation nucleate boiling. A simple correlation., *1st UK National Conference on Heat Transfer*, Vol. 2, pp. 785-793.

Dobson, R.T., 1993, Transient response of a closed loop thermosyphon, *R&D Journal*, Vol. 9, No. 1, pp. 32-38.

Dobson, R.T., 2005, Personal communications.

Dobson, R.T., 2006, A novel closed loop thermosyphon heat pipe reactor cavity cooling system for a pebble bed modular reactor, *8th Int. Heat Pipe Symp.*, 24-27 Sept. 2006, Kumamoto, pp. 384-397.

Eskom, *Nuclear Power, Future, Pebble Bed Reactor Technology*, http://www.eskom.co.za/nuclear_energy/pebble_bed/pebble_bed.html

Fukuda, K. & Kobori, T., 1979, Classification of two-phase flow instability by density wave oscillation model, *Journal of Nuclear Science and Technology*, Vol. 16, No. 2, pp. 95-108.

Greif, R., 1988, Natural circulation loops, *Journal of Heat Transfer*, Vol. 110, pp. 1243-1988.

Hsu, J-T., Ishii, M. & Hibiki, T., 1998, Experimental study on two-phase natural circulation and flow termination in a loop, *Nuclear Engineering and Design*, Vol. 186, pp. 395-409.

IAEA, 2000, Heat transport and afterheat removal for gas cooled reactors under accident conditions, (Electronic version, www.IAEC), TECDOC-1162, IAEA, Vienna.

IAEA, *50 Years of nuclear energy*, http://www.iaea.org/About/Policy/GC/GC48/Documents/gc48inf-4_ftn3.pdf

IEA, 2006, *Key world energy statistics*, http://www.iea.org/dbtw-wpd/Textbase/nppdf/free/2006/key2006.pdf

Incropera, F.P. & De Witt, D.P., 2002, Fundamentals of heat and mass transfer, 5th ed., John Wiley and Sons, Hoboken.

Infrared-thermography, *Emissivity values for common materials*, http://www.infrared-thermography.com/material-1.htm.

Jiang, S.Y., Yao, M.S., Bo, J.H. & Wu, S.R., 1995, Experimental simulation study on the start-up of the 5 MW nuclear heating reactor, *Nuclear Engineering and Design*, Vol. 158, pp. 111-123.

Kemp, Y., 2007, *Banks give Eskom power a thumbs down*, http://www.busrep.co.za/index.php?fArticleId=3646100

Khodabandeh, R. and Palm, B., 2002, Influence of system pressure on the boiling heat transfer coefficient in a closed two-phase thermosyphon loop, *International Journal of thermal sciences*, Vol. 41, pp. 619-624.

Klimenko, V.V., 1988, A generalized correlation for two-phase forced flow heat transfer, *International Journal of Heat and Mass Transfer*, Vol. 31, No. 3, pp. 541-552.

Klimenko, V.V., 1990, A general correlation for two phase forced flow heat transfer-second assessment, *International Journal of Heat and Mass Transfer*, Vol. 33, No. 10 pp. 2073-2088.

Knaani, A. and Zvirin, Y., 1990, Investigation of a two phase natural circulation loop, *Proceedings of the 9th International Heat Transfer Conference - Jerusalem*, Vol. 1, pp. 395-400.

Knaani, A. and Zvirin, Y., 1993, Bifurcation phenomena in two-phase natural circulation, *International Journal of Multiphase flow*, Vol. 19, No. 6, pp. 1129-1151.

Kröger, D.G., 2004, *Air-cooled heat exchangers and cooling towers: Thermal-flow performance evaluation and design*, Penwell Corporation, Tulsa.

Kutateladze, S.S, 1961, Boiling Heat Transfer, *International Journal of Heat and Mass Transfer*, Vol. 4, pp. 31-45.

Lee, S.Y., Kim, Y.L., 1999, An analytical investigation of role of expansion tank in semi-closed two-phase natural circulation loop, *Nuclear Engineering and Design*, Vol. 190, pp. 353-360.

Lee, Y., Rhi, S.H., 2000, Lumped and sectorial (flow pattern) methods for computer simulation of two-phase loop thermosyphons, *Proceedings of the 6th International Heat Pipe Symposium - Chiang Mai*, pp. 14-23.

Le Grange, C.N., 1996, Simulasie van ‘n geslote natuurlike konveksie sirkulasielus, Final year project for B.Eng degree at Univcersity of Stellenbosch.

Liu, H., Todreas, N.E. & Driscoll, M.J., 2000, An experimental investigation of a passive cooling unit for nuclear plant containment, *Nuclear Engineering and Design*, Vol. 199, pp. 243-255.

Liu, Z. and Winterton, R.H.S., 1991, A general correlation for saturated and subcooled flow boiling in tubes and annuli, based on a nucleate pool boiling equation, *International Journal of Heat and Mass Transfer*, Vol. 34, No. 11, pp. 2759-2766.

Matzner, D., 2004, PBMR existing and future R&D test facilities, *2nd International Topical Meeting on High Temperature Reactor Technology - Beijing*, #Paper A04, pp. 1-26.

Mangxamba, S., Bailey, C. & Prince, N., 2007, *Power cuts are bad news for all*, http://www.capeargus.co.za/index.php?fArticleId=3635973

Mikron Instrumentation Company, *Table of emissivity of various surfaces for infrared thermometry*,http://www-eng.lbl.gov/~dw/projects/DW4229_LHC_detector_analysis/ calculations/ emissivity2.pdf.

Mills, A.F., 1999, *Heat Transfer*, 2nd ed., Prentice Hall, Upper Saddle River.

Ohashi, K., Hayakawa, H., Yamada, M., Hayashi, T. & Ishii, T., 1998, Preliminary study on the application of the heat pipe to the passive decay heat removal system of the modular HTR, *Progress in Nuclear Energy*, Vol. 32, No. 3-4, pp. 587-594.

PBMR (a), *How did South Africa come to the forefront?*, http://www.pbmr.com/download/HowdidSA.pdf

PBMR (b), *Project status*, http://www.pbmr.com/index.asp?content=8

PBMR (c), *How the PBMR works*, http://www.pbmr.com/download/Operation.pdf

Sha, M.M., 1989, A general correlation for heat transfer during film condensation inside pipes, *International Journal of Heat and Mass Transfer*, Vol. 22, pp. 547-556.

Sha, W.T., Chien T.H., Sun, J.G., Chao, B.T., 2004, Analysis of large-scale tests for AP-600 passive containment cooling system, *Nuclear Engineering and Design*, Vol. 232, pp. 197-216.

Soliman, M., Schuster, J.R., Berenson, P.J., 1968, A general heat transfer correlation for annular flow condensation, *Journal of Heat Transfer*, Vol. 90, pp. 267-276.

Steiner, D. and Taborek, J., 1992, Flow boiling heat transfer in vertical tubes correlated by an asymptotic model, *Heat Transfer Engineering*, Vol. 13, No. 2, pp. 43-68.

Takada, S., 2004, Research and development on passive cooling system, *Nuclear Engineering and Design*, Vol. 233, pp. 185-195.

Thielman, J., Ge, P., Wu, Q. & Parme, L., 2005, Evaluation and optimization of General Atomic's GT-MHR reactor cavity cooling system using an axiomatic design approach, *Nuclear Engineering and Design*, Vol. 235, pp. 1389-1402.

Traviss, D.P., Rohsenow, W.M., Baron, A.B., 1973, Forced convection condensation in tubes: A heat transfer correlation for condenser design, *ASHRAE Transactions* Vol. 79, Part 1, pp. 157-165.

Van Staden, M.P., 2004, Analysis of effectiveness of the PBMR Cavity Cooling System, *2nd International Topical Meeting on High Temperature Reactor Technology - Beijing*, #Paper C20, pp. 1-16.

Vijayan, P.K., Mehta, S.K. & Date, A.W., 1991, On the steady-state performance of natural circulation loops, *International Journal of Heat and Mass Transfer*, Vol. 34, No. 9, pp. 2219-2230.

Vijayan, P.K., Patil, A.P., Pilkwal, D.S., Saha, D. & Raj, V.V., 2000, An assessment of pressure drop and void fraction correlations with data from two-phase natural circulation loops, *Heat and Mass Transfer*, Vol. 36, pp. 541-548.

Vincent, C.C.J. and Kok, J.B.W., 1992, Investigation of the overall transient performance of the industrial two-phase closed loop thermosyphon, *International Journal of Heat and Mass Transfer*, Vol. 35, No. 6, pp. 1419-1426.

Wang, S.B., Pan, C., 1998, Two-phase flow instability experiment in a natural circulation loop using the Taguchi method, *Experimental Thermal Science*, Vol. 17, pp. 189-201.

Welander, P., 1967, On the oscillatory instability of a differentially heated fluid loop, *Journal of Fluid Mechanics*, Vol. 20, No. 1, pp. 17-30.

Whalley, P.B., 1987, *Boiling, condensation and gas-liquid flow*, Clarendon Press, Oxford.

White, F.M., 1999, *Fluid mechanics*, *4th ed*., McGraw-Hill, Singapore.

Wikipedia, 2007, *Nuclear Power*, http://en.wikipedia.org/wiki/Nuclear_power

Wu, C.Y., Wang, S.B. & Pan, C., 1996, Chaotic oscillations in a low pressure two-phase natural circulation loop under low power and high inlet subcooling conditions, *Nuclear Engineering and Design*, Vol. 162, pp. 223-232.

Yang, R., Liu, R., Zhong, Y. & Liu, T., 2006, Experimental study on convective heat transfer of water flow in a heated tube under natural circulation, *Nuclear Engineering and Design*, Vol. 236, pp.1902-1908.

Yilmaz, T., 1991, Computer simulation of two-phase flow thermosyphon solar water heating system, *Energy Conversion and Management*, Vol. 32, No. 2, pp. 133-144.

APPENDIX A: THERMOPHYSICAL PROPERTIES OF MATERIALS

A.1 Properties of Water

Thermophysical properties of saturated water from 273.15 K – 380 K, Kröger (1998)

$$c_{pv} = 1.3605\text{x}10^{3} + 2.31334T - 2.46784\text{x}10^{-10}T^{5} + 5.91332\text{x}10^{-13}T^{6} \quad \textbf{\{A.1\}}$$

$$\mu_v = 2.562435\text{x}10^{-6} + 1.816683\text{x}10^{-8}T + 2.579066\text{x}10^{-11}T^{2} - 1.067299\text{x}10^{-14}T^{3} \quad \textbf{\{A.2\}}$$

$$k_v = 1.3046\text{x}10^{-2} - 3.756191\text{x}10^{-5}T + 2.217964\text{x}10^{-7}T^{2} - 1.111562\text{x}10^{-10}T^{3} \quad \textbf{\{A.3\}}$$

$$\rho_v = -4.062329056 + 0.10277044T - 9.76300388\text{x}10^{-4}T^{2} + 4.475240795\text{x}10^{-6}T^{3} - 1.004596894\text{x}10^{-8}T^{4} + 8.9154895\text{x}10^{-12}T^{5} \quad \textbf{\{A.4\}}$$

$$c_{pl} = 8.15599\text{x}10^{3} - 28.0627T + 5.11283\text{x}10^{-2}T^{2} - 2.17582\text{x}10^{-13}T^{6} \quad \textbf{\{A.5\}}$$

$$\mu_l = 2.414\text{x}10^{-5}\,\text{x}10^{247.8/(T-140)} \quad \textbf{\{A.6\}}$$

$$k_l = -6.14255\text{x}10^{-3} + 6.9962\text{x}10^{-3}T - 1.01075\text{x}10^{-5}T^{2} + 4.74737\text{x}10^{-12}T^{4} \quad \textbf{\{A.7\}}$$

$$\rho_l = (1.49343\text{x}10^{-3} - 3.7164\text{x}10^{-6}T + 7.09782\text{x}10^{-9}T^{2} - 1.90321\text{x}10^{-20}T^{6})^{-1} \quad \textbf{\{A.8\}}$$

$$h_{fg} = 3.4831814\text{x}10^{6} - 5.8627703\text{x}10^{3}T + 12.139568T^{2} - 1.40290431\text{x}10^{-2}T^{3} \quad \textbf{\{A.9\}}$$

$$T = 164.630366 + 1.832295\text{x}10^{-3}P + 4.27215\text{x}10^{-10}P^{2} + 3.738954\text{x}10^{3}P^{-1} - 7.01204\text{x}10^{-5}P^{-2} + 16.161488\ln(P) - 1.437169\text{x}10^{-4}P\ln(P) \quad \textbf{\{A.10\}}$$

A.2 Properties of Air

Thermospysical properties of air adapted from Cengel and Boles (2002)

$Pr = 0.69$

$\beta = 1/T \ \ K^{-1}$

$$k = -9.9188021\text{x}10^{-20}T^6 + 3.6893529\text{x}10^{-16}T^5 - 5.7660479\text{x}10^{-13}T^4 + 4.9974035\text{x}10^{-10}T^3 - 2.6206987x10^{-7}T^2 + 1.3662771x10^{-4}T - 2.3880862x10^{-4} \quad \textbf{\{A.11\}}$$

$$\nu = -2.1515612\text{x}10^{-22}T^6 + 7.56314\text{x}10^{-19}T^5 - 1.02857\text{x}10^{-15}T^4 + 6.6035816\text{x}10^{-13}T^3 - 1.1432998x10^{-10}T^2 + 6.2789679x10^{-8}T - 4.1066067x10^{-6} \quad \textbf{\{A.12\}}$$

A.3 Properties of Stainless Steel Heater Plate

Values for density and specific heat of steel found in textbook of Mills (1999). Emissivity value for oxidized stainless steel plate found from www.infrared-thermography.com, Cole-Parmer Technical library and Mikron Instrument Company.

$\rho = 7900 \text{ kg/m}^3$ $\qquad$ $c = 480 \text{ J/kg.K}$

$\varepsilon = 0.85$

A.4 Properties of Aluminium Fin

Values for density and specific heat of aluminium found in textbook of Mills (1999). Emissivity value for commercial aluminium sheet found from www.infrared-thermography.com, Cole-Parmer Technical library and Mikron Instrument Company.

$\rho = 2700 \text{ kg/m}^3$ $\qquad$ $c = 900 \text{ J/kg.K}$

$\varepsilon = 0.09$ $\qquad$ $\varepsilon = 0.18$ (oxidised)

APPENDIX B: DERIVATION OF DIFFERENCE EQUATIONS

B.1 Derivation of Equation 3.10

Starting from equation 3.9

$$\dot{Q}_{cr} - \dot{Q}_{r,rf} - \dot{Q}_{c,ra} = \frac{dU_r}{dt}$$

where

$$\frac{dU_r}{dt} = \frac{d(mu)_r}{dt} = u_r \frac{dm_r}{dt} + m_r \frac{du_r}{dt}$$

Since this control volume represents a solid material

$$\frac{dm_r}{dt} \approx 0$$

thus $\frac{dU_r}{dt} = m_r \frac{du_r}{dt} = m_r c_r \frac{dT_r}{dt}$

Substituting into equation 3.9 and integrating with respect to time

$$\int_t^{t+\Delta t} (\dot{Q}_{cr} - \dot{Q}_{r,rf} - \dot{Q}_{c,ra}) dt = m_r c_r \int_{T_r^t}^{T_r^{t+\Delta t}} dT_r$$

$$\Delta t(\dot{Q}_{cr} - \dot{Q}_{r,rf} - \dot{Q}_{c,ra}) = m_r c_r (T_r^{t+\Delta t} - T_r^t)$$

Rearranging the equation

$$T_r^{t+\Delta t} = T_r^t + \Delta t(\dot{Q}_{cr} - \dot{Q}_{r,rf} - \dot{Q}_{c,ra}) / (m_r c_r)$$

and writing the heat transfer rates in terms of temperatures and resistances gives equation 3.10

$$T_r^{t+\Delta t} = T_r^t + \frac{\Delta t}{m_r c_r} \left(\frac{T_c^t - T_r^t}{R_{cr}} - \frac{T_r^t - T_f^t}{R_{r,rf}} - \frac{T_r^t - T_a^t}{R_{c,ra}} \right)$$

Where $R_{cr} = \frac{1}{U_c A_{z,r}}$

$$R_{r,rf} = \left(\frac{1-\varepsilon_r}{\varepsilon_r A_{z,r}} + \frac{1}{F_{rf} A_{z,r}} + \frac{1-\varepsilon_f}{\varepsilon_f A_{z,f}} \right) \left(\frac{1}{5.67 * 10^{-8} (T_r^2 + T_f^2)(T_r + T_r)} \right)$$

$$R_{c,ra} = \frac{1}{h_{c,ra} A_{z,r}}$$

B.2 Derivation of Equation 3.12

Starting from equation 3.8

$$\frac{dQ}{dt} - \frac{dW}{dt} = \frac{d}{dt}\left(\int_{cv} e\rho dV \right) + (e\rho Av)_{out} - (e\rho Av)_{in}$$

During experimentation it was found that buoyancy driven air flow existed, it was however hampered somewhat by the lid placed on top of the heating chamber so that the flow rate was very small. An order of magnitude calculation will determine whether or not the flux terms can safely be ignored in the derivation of equation 3.12.

Assume an average temperature of 550 ºC for the heater plate with the fin temperature being 100 ºC at the top and 50 ºC at the bottom (figures based on experiment). Assume the air temperature is an average of the fin and heater plate temperature so that the air at the top of the heating chamber is at 325 ºC and the bottom at 300 ºC (This assumption is made since no data for it exists). With a linear temperature distribution a 1.25 ºC temperature difference exists between each of the twenty control volumes.

According to Incropera and De witt (2002) for free convection of gasses a typical convection heat transfer coefficient lies in the range of 2-25 W/m^{2}K. Assume a conservative heat transfer coefficient of 4 W/m^{2}K that correspond to the coefficients calculated using the correlations described in the text.

<u>Calculation of the heat transfer term:</u>

$$A_{z,f} = 0.010875 \text{ m}^2 \text{ and } A_{z,r} = 0.01125 \text{ m}^2$$

$$h_{c,ra} = h_{c,af} = 4 \text{ W/m}^2\text{K}$$

$$R_{c,af} = \frac{1}{h_{c,af} A_{z,f}} = 22.98850575 \text{ K/W}$$

$$R_{c,ra} = \frac{1}{h_{c,ra} A_{z,r}} = 22.22222222 \text{ K/W}$$

$$Q_{c,af} = \frac{T_a - T_f}{R_{c,af}} = \frac{300 - 50}{22.98850575} = 10.875 \text{ W}$$

$$Q_{c,ra} = \frac{T_r - T_a}{R_{c,ra}} = \frac{550 - 325}{22.22222222} = 10.125 \text{ W}$$

$$\underline{\Delta Q = 0.75 \text{ W}}$$

Calculation of the energy flux term:

In order to do this calculation an estimate of the velocity of the air is required. To make an estimation assume that the gain in kinetic energy of the air element is approximately equal to the work done by the buoyancy force so that:

$$0.5\rho v^2 = g\Delta\rho L$$

Rewrite in terms of velocity:

$$v = \sqrt{2gL\frac{\Delta\rho}{\rho}}$$

For three consecutive control volumes at temperatures 313.75 ºC, 315 ºC and 316.25 ºC calculate the specific heat, internal energy, density and velocity using the equations on this page and the next.

$$u_a = c_a T_a$$

$$\rho_a = 8.5233344*10^{-17}T_a^6 - 3.2630691*10^{-13}T_a^5 + 5.0903405*10^{-10}T_a^4 - 0.0000004169916T_a^3 + 0.00019258462T_a^2 - 0.049869465T_a + 6.6708097$$

$$c_a = 6.4531274*10^{-15}T_a^6 - 2.0858673*10^{-11}T_a^5 + 2.5725831*10^{-08}T_a^4 - 0.000015461597T_a^3 + 0.0051330888T_a^2 - 0.94513242T_a + 1083.449$$

The area is the cross-sectional area: fin breadth multiplied by the space between the heater plate and fin.

$$A_x = 0.145*0.1 = 0.0145 \text{ m}^2$$

The length of the control volume is L = 0.075 m.

Table B.1: Energy flux calculation values

cv #	1	2	3
T_a [K]	586.9	588.15	589.4
c_a [J/kgK]	1034.703315	1034.988	1035.275
u_a [J/kg]	324638.165	326021.4	327405.7
ρ_a [kg/m^3]	0.596674942	0.595357	0.594047
A_x [m^2]	0.0145	0.0145	0.0145

$$v_{in} = \sqrt{2gL\frac{\Delta\rho}{\rho}} = \sqrt{2gL\frac{(\rho_1 - \rho_2)}{\rho_1}} = 0.057003986 \text{ m/s}$$

$$v_{out} = \sqrt{2gL\frac{\Delta\rho}{\rho}} = \sqrt{2gL\frac{(\rho_2 - \rho_3)}{\rho_2}} = 0.056901638 \text{ m/s}$$

$$(u\rho Av)_{in} = 324638.165*0.596674942*0.0145*0.057003986 = 160.1071044 \text{ W}$$

$$(u\rho Av)_{out} = 326021.4*0.595357*0.0145*0.056901638 = 160.1461627 \text{ W}$$

$$(u\rho Av)_{out} - (u\rho Av)_{in} = 0.039058 \text{ W}$$

This order of magnitude calculation indicate that the size of the flux term is only 5% of the value of the heat transferred, this is considered small enough to allow the flux terms to disappear from the derivation. The one dimensional assumption means the dependant variables such as energy and density are constant across any cross section of the tube, varying only in the axial direction, i.e. from one control volume to the next. Therefore the integral term can be written as:

$$\frac{d}{dt}\left(\int_{cv} e\rho dV\right) = \frac{d}{dt}\left(e\rho V\right) = \frac{d\left(em\right)}{dt}$$

So that equation 3.8 becomes:

$$\frac{dQ}{dt} - \frac{dW}{dt} = \frac{d(em)}{dt}$$

Rewriting with the energy term consisting of the internal energy, *u*, the work term disappearing and the heat transfer rates corresponding to that shown in figure 7 equation 3.11 appears:

$$\dot{Q}_{c,ra} - \dot{Q}_{c,af} = \frac{d(u_a m_a)}{dt}$$

where

$$\frac{d(u_a m_a)}{dt} = m_a \frac{du_a}{dt} + u_a \frac{dm_a}{dt}$$

For a small time step and due to the low density of air $\frac{dm_a}{dt} \approx 0$ so that

$$\dot{Q}_{c,ra} - \dot{Q}_{c,af} = m_a \frac{du_a}{dt}$$

Assuming ideal gas behaviour so that internal energy and specific heat is a function of temperature alone then $\frac{du}{dt} = c_v \frac{dT}{dt}$

Thus equation 3.11 becomes

$$\dot{Q}_{c,ra} - \dot{Q}_{c,af} = m_a c_{v,a} \frac{dT_a}{dt}$$

Integrating with respect to time

$$\int_t^{t+\Delta t} (\dot{Q}_{c,ra} - \dot{Q}_{c,af}) dt = m_a c_{v,a} \int_{T_a^t}^{T_a^{t+\Delta t}} dT_a$$

$$\Delta t(\dot{Q}_{c,ra} - \dot{Q}_{c,af}) = m_a c_{v,a} (T_a^{t+\Delta t} - T_a^t)$$

Rearranging the terms

$$T_a^{t+\Delta t} = T_a^t + \Delta t(\dot{Q}_{c,ra} - \dot{Q}_{c,af}) / (m_a c_a)$$

and writing the heat transfer rates in terms of temperatures and resistances gives equation 3.12

$$T_a^{t+\Delta t} = T_a^t + \frac{\Delta t}{m_a c_a} \left(\frac{T_r^t - T_a^t}{R_{c,ra}} - \frac{T_a^t - T_f^t}{R_{c,af}} \right)$$

Where $R_{c,af} = \frac{1}{h_{c,af} A_{z,f}}$

B.3 Derivation of Equation 3.14

Start with equation 3.8

$$\frac{dQ}{dt} - \frac{dW}{dt} = \frac{d}{dt} \left(\int_{cv} e \rho dV \right) + (e \rho A v)_{out} - (e \rho A v)_{in}$$

The one dimensional assumption means the dependant variables such as energy and density are constant across any cross section of the tube, varying only in the axial direction, i.e. from one control volume to the next.

Therefore the integral term can be written as:

$$\frac{d}{dt}\left(\int_{cv} e\rho dV\right) = \frac{d}{dt}\left(e\rho V\right) = \frac{d\left(em\right)}{dt}$$

So that equation 3.8 becomes:

$$\frac{dQ}{dt} - \frac{dW}{dt} = \frac{d(em)}{dt}$$

Rewriting, with the energy term consisting of the internal energy, *u*, the work term disappearing and the heat transfer rates corresponding to that shown in figure 8, equation 3.13 appears:

$$\dot{Q}_{c,\,fba} = \frac{d(u_{ba} m_{ba})}{dt}$$

where

$$\frac{d(u_{ba} m_{ba})}{dt} = m_{ba}\frac{du_{ba}}{dt} + u_{ba}\frac{dm_{ba}}{dt}$$

For a small time step and due to the low density of air $\frac{dm_{ba}}{dt} \approx 0$ so that

$$\dot{Q}_{fba} = m_{ba}\frac{du_{ba}}{dt}$$

Assuming ideal gas behaviour so that internal energy and specific heat is a function of temperature only then

$$\frac{du}{dt} = c_v \frac{dT}{dt}$$

Thus equation 3.13 becomes

$$\dot{Q}_{c,\,fba} = m_{ab} c_{v,ba}\frac{dT_{ba}}{dt}$$

Integrating with respect to time

$$\int_{t}^{t+\Delta t} \dot{Q}_{c,fba}\, dt = m_{ba} c_{v,ba} \int_{T_{ba}^{t}}^{T_{ba}^{t+\Delta t}} dT_{ba}$$

$$\Delta t(\dot{Q}_{c,fba}) = m_{ba} c_{v,ba} (T_{ba}^{t+\Delta t} - T_{ba}^{t})$$

Rearranging the terms

$$T_{ba}^{t+\Delta t} = T_{ba}^{t} + \Delta t(\dot{Q}_{c,fba}) / (m_{ba} c_{ba})$$

and writing the heat transfer rates in terms of temperatures and resistances gives equation 3.14

$$T_{ba}^{t+\Delta t} = T_{ba}^{t} + \frac{\Delta t}{m_{ba} c_{ba}} \left(\frac{T_{f}^{t} - T_{ba}^{t}}{R_{c,fba}} \right)$$

Where $R_{c,fba} = \dfrac{1}{h_{c,fba} A_{z,f}}$

B.4 Derivation of Equation 3.16

Starting from equation 3.15

$$\dot{Q}_{r,rf} + \dot{Q}_{c,af} - \dot{Q}_{fw} - \dot{Q}_{c,fba} = \frac{dU_f}{dt}$$

where

$$\frac{dU_f}{dt} = \frac{d(mu)_f}{dt} = u_f \frac{dm_f}{dt} + m_f \frac{du_f}{dt}$$

Since this control volume represents a solid material

$$\frac{dm_f}{dt} \approx 0$$

thus $\dfrac{dU_f}{dt} = m_f \dfrac{du_f}{dt} = m_f c_f \dfrac{dT_f}{dt}$

Substituting into equation 3.15 and integrating with respect to time

$$\int_t^{t+\Delta t} (\dot{Q}_{r,rf} + \dot{Q}_{c,af} - \dot{Q}_{fw} - \dot{Q}_{c,fba})dt = m_f c_f \int_{T_f^t}^{T_f^{t+\Delta t}} dT_f$$

Rearranging the equation

$$T_f^{t+\Delta t} = T_f^t + \Delta t(\dot{Q}_{r,rf} + \dot{Q}_{c,af} - \dot{Q}_{fw} - \dot{Q}_{c,fba})/(m_f c_f)$$

and writing the heat transfer rates in terms of temperatures and resistances gives equation 3.10

$$T_f^{t+\Delta t} = T_f^t + \frac{\Delta t}{m_f c_f}\left(\frac{T_r^t - T_f^t}{(R_{r,rf}^{-1} + R_{c,af}^{-1})^{-1}} - \frac{T_f^t - T_w^t}{R_{fw}} - \frac{T_f^t - T_{ba}^t}{R_{c,fba}} \right)$$

Where $R_{fw} = \frac{1}{h_i A_z}$

B.5 Derivation of Equation 3.18

Starting from equation 3.8

$$\frac{dQ}{dt} - \frac{dW}{dt} = \frac{d}{dt}\left(\int_{cv} e\rho dV \right) + (e\rho Av)_{out} - (e\rho Av)_{in}$$

The one dimensional assumption means the dependant variables such as energy and density are constant across any cross section of the tube, varying only in the axial direction, i.e. from one control volume to the next. Therefore the integral term can be written as:

$$\frac{d}{dt}\left(\int_{cv} e\rho dV \right) = \frac{d}{dt}(e\rho V) = \frac{d(em)}{dt}$$

So that equation 3.8 becomes:

$$\frac{dQ}{dt} - \frac{dW}{dt} = \frac{d(em)}{dt} + (e\rho Av)_{out} - (e\rho Av)_{in}$$

Rewriting with the heat transfer rate and work terms handled as discussed in section 3.2.4 equation 3.17 appears taking into account $e = u$ in the control volume term and $e = u + pv = h$ across the flow boundaries and $\rho A v = \dot{m}$:

$$-\dot{S} = \frac{d}{dt}(um) + (\dot{m}h)_{out} - (\dot{m}h)_{in}$$

Integrating with respect to time

$$\int_t^{t+\Delta t} \left(\dot{m}(h_{in} - h_{out}) - \dot{S}\right)dt = \int_{U^t}^{U^{t+\Delta t}} dU$$

$$\left(\dot{m}(h_{in} - h_{out}) - \dot{S}\right)\Delta t = U^{t+\Delta t} - U^t$$

Rearranging the terms gives equation 3.18

$$U^{t+\Delta t} = U^t + \Delta t\left((\dot{m}h)_{in} - \dot{S} - (\dot{m}h)_{out}\right)$$

$$u^{t+\Delta t} = \frac{U^t}{m^{t+\Delta t}} + \frac{\Delta t}{m^{t+\Delta t}}\left((\dot{m}h)_{in} - \dot{S} - (\dot{m}h)_{out}\right)$$

This equation will be solved through an iteration process due to the new time step control volume mass term on the right hand side of the equation.

B.6 Derivation of Equation 3.21

Starting with equation 3.6

$$\sum \boldsymbol{F} = \frac{d}{dt}\left(\int_{cv} \boldsymbol{v}\rho dV\right) + (\dot{m}\boldsymbol{v})_{out} - (\dot{m}\boldsymbol{v})_{in}$$

The force and velocity are vectors, however only the force and velocity components in the direction of the flow are applicable due to the one dimensional assumption. The one dimensional assumption also means the dependant variables such as velocity and density are constant across any cross section of the tube, varying only in the axial

direction, i.e. from one control volume to the next. Therefore the integral term can be written as:

$$\frac{d}{dt}\left(\int_{cv} v\rho dV\right) = \frac{d}{dt}\left(v\rho V\right) = \frac{d\left(vm\right)}{dt}$$

So that equation 3.6 becomes:

$$\sum F = \frac{d(mv)}{dt} + (\dot{m}v)_{out} - (\dot{m}v)_{in}$$

Rewriting with the force terms reflecting figure 11

$$(P_{in} - P_{out})A_x - \rho gL\sin\theta A_x - \tau_w A_z - \tau_m A_z = \frac{d(mv)}{dt} + (\dot{m}v)_{out} - (\dot{m}v)_{in}$$

where $\rho A_x v = \dot{m}$ and $m = \rho V = \rho A_x L$ so that

$$(P_{in} - P_{out})A_x - \rho gL\sin\theta A_x - \tau_w A_z - \tau_m A_z = \frac{d(\rho A_x Lv)}{dt} + (\rho A_x Lvv)_{out} - (\rho A_x Lvv)_{in}$$

Rearrange the terms and divide by A_x

$$\frac{1}{A_x}\frac{d(\rho A_x Lv)}{dt} = (P_{in} - P_{out}) - \rho gL\sin\theta - \tau_w \frac{A_z}{A_x} - \tau_m \frac{A_z}{A_x} - (\rho Lvv)_{out} + (\rho Lvv)_{in}$$

Noting that L is independent of time so that

$$\frac{1}{A_x}\frac{d(\rho A_x Lv)}{dt} = \frac{L}{A_x}\frac{d(\rho A_x v)}{dt} = \frac{L}{A_x}\frac{d(\dot{m})}{dt}$$

The equation then becomes

$$\frac{L}{A_x}\frac{d\dot{m}}{dt} = (P_{in} - P_{out}) - \rho gL\sin\theta - \tau_w \frac{A_z}{A_x} - \tau_m \frac{A_z}{A_x} - (\rho Lvv)_{out} + (\rho Lvv)_{in}$$

Integrating around the loop it can be seen that the flux terms and pressure term cancel out. Rewriting the equation as the sum of the elements, the first term on the RH side is

the driving force and the last two terms (friction and minor loss terms, minor losses include bends and orifice plate) are the retarding forces:

$$\frac{d\dot{m}}{dt}\sum_{k=1}^{N}\frac{L_k}{A_{x,k}} = -\sum_{k=1}^{N}\rho_k g L_k \sin\theta_k - \sum_{k=1}^{N}\tau_{w,k}\frac{A_{z,k}}{A_{x,k}} - \sum_{k=1}^{N}\tau_{m,k}\frac{A_{z,k}}{A_{x,k}}$$

The friction force is calculated by $\tau_w = \frac{1}{2}C_f \rho_k v_k^2$ where C_f is the Fanning friction factor and the minor losses $\tau_m = \frac{1}{2}K\rho_k v_k^2$ where K is an empirically determined minor loss coefficient so that the equation becomes

$$\frac{d\dot{m}}{dt}\sum_{k=1}^{N}\frac{L_k}{A_{x,k}} = -\sum_{k=1}^{N}\rho_k g L_k \sin\theta_k - \sum_{k=1}^{N}\frac{1}{2}C_f\rho_k v_k^2\frac{A_{z,k}}{A_{x,k}} - \sum_{k=1}^{N}\frac{1}{2}K\rho_k v_k^2\frac{A_{z,k}}{A_{x,k}}$$

Combining the retardation terms

$$\frac{d\dot{m}}{dt}\sum_{k=1}^{N}\frac{L_k}{A_{x,k}} = -\sum_{k=1}^{N}\rho_k g L_k \sin\theta_k - \sum_{k=1}^{N}\frac{1}{2}(C_f + K)\rho_k v_k^2\frac{A_{z,k}}{A_{x,k}}$$

and noting that

$$\frac{1}{2}(C_f + K)\rho_k v_k^2\frac{A_{z,k}}{A_{x,k}} = \frac{1}{2}\frac{(C_f + K)}{\rho_k}\rho_k^2 v_k^2 A_{x,k}^2\frac{A_{z,k}}{A_{x,k}^3} = \frac{1}{2}\frac{(C_f + K)}{\rho_k}\frac{A_{z,k}}{A_{x,k}^3}\dot{m}^2$$

the equation becomes

$$\frac{d\dot{m}}{dt}\sum_{k=1}^{N}\frac{L_k}{A_{x,k}} = -\sum_{k=1}^{N}\rho_k g L_k \sin\theta_k - \sum_{k=1}^{N}\frac{1}{2}\frac{(C_f + K)}{\rho_k}\frac{A_{z,k}}{A_{x,k}^3}\dot{m}^2$$

Dividing by $\sum_{k=1}^{N}\frac{L_k}{A_{x,k}}$

$$\frac{d\dot{m}}{dt} = -\frac{\sum_{k=1}^{N} \rho_k g L_k \sin\theta_k}{\sum_{k=1}^{N} \frac{L_k}{A_{x,k}}} - \frac{\sum_{k=1}^{N} \frac{1}{2} \frac{(C_f + K)}{\rho_k} \frac{A_{z,k}}{A_{x,k}^3} \dot{m}^2}{\sum_{k=1}^{N} \frac{L_k}{A_{x,k}}}$$

and integrating with respect to time

$$\int_{\dot{m}^t}^{\dot{m}^{t+\Delta t}} d\dot{m} = \int_t^{t+\Delta t} \left(-\frac{\sum_{k=1}^{N} \rho_k g L_k \sin\theta_k}{\sum_{k=1}^{N} \frac{L_k}{A_{x,k}}} - \frac{\sum_{k=1}^{N} \frac{1}{2} \frac{(C_f + K)}{\rho_k} \frac{A_{z,k}}{A_{x,k}^3} \dot{m}^2}{\sum_{k=1}^{N} \frac{L_k}{A_{x,k}}} \right) dt$$

Rearranging the terms gives equation 3.21

$$\dot{m}^{t+1} = \dot{m}^t + \Delta t \left(-\frac{\sum_{k=1}^{N} \rho_k g L_k \sin\theta_k}{\sum_{k=1}^{N} \frac{L_k}{A_{x,k}}} - \frac{\sum_{k=1}^{N} \frac{1}{2} \frac{(C_f + K)}{\rho_k} \frac{A_{z,k}}{A_{x,k}^3} (\dot{m}^t)^2}{\sum_{k=1}^{N} \frac{L_k}{A_{x,k}}} \right)$$

B.7 Derivation of Equation 3.23

Starting from equation 3.8

$$\frac{dQ}{dt} - \frac{dW}{dt} = \frac{d}{dt}\left(\int_{cv} e\rho dV \right) + (e\rho A v)_{out} - (e\rho A v)_{in}$$

The flux terms are assumed to be negligibly small since the temperature gradient along the height of the tank will induce a very small natural circulation flow rate. The one dimensional assumption means the dependant variables such as energy and density are constant across any cross section of the tank, varying only in the axial direction, i.e. from one control volume to the next. Therefore the integral term can be written as:

$$\frac{d}{dt}\left(\int_{cv} e\rho dV \right) = \frac{d}{dt}(e\rho V) = \frac{d(em)}{dt}$$

So that equation 3.8 becomes:

$$\frac{dQ}{dt} - \frac{dW}{dt} = \frac{d(em)}{dt}$$

Rewriting with the energy term consisting of the internal energy, *u*, the work term disappearing and the heat transfer rates corresponding to that shown in Figure 12 equation 3.22 appears:

$$\dot{Q}_{c,wt} = \frac{d(u_{wt} m_{wt})}{dt}$$

where

$$\frac{d(u_{wt} m_{wt})}{dt} = m_{wt} \frac{du_{wt}}{dt} + u_{wt} \frac{dm_{wt}}{dt}$$

For a small time step and due to the assumption that the water is an incompressible single phase liquid $\frac{dm_{wt}}{dt} \approx 0$ so that

$$\dot{Q}_{c,wt} = m_{wt} \frac{du_{wt}}{dt}$$

For an incompressible liquid the internal energy and specific heat is a function of temperature alone, therefore $\frac{du}{dt} = c_v \frac{dT}{dt}$

Thus equation 3.22 becomes

$$\dot{Q}_{c,wt} = m_{wt} c_{wt} \frac{dT_{wt}}{dt}$$

Integrating with respect to time

$$\int_t^{t+\Delta t} \dot{Q}_{c,wt} dt = m_{wt} c_{wt} \int_{T_{wt}^t}^{T_{wt}^{t+\Delta t}} dT_{wt}$$

$$\Delta t\dot{Q}_{c,wt} = m_{wt}c_{wt}(T_{wt}^{t+\Delta t} - T_{wt}^{t})$$

Rearranging the terms

$$T_{wt}^{t+\Delta t} = T_{wt}^{t} + \Delta t\dot{Q}_{c,wt}/(m_{wt}c_{wt})$$

and writing the heat transfer rates in terms of temperatures and resistances gives equation 3.23

$$T_{wt}^{t+\Delta t} = T_{wt}^{t} + \frac{\Delta t}{m_{wt}c_{wt}}\left(\frac{T_{w}^{t} - T_{wt}^{t}}{R_{wt}}\right)$$

where $R_{c,wt} = \frac{1}{h_{ic}A_z} + \frac{1}{h_{c,wt}A_z}$

B.8 Derivation of Equation 3.25

Starting from equation 3.8

$$\frac{dQ}{dt} - \frac{dW}{dt} = \frac{d}{dt}\left(\int_{cv} e\rho dV\right) + (e\rho Av)_{out} - (e\rho Av)_{in}$$

The flux terms are assumed to be negligibly small since the temperature gradient along the height of the tank will induce a very small natural circulation flow rate. The one dimensional assumption means the dependant variables such as energy and density are constant across any cross section of the tank, varying only in the axial direction, i.e. from one control volume to the next. Therefore the integral term can be written as:

$$\frac{d}{dt}\left(\int_{cv} e\rho dV\right) = \frac{d}{dt}(e\rho V) = \frac{d(em)}{dt}$$

So that equation 3.8 becomes:

$$\frac{dQ}{dt} - \frac{dW}{dt} = \frac{d(em)}{dt}$$

Rewriting with the energy term consisting of the internal energy, *u*, the work term disappearing and the heat transfer rates corresponding to that shown in Figure 13 equation 3.24 appears:

$$\dot{Q}_{c,wt} - \dot{Q}_{evap} + \dot{Q}_{conv} = \frac{d(u_{wt} m_{wt})}{dt}$$

where

$$\frac{d(u_{wt} m_{wt})}{dt} = m_{wt} \frac{du_{wt}}{dt} + u_{wt} \frac{dm_{wt}}{dt}$$

For a small time step and due to the assumption that the water is an incompressible single phase liquid $\frac{dm_{wt}}{dt} \approx 0$ so that

$$\dot{Q}_{c,wt} - \dot{Q}_{evap} + \dot{Q}_{conv} = m_{wt} \frac{du_{wt}}{dt}$$

For an incompressible liquid the internal energy and specific heat is a function of temperature alone, therefore $\frac{du}{dt} = c_v \frac{dT}{dt}$

Thus equation 3.24 becomes

$$\dot{Q}_{c,wt} - \dot{Q}_{evap} + \dot{Q}_{conv} = m_{wt} c_{wt} \frac{dT_{wt}}{dt}$$

Integrating with respect to time

$$\int_t^{t+\Delta t} (\dot{Q}_{c,wt} - \dot{Q}_{evap} + \dot{Q}_{conv}) dt = m_{wt} c_{wt} \int_{T_{wt}^t}^{T_{wt}^{t+\Delta t}} dT_{wt}$$

$$\Delta t(\dot{Q}_{c,wt} - \dot{Q}_{evap} + \dot{Q}_{conv}) = m_{wt} c_{wt} (T_{wt}^{t+\Delta t} - T_{wt}^{t})$$

Rearranging the terms

$$T_{wt}^{t+\Delta t} = T_{wt}^{t} + \Delta t(\dot{Q}_{c,wt} - \dot{Q}_{evap} + \dot{Q}_{conv}) / (m_{wt} c_{wt})$$

and writing the heat transfer rates in terms of temperatures and resistances gives equation 3.25

$$T_{wt}^{t+\Delta t} = T_{wt}^{t} + \frac{\Delta t}{m_{wt} c_{wt}} \left(\frac{T_w^t - T_{wt}^t}{R_{c,wt}} - \dot{m}_{evap} h_{fg} + \frac{T_{wt}^t - T_{air}^t}{R_{c,wta}} \right)$$

where $R_{c,wta} = \frac{1}{h_{c,wt} A_{s,wt}}$

APPENDIX C: CLOSURE EQUATIONS

C.1 Boiling Heat Transfer Correlations

Chen's correlation, (Whalley1987):

$$h = h_{NB} + h_{FC} = Sh_{FZ} + Fh_l \qquad \textbf{\{C.1\}}$$

The nucleate boiling term is calculated using the Forster-Zuber equation for pool boiling and the suppression factor S

$$h_{FZ} = \frac{0.00122\Delta T_{sat}^{0.24}\Delta P_{sat}^{0.75}c_{pl}^{0.45}\rho_l^{0.49}k_l^{0.79}}{\sigma^{0.5}\lambda^{0.24}\mu_l^{0.29}\rho_g^{0.24}} \qquad \textbf{\{C.2\}}$$

Collier, as given by Carey (1992), proposed the following relations to fit Chen's original curves for the suppression factor, *S* and two phase multiplier, *F*:

$$F = 1 \qquad \text{for } X_{tt} \le 0.1 \qquad \textbf{\{C.3\}}$$

$$F = 2.35\left(0.213 + \frac{1}{X_{tt}}\right)^{0.736} \qquad \text{for } X_{tt} > 0.1 \qquad \textbf{\{C.4\}}$$

$$S = \left(1 + 2.56x10^{-6}\left[Re_l F^{1.25}\right]^{1.17}\right)^{-1} \qquad \textbf{\{C.5\}}$$

The forced convection term is calculated using *F* and a single phase liquid convective heat transfer coefficient based on the liquid mass flow rate. This coefficient is calculated using the Dittus-Boelter equation

$$Nu_l = 0.023Re_l^{0.8}Pr_l^{0.4} \qquad \textbf{\{C.6\}}$$

where

$$h_l = \frac{Nu_l k_l}{D} \text{ and } Re_l = \frac{G(1-x)D}{\mu_l} \qquad \textbf{\{C.7\}}$$

Liu and Winterton's correlation, (Liu and Winterton, 1991):

This correlation starts from the premise that

$$h^2 = \left(Sh_{pool}\right)^2 + \left(Fh_l\right)^2 \qquad \textbf{\{C.8\}}$$

Where the pool boiling heat transfer coefficient is given by Cooper's correlation

$$h_{pool} = 55 p_r^{0.12} q^{2/3} (-\log_{10} p_r)^{-0.55} M^{-0.5} \qquad \textbf{\{C.9\}}$$

and the liquid heat transfer coefficient is given by the Dittus-Boelter equation

$$h_l = 0.023(k_l / D) Re_l^{0.8} Pr_l^{0.4} \qquad \textbf{\{C.10\}}$$

Through regression expressions for F and S is found

$$F = \left(1 + xPr_l\left[\frac{\rho_l}{\rho_v} - 1\right]\right)^{0.35} \qquad \textbf{\{C.11\}}$$

$$S = \left(1 + 0.055 F^{0.1} Re_l^{0.16}\right)^{-1} \qquad \textbf{\{C.12\}}$$

These equations can be used directly if the heat transfer rate is known. However in the computer code the wall temperature rather than the heat transfer rate is known. It is therefore required to manipulate the equations as shown by Liu and Winterton.

Multiplying equation C.8 by ΔT_s squared and substituting equation C.9 gives

$$q^2 = \left(Fh_l \Delta T_s\right)^2 + \left(A_p S \Delta T_s\right)^2 q^{4/3} \qquad \textbf{\{C.13\}}$$

where

$$A_p = 55 p_r^{0.12} (-\log_{10} p_r)^{-0.55} M^{-0.5} \qquad \textbf{\{C.14\}}$$

Defining

$$q_*^3 = \left(\frac{q}{Fh_l \Delta T_s} \right)^2 \quad \textbf{\{C.15\}}$$

and

$$C = \left(A_p S / Fh_l \right)^2 \left(Fh_l \Delta T_s \right)^{4/3} \quad \textbf{\{C.16\}}$$

then equation C.13 can be rearranged to become

$$q_*^3 - Cq_*^2 - 1 = 0 \quad \textbf{\{C.17\}}$$

This is a standard cubic equation with one real root always greater than 1. The heat transfer coefficient can then be calculated by

$$h = Fh_l q_*^{3/2} \quad \textbf{\{C.18\}}$$

Steiner and Taborek's correlation, (Steiner and Taborek, 1992):

This correlation starts from the premise that

$$h = \left[(F_{nbf} h_{nb,o})^n + (F_{tp} h_l)^n \right]^{1/n} \quad \textbf{\{C.19\}}$$

Regression analysis of the Karlsruhe data bank showed the exponent n to be approximately 3 with the value of 3 taken as acceptable. The liquid only heat transfer coefficient, h_l can be calculated using the equations outlined in section 3.3.2. The two phase multiplier $F_{tp,}$ is given for quality less than 0.6 by

$$F_{tp} = \left[(1-x)^{1.5} + 1.9 x^{0.6} \left(\frac{\rho_l}{\rho_g} \right)^{0.35} \right]^{1.1} \quad \textbf{\{C.20\}}$$

The nucleate boiling correction factor, F_{nbf} is a function of pressure, heat flux, tube diameter, surface roughness and molecular weight:

$$F_{nbf} = F_{pf} + \left[\frac{\dot{q}}{\dot{q}_{of}}\right]^{nf(p_r)} + F(d) + F(R_a) + F(M) \quad \textbf{\{C.21\}}$$

where

$$F_{pf} = \left(2.816\,p_r^{0.45} + \left[3.4 + \frac{1.7}{1 - p_r^7}\right]p_r^{3.7}\right) \quad \textbf{\{C.22\}}$$

$$\dot{q}_{of} = 150000 \text{ W/m}^2 \quad \textbf{\{C.23\}}$$

$$nf(p_r) = 0.8 - 0.1\exp(1.75\,p_r) \quad \textbf{\{C.24\}}$$

$$F(d) = \left(\frac{D}{0.01}\right)^{-0.4} \quad \textbf{\{C.25\}}$$

$$F(R_a) = 1 \quad \textbf{\{C.26\}}$$

$$F(M) = 0.72 \quad \textbf{\{C.27\}}$$

The normalized nucleate boiling heat transfer coefficient, $h_{nb,o}$ for water is given as 25580 W/m^{2}K.

C.2 Condensation Heat Transfer Coefficients

Correlation of Soliman, (Soliman et al, 1968):

The correlation is given in the form

$$h = 0.036\frac{k_l \rho_l^{0.5}}{\mu_l}\mathrm{Pr}_l^{0.65}\,\tau_w^{0.5} \qquad \textbf{\{C.28\}}$$

where

$$\tau_w = \tau_i + \tau_z + \tau_a \qquad \textbf{\{C.29\}}$$

$$\tau_i = \frac{D}{4}\left(-\frac{dP}{dz}\right)_F,\ \left(-\frac{dP}{dz}\right)_F = \phi_g^2\left(-\frac{dP}{dz}\right)_v,\ \phi_g^2 = 1 + 2.85X_{tt}^{0.523} \qquad \textbf{\{C.30\}}$$

$$\tau_z = \frac{D}{4}(1-\alpha)(\rho_l - \rho_v)g\sin\theta,\quad \alpha = \left[1 + \left(\frac{1-x}{x}\right)\left(\frac{\rho_v}{\rho_l}\right)^{2/3}\right]^{-1} \qquad \textbf{\{C.31\}}$$

$$\tau_a = \frac{D}{4}\left(\frac{G^2}{\rho_v}\right)\left(\frac{dx}{dz}\right)\sum_{n=1}^{5} a_n\left(\frac{\rho_v}{\rho_l}\right)^{n/3} \qquad \textbf{\{C.32\}}$$

$$a_1 = 2x - 1 - \beta x \qquad \textbf{\{C.33\}}$$

$$a_2 = 2(1-x) \qquad \textbf{\{C.34\}}$$

$$a_3 = 2(1 - x - \beta + \beta x) \qquad \textbf{\{C.35\}}$$

$$a_4 = x^{-1} - 3 + 2x \qquad \textbf{\{C.36\}}$$

$$a_1 = \beta(2 - x^{-1} - x) \qquad \textbf{\{C.37\}}$$

For flow in round tubes and Re number greater than 2000 the flow is considered turbulent and the value of β is 1.25, for Re number less than 2000 the flow is considered as laminar and the value of β is 2.0.

Correlation of Travis, (Travis et al, 1973):

The proposed correlation is given in the form

$$Nu = \frac{0.15 Pr_l Re_l^{0.9}}{F_T}\left[\frac{1}{X_{tt}} + \frac{2.85}{X_{tt}^{0.476}}\right] \qquad \textbf{\{C.38\}}$$

where

$$\begin{aligned} F_T &= 5Pr_l + 5\ln(1+5Pr_l) + 2.5\ln(0.0031 Re_l^{0.812}) && for \;\; Re_l > 1125 \\ &= 5Pr_l + 5\ln(1+Pr_l[0.0964 Re_l^{0.585} - 1]) && for \;\; 50 < Re_l < 1125 \\ &= 0.707 Pr_l Re_l^{0.5} && for \;\; Re_l < 50 \end{aligned} \qquad \textbf{\{C.39\}}$$

$$Re_l = \frac{G(1-x)D}{\mu_l} \qquad \textbf{\{C.40\}}$$

Shah's correlation, (Shah, 1989):

The proposed correlation takes the form

$$\frac{h}{h_{lo}} = (1-x)^{0.8} + \frac{3.8 x^{0.76}(1-x)^{0.04}}{P_r^{0.38}} \qquad \textbf{\{C.41\}}$$

Where h_{lo} is calculated using the Dittus Boelter equation

$$h_{lo} = 0.023\left(\frac{k_l}{D}\right) Re_l^{0.8} Pr_l^{0.4} \qquad \textbf{\{C.42\}}$$

This correlation was recommended for $11 \le G \le 211 \;\; kg/m^2 s$, $0 \le x \le 1$ and $1 \le Pr \le 13$

Correlation of Chen, (Chen et al, 1987):

The correlation takes the form

$$Nu_x = \left[\left(0.31 Re_x^{-1.32} + \frac{Re_x^{2.4} Pr_l^{3.9}}{2.37 * 10^{14}} \right)^{1/3} + \frac{A_D Pr_l^{1.3}}{771.6} (Re_{ter} - Re_x)^{1.4} Re_x^{0.4} \right]^{1/2} \quad \textbf{\{C.43\}}$$

where

$$Nu_x = \frac{h v_l^{2/3}}{k_l g^{1/3}} \quad \textbf{\{C.44\}}$$

$$Re_x = \frac{G(1-x)D}{\mu_l} \quad \textbf{\{C.45\}}$$

$$A_D = \frac{0.252 \mu_l^{1.177} \mu_v^{0.156}}{D^2 g^{2/3} \rho_l^{0.553} \rho_v^{0.78}} \quad \textbf{\{C.46\}}$$

$$Re_{ter} = \frac{GD}{\mu_l} \quad \textbf{\{C.47\}}$$

C.3 Void Fraction, CISE Correlation, (Whalley, 1987):

The general equation for void fraction is

$$\alpha = \frac{1}{1 + \left(S \frac{1-x}{x} \frac{\rho_g}{\rho_l} \right)} \quad \textbf{\{C.48\}}$$

The CISE correlation determines the slip factor to be used in the equation above.

$$S = 1 + E_1 \left(\frac{y}{1 + yE_2} - yE_2 \right)^{0.5} \quad \textbf{\{C.49\}}$$

where

$$y = \frac{\beta}{1 - \beta} \quad \textbf{\{C.50\}}$$

$$\beta = \frac{\rho_l x}{\rho_l x + \rho_g (1 - x)} \quad \textbf{\{C.51\}}$$

$$E_1 = 1.578 Re^{-0.19} \left(\frac{\rho_l}{\rho_g} \right)^{0.22} \quad \textbf{\{C.52\}}$$

$$E_2 = 0.0273 WeRe^{-0.51} \left(\frac{\rho_l}{\rho_g} \right)^{-0.08} \quad \textbf{\{ C.53\}}$$

$$Re = \frac{GD}{\mu_l} \quad \textbf{\{C.54\}}$$

$$We = \frac{G^2 D}{\sigma \rho_l} \quad \textbf{\{C.55\}}$$

C.4 Two-phase Multiplier, Friedel Correlation, (Whalley, 1987):

The two phase multiplier is given by

$$\phi_{lo}^2 = C_{F1} + \frac{3.24 C_{F2}}{Fr^{0.045} We^{0.035}} \quad \textbf{\{C.56\}}$$

where

$$E = (1 - x)^2 + x^2 \frac{\rho_l}{\rho_g} \frac{C_{f,go}}{C_{f,go}} \quad \textbf{\{C.57\}}$$

$$F = x^{0.78} (1 - x)^{0.224} \quad \textbf{\{C.58\}}$$

$$H = \left(\frac{\rho_l}{\rho_g}\right)^{0.91} \left(\frac{\mu_g}{\mu_l}\right)^{0.19} \left(1 - \frac{\mu_g}{\mu_l}\right)^{0.7} \quad \textbf{\{C.59\}}$$

$$Fr = \frac{G^2}{gD\rho_h^2} \quad \textbf{\{C.60\}}$$

$$We = \frac{G^2 D}{\sigma \rho_h} \quad \textbf{\{C.61\}}$$

$$\rho_h = \left(\frac{x}{\rho_g} + \frac{1-x}{\rho l}\right)^{-1} \quad \textbf{\{C.62\}}$$

APPENDIX D: CALIBRATION OF EXPERIMENTAL APPARATUS

D.1 Thermocouple tests

The accuracy of the thermocouples used in the experiments was verified by comparison with a calibrated sub-standard platinum resistance thermometer, model number 935-14-72. Table D.1 shows the comparison for the 5 K-type thermocouples used to measure the temperatures of the heater plate. Table D.2 shows the comparison for the 4 T-type thermocouple probes used to measure the temperatures of the working fluid. Table D.3 shows the comparison for the 6 T-type thermocouples used to measure the temperatures of the fins.

For the K-type thermocouples the standard deviation at each of the measured points lies between 0.100 and 0.182 with a maximum error of 1.5 %. For the T-type thermocouple probes the standard deviation at each of the measured points lies between 0.050 and 0.126 with a maximum error of 1.27 %. For the T-type thermocouples the standard deviation at each of the measured points lies between 0.052 and 0.098 with a maximum error of 0.72 %.

Table D.1: K-Type thermocouples

Temperatures [ºC]						**S.D.**	**Error %**				
PRT	**#1**	**#2**	**#3**	**#4**	**#5**		**#1**	**#2**	**#3**	**#4**	**#5**
90.66	89.5	89.7	89.5	89.4	89.7	0.134	1.27	1.05	1.27	1.38	1.05
85.41	84.4	84.7	84.7	84.6	84.6	0.122	1.18	0.83	0.83	0.94	0.94
78.86	78.0	78.3	78.2	78.0	78.2	0.134	1.09	0.71	0.83	1.09	0.83
74.94	74.2	74.4	74.3	74.1	74.3	0.114	0.98	0.71	0.85	1.11	0.85
69.71	69.1	69.3	69.3	69.2	69.1	0.100	0.88	0.59	0.59	0.73	0.88
64.50	63.8	63.8	64.2	63.9	64.1	0.182	1.08	1.08	0.46	0.93	0.62
59.29	58.6	58.8	58.6	58.5	58.8	0.134	1.16	0.83	1.16	1.33	0.83
54.09	53.4	53.6	53.4	53.4	53.6	0.110	1.28	0.91	1.28	1.28	0.91
48.90	48.4	48.6	48.3	48.4	48.5	0.114	1.03	0.62	1.23	1.03	0.82
43.72	43.1	43.3	43.1	43.1	43.4	0.141	1.42	0.96	1.42	1.42	0.73
38.55	38.2	38.3	38.1	38.1	38.3	0.100	0.90	0.64	1.16	1.16	0.64
33.38	33.0	33.2	32.9	32.9	33.1	0.130	1.14	0.54	1.44	1.44	0.84
28.22	27.9	28.0	27.8	27.8	28.0	0.100	1.15	0.79	1.50	1.50	0.79

Table D.2: T-type thermocouple probes

Temperatures [ºC]					S.D.	Error %			
PRT	**#1**	**#2**	**#3**	**#4**		**#1**	**#2**	**#3**	**#4**
90.66	89.6	89.6	89.5	89.5	0.058	1.16	1.16	1.27	1.27
85.41	84.4	84.5	84.5	84.5	0.050	1.18	1.06	1.06	1.06
78.86	78.1	78.1	78.0	78.1	0.050	0.96	0.96	1.09	0.96
74.94	74.3	74.4	74.1	74.3	0.126	0.85	0.71	1.11	0.85
69.71	69.1	69.2	69.1	69.2	0.058	0.88	0.73	0.88	0.73
64.50	64.1	64.2	64.0	64.0	0.096	0.62	0.46	0.77	0.77
59.29	58.8	58.9	58.7	58.8	0.082	0.83	0.66	1.00	0.83
54.09	53.6	53.7	53.5	53.7	0.096	0.91	0.73	1.09	0.73
48.90	48.7	48.7	48.5	48.7	0.100	0.41	0.41	0.82	0.41
43.72	43.5	43.5	43.3	43.5	0.100	0.50	0.50	0.96	0.50
38.55	38.4	38.5	38.3	38.5	0.096	0.38	0.12	0.64	0.12
33.38	33.3	33.3	33.1	33.2	0.096	0.24	0.24	0.84	0.54
28.22	28.2	28.2	28.0	28.2	0.100	0.09	0.09	0.79	0.09

Table D.3: T-type thermocouples

Temperatures [ºC]							S.D.	Error %					
PRT	**#1**	**#2**	**#3**	**#4**	**#5**	**#6**		**#1**	**#2**	**#3**	**#4**	**#5**	**#6**
88.03	87.5	87.4	87.5	87.4	87.4	87.4	0.052	0.60	0.72	0.60	0.72	0.72	0.72
84.10	83.8	83.9	83.8	83.9	83.8	83.8	0.052	0.36	0.24	0.36	0.24	0.36	0.36
80.17	79.9	79.9	79.9	79.9	79.7	79.8	0.084	0.34	0.34	0.34	0.34	0.59	0.46
76.24	76.3	76.3	76.3	76.3	76.2	76.1	0.084	0.08	0.08	0.08	0.08	0.05	0.18
72.32	72.0	72.0	71.9	71.9	71.9	71.9	0.052	0.44	0.44	0.58	0.58	0.58	0.58
68.41	68.2	68.1	68.1	68.1	68.1	68.0	0.063	0.31	0.45	0.45	0.45	0.45	0.60
64.50	64.8	64.6	64.6	64.6	64.6	64.5	0.098	0.47	0.16	0.16	0.16	0.16	0.00
60.60	60.3	60.3	60.3	60.4	60.2	60.3	0.063	0.50	0.50	0.50	0.33	0.66	0.50
56.70	56.5	56.5	56.6	56.6	56.5	56.5	0.052	0.35	0.35	0.18	0.18	0.35	0.35
52.27	52.1	52.1	52.2	52.2	52.1	52.1	0.052	0.33	0.33	0.13	0.13	0.33	0.33
48.90	48.9	48.8	48.8	48.8	48.8	48.7	0.063	0.00	0.20	0.20	0.20	0.20	0.41
45.02	44.8	44.8	44.8	44.8	44.8	44.8	0.000	0.49	0.49	0.49	0.49	0.49	0.49
41.13	41.2	41.1	41.2	41.2	41.1	41.1	0.055	0.17	0.07	0.17	0.17	0.07	0.07

D.2 Orifice Plate Calibration

The orifice plate calibration was done once the entire system was installed. A total of five sets of calibration data were obtained using both pressure transducers and are plotted on figures 31 and 32. An attempt was made to fit a single polynomial curve through the data in order to approximate the mass flow rate from the measured pressure drop across the orifice plate. Looking at figure 31 it can be seen that the low order polynomial curves grossly underestimate the flow rates at low pressures which is exactly the region were the system works most of the time.

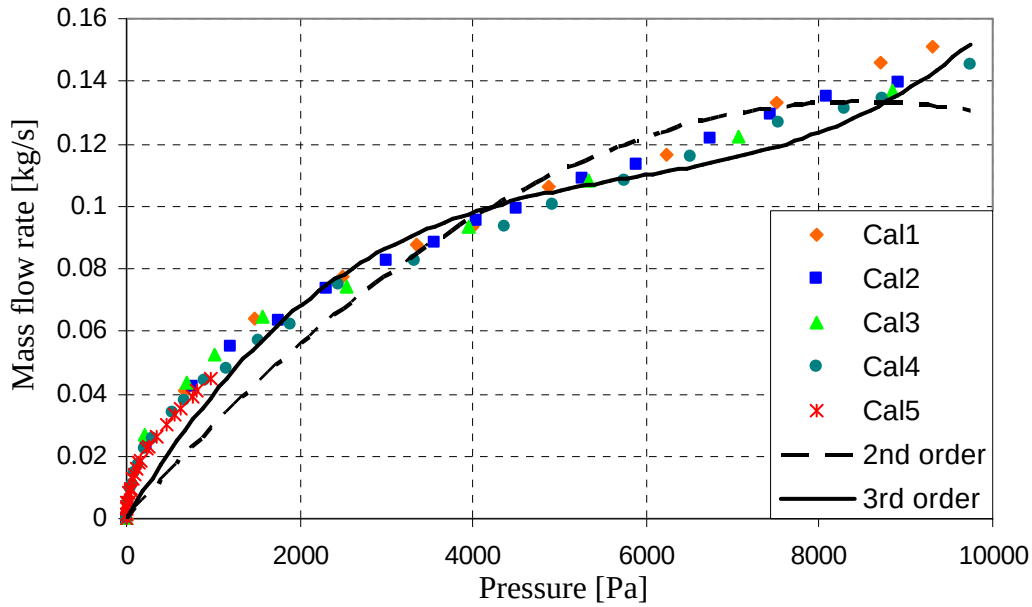

Figure 31: Polynomial curve fit to data

It was therefore decided to divide the range up into three regions and fit curves through each region that approximate the data better.

The first region lies between 0 and 165 Pa and the curve is given by the equation D.1 with an R^2 of 0.999.

$$\dot{m} = -3.675902*10^{-14}(\Delta P)^6 + 1.981716*10^{-11}(\Delta P)^5 - 4.125673*10^{-9}(\Delta P)^4 + 4.173198*10^{-7}(\Delta P)^3 - 2.153560*10^{-5}(\Delta P)^2 + 6.429589(\Delta P) \quad \textbf{\{D.1\}}$$

The second region lies between 165 Pa and 1 000 Pa and the curve is given by the equation D.2 with an R^2 of 0.998.

$$\dot{m} = -1.196975 * 10^{-8} (\Delta P)^2 + 4.537928 * 10^{-5} (\Delta P) + 1.202012 * 10^{-2} \quad \{D.2\}$$

The third region lies between 1 000 Pa and 10 000 Pa and the curve is given by equation D.3 with an R^2 value of 0.997.

$$\dot{m} = 1.620223 * 10^{-13} (\Delta P)^3 - 3.123890 * 10^{-9} (\Delta P)^2 + 2.853950 * 10^{-5} (\Delta P) + 2.107825 * 10^{-2} \quad \{D.3\}$$

These three curves are plotted in figure 32. It will be noted that there exist discontinuities at both of the transition points. At 165 Pa, equation D.2 predicts a value 4.7 % larger than equation D.1. While at 1000 Pa, equation D.3 predicts a value 2.7 % larger than equation D.2. These discrepancies will have a very small influence on the final result and is thus tolerable.

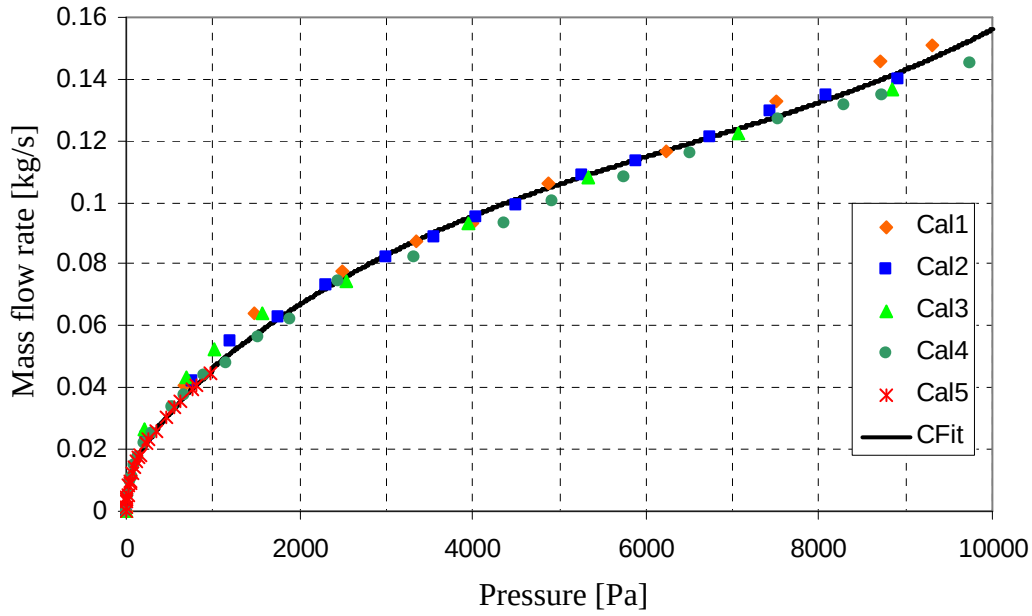

Figure 32: Orifice calibration curve

APPENDIX E: SAMPLE CALCULATIONS

Sample calculations for one time step are shown for a control volume situated in the middle of the evaporator section of the loop. The calculations for the accompanying control volumes for the air and fins are also shown for the sake of clarity. The values calculated by the computer program were compared to the values below and found to correspond.

The initial values given in double precision for time t were as follows:

$\Delta t = 0.0025$ s

$\dot{m} = 9.15063530144826 * 10^{-3}$ kg/s

$T_r = 549.603116131472$ ºC

$T_a = 295.734395388914$ ºC

$T_f = 42.9779361029936$ ºC

$T_w = 37.2476724136036$ ºC

$T_{ba} = 42.6468702339214$ ºC

E.1 Geometric and Material Property Values

Control volume length: $L = 0.075$ m

Tube diameter: $D_i = 0.0254$ m

Cross-sectional area of tube control volume:

$$A_x = \frac{\pi D_i^2}{4}$$
$$= 5.06707479 * 10^{-4} \text{ m}^2$$

Surface area of tube control volume:

$$A_z = \pi D_i L$$
$$= 5.9844734 * 10^{-3} \text{ m}^2$$

Space between fin and heater plate: $L_{space} = 0.1$ m

Fin breadth: $B_{fin} = 0.145$ m

Fin thickness: $t_{fin} = 0.003$ m

Volume of fin control volume:

$$V_{fin} = LB_{fin}t_{fin}$$
$$= 0.00003625 \text{ m}^3$$

Surface area of fin cv:

$$A_{z,f} = LB_{fin}$$
$$= 0.010875 \text{ m}^2$$

Fin density: $\rho_f = 2700$ kg/m^3

Specific heat of fin: $c_f = 900$ J/kgK

Emissivity of fin: $\varepsilon_f = 0.18$

Mass of fin control volume:

$$m_f = \rho_f V_f$$
$$= 0.0880875 \text{ kg}$$

Heater plate breadth: $B_{rpv} = 0.15$ m

Surface area of heater plate control volume:

$$A_{z,r} = LB_{rpv}$$
$$= 0.01125 \text{ m}^2$$

Emissivity of heater plate: $\varepsilon_r = 0.85$

View factor: $F_{rf} = 1$

Thermophysical properties of air adapted from Cengel and Boles (2002). Equations require temperatures to be given in Kelvin.

Density of air:

$$\rho_a = 8.5233344*10^{-17}T_a^6 - 3.2630691*10^{-13}T_a^5 + 5.0903405*10^{-10}T_a^4$$
$$- 0.0000004169916T_a^3 + 0.00019258462T_a^2 - 0.049869465T_a$$
$$+ 6.6708097$$
$$= 6.16520818295826*10^{-1} \text{ kg/m}^3$$

Volume of air control volume: $V_a = LL_{space} B_{fin} = 0.0010875 \text{ m}^3$

Mass of air control volume: $m_a = \rho_a V_a = 6.70466389896711 * 10^{-4} \text{ kg}$

Specific heat of air:

$$\begin{aligned} c_a &= 6.4531274 * 10^{-15} T_a^6 - 2.0858673 * 10^{-11} T_a^5 + 2.5725831 * 10^{-08} T_a^4 \\ &\quad - 0.000015461597 T_a^3 + 0.0051330888 T_a^2 - 0.94513242 T_a + 1083.449 \\ &= 1030.7353038436 \text{ J/kgK} \end{aligned}$$

Density of air at back of fin:

$$\begin{aligned} \rho_{ba} &= 8.5233344 * 10^{-17} T_{ba}^6 - 3.2630691 * 10^{-13} T_{ba}^5 + 5.0903405 * 10^{-10} T_{ba}^4 \\ &\quad - 0.0000004169916 T_{ba}^3 + 0.00019258462 T_{ba}^2 - 0.049869465 T_{ba} \\ &\quad + 6.6708097 \\ &= 1.11793063167137 \text{ kg/m}^3 \end{aligned}$$

Volume of air control volume: $V_{ba} = 0.05 L B_{fin} = 0.00054375 \text{ m}^3$

Mass of air control volume: $m_{ba} = \rho_{ba} V_{ba} = 6.07874780971308 * 10^{-4} \text{ kg}$

Specific heat of air:

$$\begin{aligned} c_{ba} &= 6.4531274 * 10^{-15} T_{ba}^6 - 2.0858673 * 10^{-11} T_{ba}^5 + 2.5725831 * 10^{-08} T_{ba}^4 \\ &\quad - 0.000015461597 T_{ba}^3 + 0.0051330888 T_{ba}^2 - 0.94513242 T_{ba} + 1083.449 \\ &= 1006.6942474528 \text{ J/kgK} \end{aligned}$$

Properties of water (working fluid) valid from 275 K – 380 K, Kröger(1998). Equations require temperatures to be given in Kelvin.

Specific heat of water (liquid):

$$\begin{aligned} c &= 8155.99 - 28.0627 T_w + 0.0511283 T_w^2 - 2.17582 * 10^{-13} T_w^6 \\ &= 4176.84108249178 \text{ J/kgK} \end{aligned}$$

Density of water (liquid):

$$\begin{aligned} \rho &= \left(1.49343810^{-3} - 3.7164 * 10^{-6} T_w + 7.09782 * 10^{-9} T_w^2 - 1.90321 * 10^{-20} T_w^6\right)^{-1} \\ &= 993.346321796206 \text{ J/kgK} \end{aligned}$$

Dynamic viscosity:

$$\mu = 0.00002414 * 10^{(247.8/(T_w - 140))}$$
$$= 6.87040726828043 * 10^{-4} \text{ J/kgK}$$

E.2 Heat Transfer Resistances

Air Side Convection Heat Transfer Coefficient

The calculation of the air side convection heat transfer coefficient is based on the work of Hollands on thin air layers in large aspect ratio enclosures as described by chapter 4 of Mills (1999):

Perform a numerical integration over the length of the fin to find the average film temperature to be used in the isothermal correlation of Hollands to give an engineering estimate of the heat transferred. Apply the same method to find an average temperature difference between the heater plate and fin.

$T_{film,air} = 515.312107950311$ K

$\Delta T = 406.197733304903$ K

Prandtl number: $\text{Pr}_a = 0.69$

Thermal expansion coefficient:

$$\beta_a = 1/T_{film,air}$$
$$= 1/515.312107950311$$
$$= 1.94057151883655 * 10^{-3} \text{ K}^{-1}$$

Kinematic viscosity of air:

$$\nu_a = -2.1515612 * 10^{-22} T_{film,air}^6 + 7.56314 * 10^{-19} T_{film,air}^5$$
$$- 1.02857 * 10^{-15} T_{film,air}^4 + 6.6035816 * 10^{-13} T_{film,air}^3$$
$$- 1.1432998 * 10^{-10} T_{film,air}^2 + 6.2789679 * 10^{-8} T_{film,air} - 4.1066067 * 10^{-6}$$
$$= 3.91766909338551 * 10^{-5} \text{ m}^2/\text{s}$$

Thermal conductivity of air:

$$\begin{aligned} k_a &= -9.9188021 * 10^{-20} T_{film,air}^6 + 3.6893529 * 10^{-16} T_{film,air}^5 \\ &\quad - 5.7660479 * 10^{-13} T_{film,air}^4 + 4.9974035 * 10^{-10} T_{film,air}^3 \\ &\quad - 2.6206987 * 10^{-7} T_{film,air}^2 + 1.3662771 * 10^{-4} T_{film,air} - 2.3880862 * 10^{-4} \\ &= 3.98490124286148 * 10^{-2} \text{ W/mK} \end{aligned}$$

Rayleigh number:

$$\begin{aligned} Ra_L &= \frac{g\beta_a \Delta T L_{space}^3 \Pr_a}{\nu_a^2} \\ &= 3476400.03722606 \end{aligned}$$

Nusselt number: $Nu_L = \max\{Nu_1, Nu_2, Nu_3\}$

$$\begin{aligned} Nu_1 &= 0.0605 Ra_L^{1/3} \\ &= 9.16498918085412 \end{aligned}$$

$$\begin{aligned} Nu_2 &= \left(1 + \left[\frac{0.104 Ra_L^{0.293}}{1 + (6310 / Ra_L)^{1.36}} \right]^3 \right)^{1/3} \\ &= 8.58483766104984 \end{aligned}$$

$$\begin{aligned} Nu_3 &= 0.242 \left(\frac{Ra_L}{1.5 / L_{space}} \right)^{0.272} \\ &= 6.9679629760592 \end{aligned}$$

Heat transfer coefficient:

$$\begin{aligned} h_{c,af} &= \frac{Nu_1 k_a}{L_{space}} \\ &= 3.65215767775976 \text{ W/m}^2\text{K} \end{aligned}$$

Water Side Convection Heat Transfer Coefficient

$$\Delta T = T_f - T_w = 5.73026368939003 \text{ K}$$

$$T_{film} = \left(T_f + T_w\right)/2 = 313.262804258299 \text{ K}$$

$$T_{wall} = T_f = 316.127936102994 \text{ K}$$

Thermophysical properties of water adapted from Mills (1999). Equations require temperatures to be given in Kelvin and are valid in the range 275K to 500K

Thermal expansion coefficient:

$$\begin{aligned}\beta = &-6.5804074*10^{-17}T_{film}^6 + 1.6037129*10^{-13}T_{film}^5 \\ &- 1.6174215*10^{-10}T_{film}^4 + 8.6489874*10^{-8}T_{film}^3 \\ &- 2.5892029*10^{-5}T_{film}^2 + 0.0041248074T_{film} - 0.27372844 \\ = &\ 3.88223098613361*10^{-4} \text{ K}^{-1}\end{aligned}$$

Surface tension:

$$\begin{aligned}\sigma = &-1.6026051*10^{-15}T_{film}^6 + 3.7613623*10^{-12}T_{film}^5 \\ &- 3.647111*10^{-9}T_{film}^4 + 1.869796*10^{-6}T_{film}^3 \\ &- 5.3472746*10^{-4}T_{film}^2 + 0.080744631T_{film} - 4.9407974 \\ = &\ 6.95644866645084*10^{-2} \text{ N/m}\end{aligned}$$

Enthalpy of vaporization:

$$\begin{aligned}h_{lv} = &-3.2097273*10^{-9}T_{film}^6 + 7.1827735*10^{-6}T_{film}^5 \\ &- 6.6553531*10^{-3}T_{film}^4 + 3.2514176T_{film}^3 \\ &- 881.81423T_{film}^2 + 123484.94T_{film} - 4239106.2 \\ = &\ 2.40547532757911*10^6 \text{ J/kg}\end{aligned}$$

Prandtl number at wall temperature:

$$\begin{aligned}\text{Pr}_{wall} = &\ 2.6244157*10^{-12}T_{film}^6 - 6.3680073*10^{-9}T_{film}^5 \\ &+ 6.4093506*10^{-6}T_{film}^4 - 3.4260841*10^3T_{film}^3 \\ &+ 1.0262977T_{film}^2 - 163.46148T_{film} + 10827.083 \\ = &\ 4.02459267185077\end{aligned}$$

Thermal conductivity:

$$\begin{aligned} k_l &= -2.2253838*10^{-15}T_{film}^6 + 5.1513299*10^{-12}T_{film}^5 \\ &\quad - 5.0404666*10^{-9}T_{film}^4 + 2.6841228*10^{6}T_{film}^3 \\ &\quad - 8.2948763*10^{-4}T_{film}^2 + 0.14295254T_{film} - 10.159996 \\ &= 6.32011329853263*10^{-1} \text{ W/mK} \end{aligned}$$

Dynamic viscosity (liquid)

$$\begin{aligned} \mu_l &= 2.5476417*10^{-16}T_{film}^6 - 6.2014525*10^{-13}T_{film}^5 \\ &\quad + 6.2644683*10^{-10}T_{film}^4 - 3.3627479*10^{-7}T_{film}^3 \\ &\quad + 1.0123043*10^{-4}T_{film}^2 - 0.016218788T_{film} + 1.0821869 \\ &= 6.5152286951875*10^{-4} \text{ kg/ms} \end{aligned}$$

Dynamic viscosity (vapour)

$$\begin{aligned} \mu_g &= -4.4135362*10^{-13}T_{film}^3 + 5.1529319*10^{-10}T_{film}^2 \\ &\quad - 1.523527*10^{-7}T_{film} + 2.0248505*10^{-5} \\ &= 9.52172150581826*10^{-6} \text{ kg/ms} \end{aligned}$$

Specific heat (liquid)

$$\begin{aligned} c_l &= 1.9820742*10^{-11}T_{film}^6 - 4.750386*10^{-8}T_{film}^5 + 4.744802*10^{5}T_{film}^4 \\ &\quad - 2.5237881*10^{2}T_{film}^3 + 7.538464T_{film}^2 - 1198.8961T_{film} + 83463.034 \\ &= 4.17367511921913*10^{3} \text{ J/kgK} \end{aligned}$$

Prandtl number (liquid):

$$\text{Pr}_l = c_l \mu_l / k_l = 4.30252538470157$$

Density (liquid):

$$\begin{aligned} \rho_l &= 3.6622841*10^{-13}T_{film}^6 - 4.896556*10^{-10}T_{film}^5 + 1.2449597*10^{-7}T_{film}^4 \\ &\quad + 1.16732*10^{-4}T_{film}^3 - 0.089134061T_{film}^{-2} + 22.730535T_{film} - 1037.8816 \\ &= 9.92072187449987*10^{2} \text{ kg/m}^3 \end{aligned}$$

Density (vapour):

$$\begin{aligned} \rho_g &= 4.2122072*10^{-14}T_{film}^6 - 8.5900137*10^{-11}T_{film}^5 + 7.7872598*10^{-8}T_{film}^4 \\ &\quad - 3.8554549*10^{-5}T_{film}^3 + 0.010756854T_{film}^{-2} - 1.5883188T_{film} + 96.639269 \\ &= 5.20141454173739*10^{-2} \text{ kg/m}^3 \end{aligned}$$

Reynolds number: $\mathrm{Re}_l = \dfrac{4(1-x)\dot{m}}{\pi \mu_l D_i} = 704.041053523945$

Nusselt number:

$$Nu = 0.17\,\mathrm{Re}^{0.33}\,\mathrm{Pr}_l^{0.43}\left(\frac{\mathrm{Pr}_l}{\mathrm{Pr}_{wall}}\right)^{0.25}\left(\frac{9.81 D_i^3 \beta \Delta T}{\nu^2}\right)^{0.1}$$
$$= 11.0096382357401$$

Heat transfer coefficient:

$$h_i = \frac{Nu * k_l}{D_i}$$
$$= 273.945515849349\ \mathrm{W/m^2K}$$

Heat transfer coefficient times 6: $h_i = 1643.67309509609\,\mathrm{W/m^2\ K}$

<u>Resistances:</u>

$$R_{r,rf} = \left(\frac{1-\varepsilon_r}{\varepsilon_r A_{z,r}} + \frac{1}{F_{rf} A_{z,r}} + \frac{1-\varepsilon_f}{\varepsilon_f A_{z,f}}\right)\left(\frac{1}{5.67 * 10^{-8}(T_r^2 + T_f^2)(T_r + T_f)}\right)$$
$$= 10.435025541447\ \mathrm{K/W}$$

$$R_{c,af} = \frac{1}{h_{c,af} A_{z,f}} = 25.1779991725085\ \mathrm{K/W}$$

$$R_{c,fba} = \frac{1}{h_{c,fba} A_{z,f}} = 18.3908045977012\ \mathrm{K/W}$$

$$R_{c,ra} = \frac{1}{h_{c,ra} A_{z,r}} = 24.3387325334248\ \mathrm{K/W}$$

$$R_w = \frac{1}{h_i A_z} = 0.101657564554374\ \mathrm{K/W}$$

E.3 Temperatures

Fin temperature at next time step:

$$T_f^{t+\Delta t} = T_f^t + \frac{\Delta t}{m_f c_f}\left(\frac{T_r^t - T_f^t}{(R_{r,rf}^{-1} + R_{c,af}^{-1})^{-1}} - \frac{T_f^t - T_w^t}{R_{fw}} - \frac{T_f^t - T_{ba}^t}{R_{c,fba}}\right)$$
$$= 316.128006267517 \text{ K}$$

Air temperature at next time step:

$$T_a^{t+\Delta t} = T_a^t + \frac{\Delta t}{m_a c_a}\left(\frac{T_r^t - T_a^t}{R_{c,ra}} - \frac{T_a^t - T_f^t}{R_{c,af}}\right)$$
$$= 568.885812981328 \text{ K}$$

Air temperature at next time step at back of fin:

$$T_{ba}^{t+\Delta t} = T_{ba}^t + \frac{\Delta t}{m_{ba} c_{ba}}\left(\frac{T_f^t - T_{ba}^t}{R_{c,fba}}\right)$$
$$= 315.796943777029 \text{ K}$$

Working fluid:

Internal energy:

$$u^t = cT_w^t + xu_{fg}$$
$$= 155577.608364335 \text{ J/kg}$$

Heat transfer to control volume: $\dot{S} = \frac{T_f^t - T_w^t}{R_w} = 56.3682959995079 \text{ W}$

Enthalpy entering control volume:

$$h_{in} = c_{k-1}T_{k-1} + xh_{fg}$$
$$= 4176.99613317836 * 35.8742371923017$$
$$= 149846.550032967 \text{ J/kgK}$$

Enthalpy leaving control volume:

$$h_{out} = cT_k + xh_{fg}$$
$$= 4176.84108249178 * 37.2476724136036$$
$$= 155577.608364335 \text{ J/kgK}$$

Internal energy at next time step:

$$u^{t+\Delta t} = \frac{U^t}{m^{t+\Delta t}} + \frac{\Delta t}{m^{t+\Delta t}}\left((\dot{m}h)_{in} - \dot{S} - (\dot{m}h)_{out}\right)$$
$$= 155577.868327934 \text{ J/kgK}$$

Due to $u^{t+\Delta t} < u_{sat}$:

Quality at next time step: $x^{t+\Delta t} = 0$

Temperature at next time step:

$$T^{t+\Delta t} = u^{t+\Delta t} / c$$
$$= 37.2477346528878 \text{ °C}$$
$$= 310.3977346528878 \text{ K}$$

E.4 Mass flow rate

Void fraction at next time step: $\alpha^{t+\Delta t} = 0$

Density at next time step:

$$\rho^{t+\Delta t} = \alpha^t \rho_g^t + \left(1 - \alpha^t\right)\rho_l^t$$
$$= 993.34632179606 \text{ kg/m}^3$$

Liquid only Reynolds number: $\text{Re}_{lo} = \frac{4\dot{m}}{\pi \mu_l D_i} = 667.644332481808$

Fanning friction factor: $C_f = \frac{16}{\text{Re}_{lo}} 2.39648555699167 * 10^{-2}$

Gravity term: $\frac{\sum_{k=1}^{N} \rho_k g L_k \sin\theta_k}{\sum_{k=1}^{N} \frac{L_k}{A_{x,k}}} = 1.16677820709083 * 10^{-3} \text{ kg/s}^2$

Friction and minor loss term:

$$\frac{\sum_{k=1}^{N}\frac{1}{2}\frac{(C_f+K)}{\rho_k}\frac{A_{z,k}}{A_{x,k}^3}(\dot{m}^t)^2}{\sum_{k=1}^{N}\frac{L_k}{A_{x,k}}} = 1.16624939579674*10^{-3}\ \text{kg/s}^2$$

Mass flow rate at next time step:

$$\dot{m}^{t+\Delta t} = \dot{m}^t + \Delta t\left(-\frac{\sum_{k=1}^{N}\rho_k g L_k \sin\theta_k}{\sum_{k=1}^{N}\frac{L_k}{A_{x,k}}} - \frac{\sum_{k=1}^{N}\frac{1}{2}\frac{(C_f+K)}{\rho_k}\frac{A_{z,k}}{A_{x,k}^3}(\dot{m}^t)^2}{\sum_{k=1}^{N}\frac{L_k}{A_{x,k}}}\right)$$
$$= 9.15063662347649*10^{-3}\ \text{kg/s}$$

E.5 Pressure

Friction pressure change over control volume:

$$\Delta P_f = \frac{1}{2}\frac{(C_{f,k}+K_k)}{\rho_k}\frac{A_{z,k}}{A_{x,k}^3}(\dot{m}^t)^2 = 4.64643145735098*10^{-2}\ \text{Pa}$$

Gravitational pressure change over control volume:

$$\Delta P_g = -\rho_k g L_k \sin\theta_k = -730.854572567556\ \text{Pa}$$

Momentum pressure change over control volume:

$$\Delta P_a = \left(\frac{\dot{m}}{A_{x,k}}\right)^2\frac{1}{\rho_k} - \left(\frac{\dot{m}}{A_{x,k-1}}\right)^2\frac{1}{\rho_{k-1}} = 1.5889238629645*10^{-4}\ \text{Pa}$$

Total pressure change:

$$\Delta P = \Delta P_f - \Delta P_g - \Delta P_a = 730.900877989743\ \text{Pa}$$

Control volume outlet pressure at next time step:

$$P_e^{t+\Delta t} = P_i - \Delta P = 113593.464880239\ \text{Pa}$$

Control volume nodal pressure at next time step:

$$P_n^{t+\Delta t} = \left(P_i^{t+\Delta t} + P_e^{t+\Delta t}\right)/2 = 113958.915319234\ \text{Pa}$$

Control volume saturation temperature at next time step:

$$T_{sat}^{t+\Delta t} = 164.630366 + 0.001832295P_n^t + 4.27215x10^{-10}\left(P_n^t\right)^2 + 3738.954\left(P_n^t\right)^{-1}$$
$$- 701204\left(P_n^t\right)^{-2} + 16.161488\ln(P_n^t) - 0.0001437169P_n^t\ln(P_n^t)$$
$$= 376.398651886096\ \text{K}$$